Influence of Petroleum Deposit Geometry on Long Term Persistence of Residual Crude Oil

Bocheng Li

Thesis submitted to the faculty of the Virginia Polytechnic Institute and State University in partial fulfillment of the requirements for the degree of

Master of Science
In
Civil and Environmental Engineering

Mark A. Widdowson, Chair
Gregory D. Boardman
Glenn E. Moglen

May 11, 2015
Blacksburg, Virginia

Keywords: Petroleum oil deposit, geometry, numerical model, biodegradation, Deepwater Horizon oil spill, SEAM3D

Influence of Petroleum Deposit Geometry on Long Term Persistence of Residual Crude Oil

Bocheng Li

ABSTRACT

Following the DWH oil spill event, crude oil reaching the shoreline of Gulf of Mexico produced petroleum oil deposit with a range of distinct geometries, including sphere tar balls and horizontal tar sheets. Numerical models were developed based on the Deep Water Horizon oil spill conditions to evaluate the influence of deposit geometry on long term persistence of residual NAPL oil. Two extreme deposit geometries were modeled in this study: the horizontal tar sheet and the spherical tar ball. Both two-dimensional modeling approach and three-dimensional modeling approach were applied to compare two contrasting geometries. The two-dimensional model results showed that sheet geometry deposits exhibited a greater obstruction to groundwater flow relative to the spherical deposits and induced a larger sulfate reducing zone downgradient of the NAPL source, resulting in significantly greater sulfate-based biodegradation of benzene. Three-dimensional models were constructed to assess the influence of key geometry parameters on oil deposit fate and persistence. Three parameters affecting deposit's geometric structure were recognized, including the upper horizontal area of the sheet deposit, the thickness of the sheet deposit, and the radius of the sphere deposit. The three-dimensional model results suggested that thickness of the sheet deposit and radius of the sphere deposit were important geometry factors impacting the fate and long term persistence of residual NAPL oil in the coastal environment. However, the influence of deposit geometry differed depending on the solubility of the different NAPL components. When high solubility compound and low solubility compound both exist in the oil deposit, the influence of deposit geometry on benzene degradation was significant, while the influence on naphthalene was almost negligible.

Dedicated to my parents,

Shijiang Li and Aihua Bai, who always supporting and encouraging me to go on every adventure

Acknowledgements

Foremost, I wish to express my sincere thanks to my advisor Dr. Mark Widdowson for the continuous support of my study and research, for his patience, motivation, and encouragement. His valuable guidance helped me in all the time of research and writing of this thesis. I appreciate his immense knowledge and skills in many areas. I couldn't have imagined having a better advisor and mentor during my study time at Virginia Tech.

Besides my advisor, I would like to thank the rest of my thesis committee: Dr. Gregory Boardman and Dr. Glenn Moglen for their involvement, patience, encouragement, and insightful advices.

I would like to thank Charles E. Via Department of Civil and Environmental Engineering at Virginia Tech for providing me with all the necessary facilities for the research.

Special thanks goes to Carlos ManPena, Marian Alicea, Masud Rana, and Bojun Xu, who provided valuable suggestions through my research and helped my keep things in perspective. Also, I want to acknowledge the graduate students in Patton Hall 222, for providing a much needed form of escape from my studies.

Finally, I would like to thank my family for the support they provided me through my entire life. Without those love and spiritual encouragement, I would not have finished this thesis.

Table of Contents

List of Figures

List of Tables

Chapter 1 Introduction and Objectives

1.1 Deepwater Horizon Explosion

Oil and gas in the Gulf of Mexico (GOM) Offshore region is a principal source of oil and natural gas in the United States. The Gulf region (Figure 1.1), which covers offshore Texas, Louisiana, Mississippi, and Alabama, is a major contributor to U.S. oil and natural gas production, supplying approximately 25 percent of the nation's domestic oil and 14 percent of the Nation's domestic gas production in 2007 (Nixon et al., 2009). In 2014, Federal leases in the Gulf of Mexico produced 509 million barrels of oil, which made up 16 percent of the US oil production that year (US Energy Information Administration, 2014). Since 1997, interest in the oil and gas potential of the deepwater areas of the GOM increased with significant support from the Federal government. In 2009, it has been reported that deepwater wells (water depth over 1000 ft) and ultra-deepwater wells (water depth over 5000 ft) like Deepwater Horizon (DWH) contributed a very important part of the total GOM production, providing approximately 70 percent of the oil and 36 percent of the gas in the region (Nixon et al., 2009). However, activities related to crude oil exploration and transportation have resulted in numerous accidental oil spills. Active petroleum vents and slicks were identified in the deep water of GOM (Kornacki et al., 1994). Consequently, small oil seeps or spills in GOM have been quite common. According to the U.S. Department of Interior estimates, about 1,800 total barrels of oil were spilled in U.S. waters as a result of blowouts between 1970 and 2010 (Hamilton, 2011).

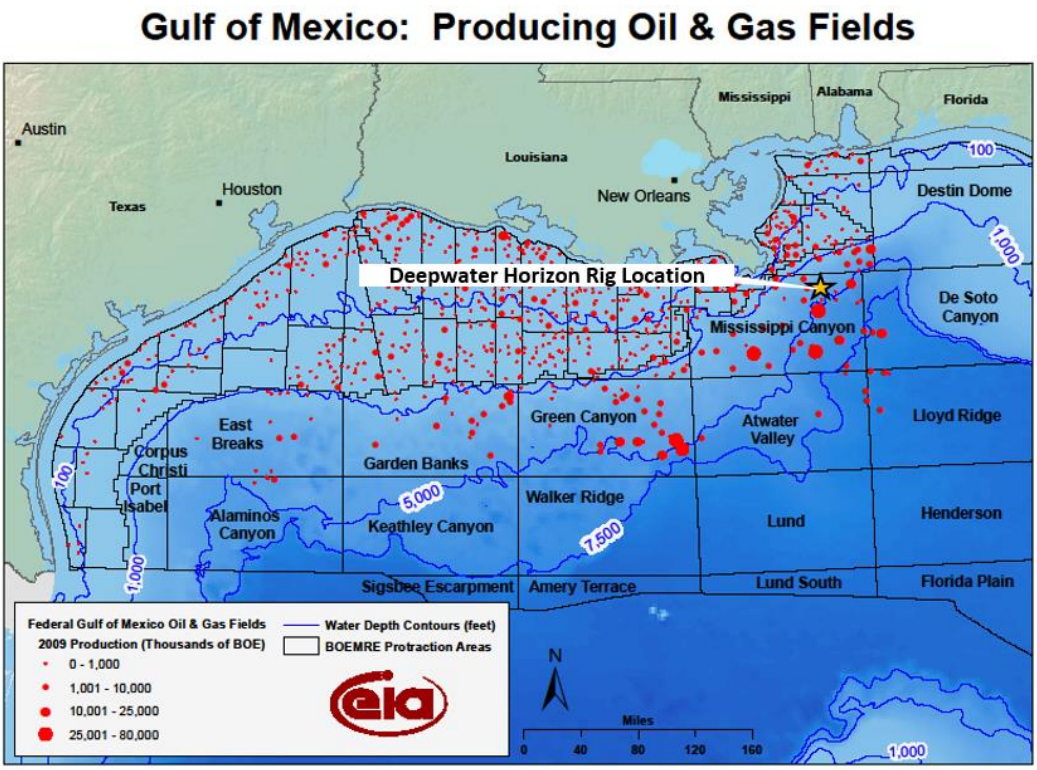

Figure 1.1. Offshore oil and gas fields in the United States Federal zone, Gulf of Mexico (U.S. Energy Information Administration, 2010, retrieved from http://www.eia.gov/pub/oil_gas/natural_gas/data_publications/crude_oil_natural_gas_reserves/current/pdf/gomwaterdepth.pdf, used under fair use, 2015)

Deepwater Horizon (DWH) was an ultra-deepwater offshore oil drilling rig owned by Transocean. The DWH oil rig was built in 2001 in South Korea and then leased to British Petroleum (BP) until September 2013 (Paganie, 2009). In September 2009, the rig reached the deepest oil well in history at a vertical depth greater than 10 km beneath the seafloor located southeast of Houston, Texas (Latham, 2011). On April 20, 2010 the DWH oilrig exploded while drilling at the Macondo Prospect located 66 km southeast of the Louisiana coast in Mississippi Canyon Block 252 (Office of the Maritime Administrator, 2011). A loss of well control resulted in a release of liquid and gaseous hydrocarbons onto and around DWH. This blowout culminated in explosions and fire that killed 11 crewmen. Considered as the largest accidental marine oil spill in the history, the DWH oil spill caused enormous losses to humans, the economy, and the environment. It is estimated by US government that a total amount of 4.9 million barrels of crude oil were spilled impacting a coastal area of 68,000 mi^2 directly (Figure 1.2).

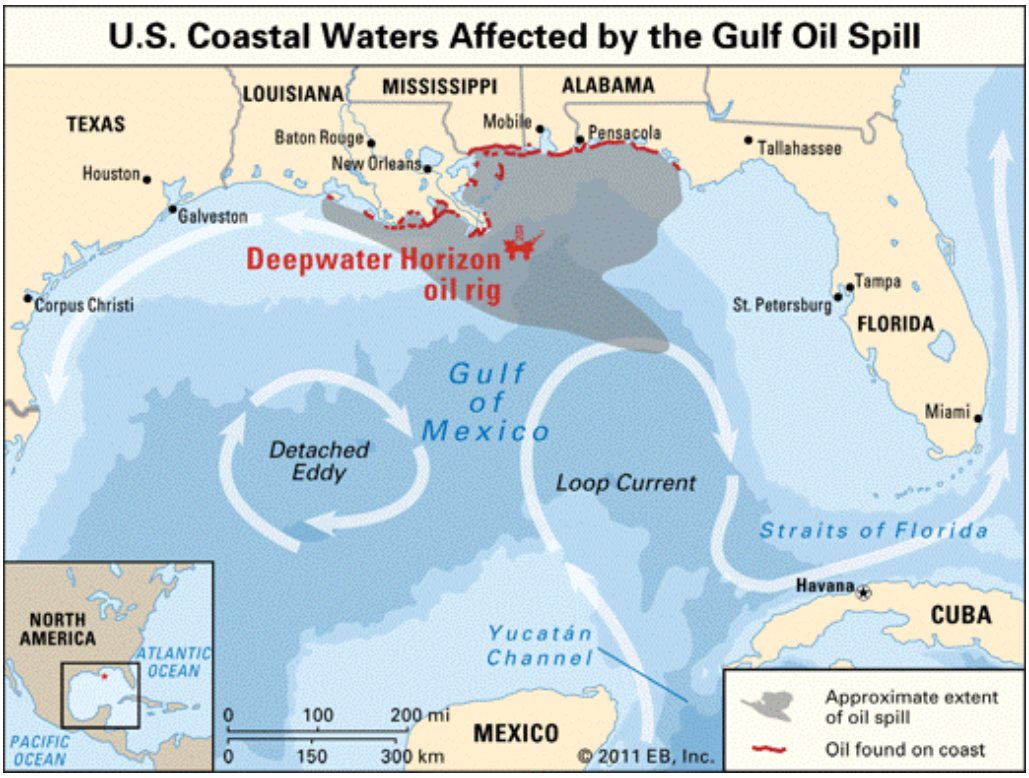

Figure 1.2. Impact of the DWH spill on the GOM offshore (Encyclopedia Britannica, 2011, retrieved from http://www.britannica.com/event/Deepwater-Horizon-oil-spill-of-2010/images-videos, used under fair use, 2015)

1.2 Efforts in Response to Gulf of Mexico Oil Spill

Oil spilled from the DWH explosion impacted five states in the U.S. A variety of techniques were used immediately in response to the oil spill, which includes containment, dispersal and removal. The crude oil emanating from the DWH was a complex mixture of petroleum hydrocarbons with different densities primarily in the form of a water-in-oil emulsion (Elango et al., 2014). Because the oil was highly emulsified, it did not evaporate or combust as easily as regular oil, and the emulsified oil was not readily subject to biodegradation or elusion, which essentially increased the difficulty in cleaning up the spilled oil (Board and Board, 2002).

Miles of containment boom were deployed to capture the oil on the surface. The containment boom was designed to extend 18-48 inches above and below the water surface and are effective only in relatively slow-moving waters. More than 9,100,000 feet of one time use sorbent boom and 4,200,000 feet of containment booms were assigned by British Petroleum to contain the spill (Butler, 2011)

Injection of dispersants is a notable strategy that has been well-studied to minimize the adverse impact of oil. It can greatly increase the surface area available for dissolution of oil and microbial colonization (Atlas and Hazen, 2011), and dispersed oil is thought to lessen the harm to the environmental ecosystem (Jefferson and Bowling, 2011). Dispersants COREXIT 9500 and COREXIT EC9527A were directly injected to the wellhead of DWH after the explosion. By July 2010, more than 1.8 million US gallons of dispersant had been used (Butler, 2011). However, despite the effectiveness of dispersants combating oil impact in general, this use of dispersant at DWH was questioned for its deep injection depth at 4,900 ft near the wellhead and the dispersant toxicity effect on environment.

Removal approaches to treat the spilled oil included controlled burns, skimming, and siphoning from the wellhead. British Petroleum, along with the U.S. Coast Guard carried out 411 controlled burns and approximately 265,000 barrels of oil were remediated (Butler, 2011). Oil was also collected by using skimmers. More than 60 open water skimmers including 12 purpose-built vessels were deployed after the DWH explosion (Butler, 2011).

As the largest emergency response to a marine oil spill in petroleum industry, National Incidents Command's Flow Rate Technical Group (FRTG)'s oil budget calculator for the Deepwater Horizon well oil release estimated that 3% was skimmed, 5% was burned, 8% was chemically dispersed, 16% was naturally dispersed, 17% was captured, 25% was evaporated or dissolved, and 26% was residual remained. The "chemically dispersed" fraction includes dispersal at the surface and at the wellhead, while "naturally dispersed" was mostly at the wellhead; the "residual remaining" is the residual oil remaining as surface sheen, floating tar balls, and oil washed ashore or buried in sediments. Based on the estimates, approximately 75% of the spill still remained in the Gulf environment and a plus or minus 10% uncertainty exists in the volume of the spill (Kerr, 2010).

1.3 Long Term Persistence of Crude Oil and Role of Geometry

Large amounts of crude oil MC252, a light paraffinic crude oil (Daling et al, 2014), was transported by ocean currents and deposited onto the beaches along the Gulf of Mexico. Coastal headland Fourchon Beach located at the Louisiana Gulf Coast found MC252 crude oil first reaching its shoreline in May 2010 (Urbano et al., 2013). Figure 1.3 shows the amount of oil on the coastline on August 7, 2010. The crude oil reaching from the DWH blowout was in a form of water-in-oil emulsion. As the oil emulsions reached the sandy beach shorelines, mixed with sand and shell in the subtidal and intertidal areas of the beach, it started to produce several unique oil forms including surface residue balls, which is oil-sand aggregates typically 0.5-10 cm in diameter, and oil mats, leading to a formation of large sheet deposit (Singh et al., 2012; Elango, 2014). As the slick of oil on the Gulf reduced in volume and mass, long term persistence of crude oil reaching the beach became an ecosystem threat and a concern for clean-up efforts.

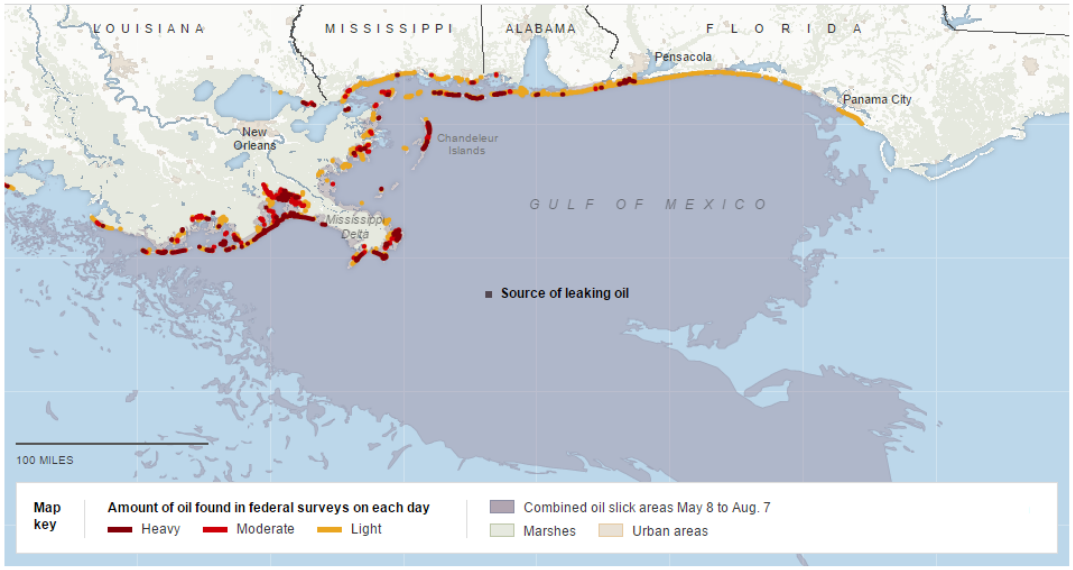

Figure 1.3. Spilled oil on the coastline on August 7, 2010 (Aigner et al., 2010, retrieved from http://www.nytimes.com/interactive/2010/05/27/us/20100527-oil-landfall.html, used under fair use, 2015)

Mainly composed of petroleum hydrocarbon compounds (PHCs), crude oil is a rich source of organic carbon which includes readily biodegradable compounds, especially under aerobic conditions. Most of oil components are water-soluble to a certain degree. Compounds with low molecular weight like aliphatic and aromatic hydrocarbons have relatively high solubility in the seawater. Crude oil dissolved in

the groundwater is then utilized by microorganisms in microbial metabolism (Blumer et al., 1973). Therefore, dissolution and biodegradation play an important role in determining the long term persistence of PHCs. A variety of factors including oil composition, limiting nutrients for biodegradation, and aquifer characteristics impact dissolution and biodegradation of PHCs (Urbano et al., 2013; Vilcáez et al, 2013; Kiruri et al., 2013). However, contaminant source geometry as one potentially key factor impacting the persistence of PHCs in coastal environments has been overlooked in the models.

Crude oil present in coastal sand is generally considered to behave as a non-aqueous phase liquid (NAPL). In the case of a NAPL contamination source, NAPL source geometry was recently acknowledged as an important factor impacting the persistence of PHCs in the subsurface (Singh et al., 2012). First, NAPL surface area is dictated by the geometry, which then drives NAPL dissolution rate and available area for microbial colonization (Widdowson, 2004). Furthermore, from the perspective of hydrology groundwater flow, NAPL geometry could potentially form a localized obstruction to flow, and thus, impact the recharge condition (Ewing and Berkowitz, 1998). The flow change within the NAPL source causes a deficit of essential nutrients and electron acceptor in and around the NAPL source. This vacant area of nutrients and electron acceptors could have a dramatic impact on the biodegradation potential and thus the ultimate fate and persistence of the NAPL (Singh et al., 2012). In the case of an oil spill, PHCs are an abundant source of electron donors so that the limiting factors for biodegradation become the availability of nutrients and electron acceptors. Therefore, the geometry of NAPL source plays an important role in deciding microbial colonization (Abed et al., 2011; Amos et al., 2008), fate and long term persistence of oil deposited in the coastal environment.

1.4 Biodegradation Model to Investigate on Effect of Geometry

Crude oil is a complex mixture composed of different classes of organic hydrocarbons. To account for biodegradation processes so as to evaluate the long term persistence of crude oil, mathematical modeling is a powerful, well studied tool. For example, a biodegradation model could be developed for simulating microbial growth-degradation processes in porous media (Molz et al., 1986); a

numerical model was developed by Li and Boufadel (2010) to study the long term persistence of oil after another major oil spill happened in 1989, the Exxon Valdez oil spill in Alaska; Vilcáez and Li (2013) built a model for the biodegradation of oil droplets under conditions relevant to the DWH oil spill.

Field observations after oil traveled to the beach suggest that oil could interact with sand and other particulate matter to deposit stable geometries in Gulf of Mexico. While a range of geometries were found in the coastal area, two extreme geometries were identified as "horizontal tar sheet" and "sphere tar ball" (Singh et al., 2012).It is hypothesized in this study that the horizontal sheet deposit has more impact on redox conditions around the oil deposit than the sphere tar ball deposit. Sheet deposit is assumed to encourage formation of anaerobic conditions below the deposit.

1.5 Objectives and Roadmap

The overall objective of this study was to investigate the effect of crude oil deposit geometry on long term persistence of petroleum deposits. Divergent geometries of horizontal tar sheet and sphere tar ball were modeled to explain and account for the long term persistence of oil deposit. Both two-dimensional and three-dimensional numerical models were developed based on DWH oil spill conditions. The impact of geometry was studied by comparing biodegradation efficiency through use of a sheet model and a sphere model. By altering geometry structures of sheet deposits and sphere deposits in the numerical model, key parameters of geometry were examined.

In order to achieve this objective, numerical computer models were built based on field conditions. The overlying purpose of these numerical models design was to simulate the petroleum oil deposit, observe the groundwater flow distribution as well as development of the redox gradient around the petroleum deposit, and calculate the mass depletion difference between the two geometries, which is ascribable to aqueous phase transportation and biodegradation. This study began with a two-dimensional model design aimed at observing groundwater flow distribution and comparing biodegradation efficiency. In order to understand geometry influence on divergent biodegradation processes, two-dimensional

models were developed under different biodegradation pathways. Based on the DWH oil spill conditions, a set of three-dimensional models were developed afterwards to assess geometry key parameters' influence on oil deposit fate and persistence.

1.6 Organization of this Thesis

A summary of the approach achieving the overall objective of this thesis is:

1) Comparison of groundwater flow distribution and biodegradation under diverse pathways applying two-dimensional numerical models.
2) Quantify the effect of key geometry parameters on transportation and biodegradation applying three-dimensional numerical models.

Chapter 1 is a general introduction and background to this. A brief history of DWM oil spill incident at the GOM and the role of geometry related to long term persistence of oil deposit are provided. Chapter 1 also contains a brief statement of the objective of this study and organization of this thesis.

Chapter 2 will review the literature on models for the persistence of oil and PHCs in coastal soils. It begins with a discussion about oil composition and properties. Further, the chapter deals with biodegradation behavior of petroleum hydrocarbons under various redox conditions. This is then followed by a brief overview of current biodegradation models in assessing long term persistence of petroleum hydrocarbons in the subsurface. Lastly, the role of deposit geometry which is hypothesized to play in long term persistence of petroleum hydrocarbon, in this study, is discussed in terms of development of electron acceptor gradient and redox conditions.

Chapter 3 details the specific design of the numerical models and presents development of conceptual and mathematical models. Chapter 4 describes data analysis and model parameters. Chapter 5 is the results from numerical model simulations and a discussion of its findings. Chapter 6 is the summary of the conclusions from this study.

Chapter 2 Literature review

2.1 Oil Composition and Properties

Crude oil is a mixture of hydrocarbon compounds ranging from smaller, volatile compounds to very large, nonvolatile compounds (Ancheyta and Speight, 2007). The chemical composition of crude oil varies according to the geological formation region and greatly influences the properties of the oil. In general, petroleum hydrocarbon compounds (PHCs) found in oils is characterized by their structure. A common method of classification is by SARA—saturates, aromatics, resins, and asphaltenes (Fingas and Brown, 2011). The saturate group of components in oil consists primarily of alkanes. It includes straight-chain alkanes and branched-chain alkanes and also cycloalkanes. The straight-chain alkanes and branched-chain alkanes are saturated hydrocarbons with no ring structures. Crude oil typically contains large amount of alkanes, making up 50 to 90% of the composition of the oil (Fingas and Brown, 2011). Although alkanes are chemically inert, most of them can be efficiently degraded by several microorganisms under both aerobic and anaerobic biodegradation pathways (Caldwell et al, 1998; Lee and Choi, 1999; Rojo, 2009).

Aromatic compounds include at least one benzene ring of six carbons. The most common aromatic compounds found in oil are often referred to as BTEX, or Benzene, Toluene, Ethyl-benzene, and Xylenes. Because of the stability of benzene ring, aromatics are very persistent and can have toxic effects on the environmental. BTEX make up between 0 to 2.5% of the composition of the oil (Fingas and Brown, 2011). Experiments and simulations demonstrate that BTEX are very readily biodegraded by many marine microorganisms. Previous study also indicates that BTEX were better growth substrates than multi-ring aromatics, resulting in faster growth and higher yield coefficients (Chen et al., 1992; Atlas, 1995; Godsy et al, 1999; Reardon et al, 2000). Polycyclic aromatic hydrocarbons (PAHs) are compounds consisting of at least two benzene rings. PAHs make up between 0 to 40% of the composition of the oil (Fingas and Brown, 2011). Although PAH may undergo adsorption, volatilization, photolysis,

and chemical degradation, microbial degradation is the major degradation process. The biodegradation of PAHs have been observed under both aerobic and anaerobic conditions (Haritash and Kaushik 2009; Desai et al., 2008; Allan et al., 2012). Resins and asphaltenes are both classes of polar compounds, which have significant molecular charge as a result of bonding with compounds such as Sulphur, nitrogen, or oxygen. Polar compounds usually make up between 0 to 5% of the composition of the crude oil (Jobson et al., 1972). Due to its chemical structure complexity, polar compounds are extremely resilient in terms of microbial degradation (Atlas, 1995).

Oil released to oceans undergoes various processes altering the composition and concentration of the oil. The processes, collectively known as weathering, including chemical, physical and biological processes, have significant influence on the toxicity and persistence of the oil washed to salt marshes or deposited in sediments (Liu et al., 2012). The important weathering processes include evaporation, dissolution, biodegradation and photoxidation (Hunt, 1996; Fingas, 1999; Plata et al, 2008). Weathering of oil after large oil spills like Exxon Valdez in Alaska has been well documented (Wang and Fingas, 1995). However, there are couple unique features in the DWH oil spill. As a typical light Louisiana crude oil, the DWH oil contains saturated n-alkanes, PAHs and alkylated PAHs, with low-molecular-weight hydrocarbons over 50% of the composition (Ryerson et al., 2011). The long vertical travel distance for the oil after wellhead blowout along with application of dispersant could have impact on weathering of crude oil. Field study examined the composition of petroleum hydrocarbons in oil mouse collected from the sea surface, salt marshes, and in oil deposited sediments (Liu et al., 2012). The petroleum hydrocarbon data reveal that the oil deposit collected in the sediments was subjected to a light to moderate degree of weathering, as supported by the presence of short-chained n-alkanes, BTEX and C_3-benzenes.

2.2 Biodegradation of Petroleum Hydrocarbons

In order to combat the adverse environmental impact of marine oil spill, numerous physical means were used to remove or disperse the oil. However, microbial degradation is the major and ultimate natural mechanism by which one could clean up the petroleum hydrocarbon contamination (Leahy and

Colwell, 1990; Atlas and Hazen, 2011). Biodegradation of petroleum hydrocarbons is a complex process that depends on the nature and on the amount of the hydrocarbons present (Atlas, 1981). A number of limiting factors affecting the biodegradation of petroleum hydrocarbons have been discussed (Das and Chandran, 2010). The composition and inherent biodegradability of the petroleum hydrocarbon component is the first and foremost important factor taking into account. Temperature plays an important role in terms of physical factors by affecting the chemistry of the pollutants as well as affecting the microbial activities (Atlas, 1975). Nutrients are also very important ingredients for successful biodegradation of petroleum hydrocarbons especially nitrogen, phosphorus and sometimes iron (Atlas, 1985).

Biodegradation of petroleum hydrocarbon, in essence, is redox chemical reaction happened between electron acceptors and electron donors. The energy released from the redox reaction was then utilized by microbes for microbial growth. Typically, petroleum hydrocarbons are electron donors. Electron acceptors differs from oxygen (O2), sulfate (SO42-), nitrate (NO3-), ferric ions (Fe(III)), oxidized manganese (Mn(IV)), and carbon dioxide (CO2) (Jørgensen, 1989).

The availability of electron acceptors determines the sequence of biodegradation processes. The most rapid degradation of the majority of petroleum hydrocarbons is aerobic biodegradation. Under aerobic conditions a class of enzymes belonging to oxygenases attacks the C-H bond, whereas anaerobic hydrocarbon degraders use alternate enzyme mechanisms (Boll and Heider, 2010). Anaerobic biodegradation occurs in the absence of oxygen and usually exhibit lower microbial growth rates than aerobic degradation. This is ascribable to thermodynamic limitations of anaerobic terminal electron acceptor (TEA) and fermentation processes. Table 2.1 exhibits the redox reactions with Gibbs free energy supplied by TEA considered in this study. When multiple EAs are available, microbes tend to utilize them in sequence, starting with the one that provides the highest Gibbs free energy (Waddill and Widdowson, 1998). The table shows that highest energy is available for microbes when oxygen is utilized by microorganisms as a TEA, followed by sulfate and methanogenesis (Jakobsen, 2007).

2.3 Numerical Models Assessing Fate and Persistence of Petroleum Hydrocarbon

Mathematical models developed to simulate both transportation and biogeochemical (coupled organic and inorganic reaction processes) processes have been employed to account for long term persistence of PHCs in the environment. Biodegradation models are classified by considering the complete biodegradation process as either a single- or as a two-step process (Brun and Engesgaard, 2002). The single-step biodegradation models identify substrate and electron acceptor for the reaction, and the consumption of both the electron donor and acceptor are treated kinetically (Schäfer and Therrien, 1995). The two-step biodegradation approach split the biodegradation processes into two half-cell reactions. The first reaction consumes the substrate and donates electrons; the second step balances the donated electrons by reacting with electron acceptors. The single-step models have found inspiration in classical biodegradation transport with complex bacterial growth relations based on Monod kinetics. The two-step process models rely on the Partial Equilibrium Approach (PEA) to assume the organic degradation step, and not the electron acceptor consumption step, is rate limiting. The two-step model shows advantages simulating complex geochemical reactions; however, it has some limitations in biomass growth simulation (Jakobsen and Postma, 1999). Brun and Engesgaard (2002) developed a three-dimensional, two-step PEA model that allows Monod kinetics and biomass growth, features usually included only in one-step process models.

Table 2.1. Electron Acceptors and Gibbs free energy

Reaction	Gibbs Free Energy (ΔG°kj/mol)	Reaction Type
$\frac{1}{4}O_2 + H^+ + e^- = \frac{1}{2}H_2O$	-118.6	Oxidation Reduction
$\frac{1}{8}SO_4^{2-} + \frac{19}{16}H^+ + e^- = \frac{1}{16}H_2S + \frac{1}{16}HS^- + \frac{1}{2}H_2O$	-26.76	Sulfate Reduction
$\frac{1}{8}CO_2 + H^+ + e^- = \frac{1}{8}CH_4 + \frac{1}{4}H_2O$	-16.29	Methanogenesis

In order to get numerical solutions to predict the fate of petroleum hydrocarbon in the environment, code or software packages were developed in the past based on numerical analysis. Baehr and Corapcioglu (1987) constructed a numerical model to simulate spilled hydrocarbon trapped in soil. The solution was obtained by using a finite difference scheme and a method of forward projection to predict mass removed from the soil, entering either the atmosphere or groundwater, or is biodegraded. Nicol et al (1994) completed a framework for numerically modeling the biodegradation of petroleum hydrocarbons within a flooded column of porous media. The petroleum hydrocarbon was classified to 8 components, and a specific microbial population is associated with each degradable class. Monod kinetics were used to model the biological processes and a variable step, variable order, backward differentiation method was used to solve the numerical equations.

After oil spill accidents, numerical models were routinely constructed by researchers based on the specific field conditions. Uraizee et al. (1997) developed a mathematical model to account for the dependence of biodegradation of crude oil through a putative bioavailability parameter. Boufadel et al. (1999) constructed a two-dimensional model evaluate the solute on water density and viscosity by using the MARUN model. Cirpka et al. (1999) built numerical models to account for the effect of mixing between substrates in heterogeneous aquifer on microbial activity. Essaid et al. (2003) used the U.S. Geological Survey (USGS) solute transport and biodegradation code BIOMOC combined with the USGS universal inverse modeling code UCODE to quantify BTEX dissolution and biodegradation at a crude oil spill site located near Bemidji, MN. Li and Boufadel (2010) carried out two-dimensional variable density and saturation simulations using the finite-element model MARUN to account for the long term persistence of oil from the Exxon Valdez spill. Vilc áez et al. (2013) developed a numerical model for the biodegradation of oil droplets, and applied the model to estimate the time scale of biodegradation of DWH oil spill in Gulf of Mexico. Torlapati and Boufadel (2014) used numerical model BIOB to simulate the biodegradation of oil entrapped in the sediment. Xu et al. (2015) used the Hydrocarbon Spill

Screening Model (HSSM) combined with the modified Modular Three-Dimensional Multispecies Transport Model (MT3DMS) to predict the fate of spilled gasoline in soil and groundwater.

2.4 Role of Geometry of Petroleum Deposits

Geometry effect of the contaminant source has been considered as an emerging factor impacting the fate of NAPLs in the subsurface. Following the DWH oil spill event, crude oil reaching the shoreline of Gulf of Mexico was primarily in the form of a water-in-oil emulsion (Urbano et al., 2013). Mixed with sand and shell in the beach, the water-in-oil emulsion produced petroleum oil deposit with a range of distinct geometries (Elango et al., 2014).

Source zone geometry and size are known to be significant in almost all NAPL modeling studies of predicting time of remediation for petroleum contaminated groundwater systems (Hosseini, 2011). NAPL geometry determines the surface area of NAPL, which drives dissolution rates and area available for microbial activities (Widdowson et al., 2004). Measurement of hydraulic conductivity in oil sand deposit found that NAPL contamination could drastically decrease the hydraulic conductivity of the sand sediment (Suthaker and Scott, 1996). With a relatively low hydraulic conductivity, NAPL source forms a local obstruction to the groundwater flow. Therefore, groundwater flow distribution could be potentially influenced by NAPL geometry (Ewing and Berkowitz, 1998).

In case of NAPL contamination, biodegradation processes while TEAs and nutrients were consumed along with the substrate. When multiple EAs are available subsurface, microbes tend to utilize them in sequence (Waddill and Widdowson, 1998). Depletion of a TEA results in sequential use of other TEAs present in the surrounding, until the region has been depleted of all TEAs and fermentative conditions set in. Singh et al. (2012) investigated the geometry influence of petroleum deposit on local gradient of electron acceptors and microbial community composition. Their results indicated that petroleum deposits that are spread horizontally into sheets obstruct recharge to a greater extent than tar

balls. Due to the lower surface area to volume ratio and higher obstruction to flow, horizontal tar sheet deposit is more persistent in the environment and may be a greater priority for cleanup than tar balls.

Overall, source geometry is a well-known factor considered in most current models for NAPL contamination in groundwater, and its extension to petroleum oil deposit in coastal environment stands as an interesting prospect in improving models predicting the fate and long term persistence of spilled crude oil.

Chapter 3 Model Development

3.1 Conceptual Model

Conceptually, the problem concerned in this thesis is the biodegradation of petroleum hydrocarbon compounds (PHC) within a porous medium where a residual petroleum source is present. For this problem the porous medium is conceptualized as the saturated zone beneath the water table. The source is conceptualized as a freshly-deposited crude oil. The oil phase is represented as a multi-component non-aqueous phase liquid (NAPL). Two different geometries were adopted for the NAPL source; crude oil deposited as a spherical tar ball and as a horizontal sheet representing two diverse geometric structures.

The groundwater flow model MODFLOW (Banta and McDonald, 2000) was used to simulate the groundwater flow field of the aquifer. MODFLOW could solve groundwater flow equations based on the finite-difference method. MODFLOW-2005 released by the USGS simulates steady and nonsteady flow in an irregularly shaped flow system in which aquifer layers can be confined or unconfined. Hydraulic parameters (i.e., hydraulic conductivity, dispersivity, specific storage and specific yield) may be specified spatially different. Specific head and flux boundaries can be simulated as a head dependent flux across the model's outer boundary. MODFLOW can be paired with a solute transport simulation package like SEAM3D (Waddill and Widdowson, 1998) to simulate pollutant transport.

The numerical model SEAM3D (sequential electron acceptor model, 3 dimensional) was used to simulate subsurface solute transport coupled with aerobic and sequential anaerobic biodegradation and dissolution of PHCs from the NAPL source. SEAM3D can depict multiple solutes in a three-dimensional, anisotropic, heterogeneous domain as influenced by advection, dispersion, sorption and biodegradation. The solutes include biodegradable carbon substrates, mineral nutrients, and electron acceptors (EAs) for microbial growth. Petroleum hydrocarbon compounds are substrates in this study that serve as electron donors. Biodegradation of PHCs is described using Monod kinetics (Bailey and Ollis, 1977). The

modified Monod equations include effects of EA and nutrient availability, inhibition (Widdowson et al., 1988) and threshold concentrations (Button, 1985) were used to represent substrate uptake rate and biomass growth.

The NAPL source mass was specified at model cells in the numerical domain with a specified initial mass in order to generate different geometries. Dissolution of contaminants from the NAPL into the aqueous phase was simulated with a single uniform dissolution rate coefficient for all the petroleum hydrocarbons. It is assumed that the NAPL has reached its residual saturation state, and aqueous phase constituents are assumed to be the only mobile phase. This includes PHCs, electron acceptors and products resulting from the biodegradation of PHCs. Thus, the NAPL is assumed to be immobile. This assumption is valid based on the time scale for aqueous phase transport which is much greater than the time period of NAPL mobility. The composition of the multi-component NAPL and rationale are described in Chapter 4.

Both aerobic biodegradation and anaerobic biodegradation were considered in this study. Multiple electron acceptors were taken into account including oxygen (O_2), sulfate (SO_4^{2-}), and carbon dioxide (CO_2). However, for this study nitrate (NO_3^-), oxidized manganese (Mn(IV)), and ferric iron (Fe(III)) reduction were not considered due to their low concentration in the seawater environment (Gros et al., 2008). In case of methanogenic biodegradation, methane (CH_4) is the primary end product. Mineral nutrients (ammonia nitrogen and phosphorus) were not considered because these are not typically present in the oligotrophic environments (i.e., beach sand). Spatially uniform biodegradation rates were also assumed during model development.

3.2 Mathematical Model

The mathematical model that serves as the basis for the SEAM3D codes is fully described in (Waddill and Widdowson, 1998). The description in Section 3.2 explains the equations of solution pertaining to the current study.

3.2.1 Equations of Aqueous Phase Mass Balance

The transport of different solute species in SEAM3D model is solved by the advection-dispersion equation. Three classes of solute, which includes hydrocarbon substrate, electron acceptor and biodegradation product, were considered for both two-dimensional and three-dimensional models in this study. For each hydrocarbon substrate, the transport governing equation is written as

$$-\frac{\partial}{\partial x_i}(\overline{V_i}S_{ls}) + \frac{\partial}{\partial x_i}\left(D_{ij}\frac{\partial S_{ls}}{\partial x_j}\right) + \frac{q_s}{\theta}S_{ls}^{*} - R_{sink,ls}^{bio} + R_{source,ls}^{NAPL} = R_{ls}\frac{\partial S_{ls}}{\partial t} \quad (3.1)$$

where S_{ls} is the aqueous phase substrate concentration [$M_{ls}\,L^{-3}$] for ls=1,2,…,NS (number of substrates); S_{ls}^{*} is the substrate point source concentration [$M_{ls}\,L^{-3}$]; $\overline{V_i}$ is the average pore water velocity [$L\,T^{-1}$]; x_i is the distance [L]; D_{ij} is the tensor for the hydrodynamic dispersion coefficient [$L^2\,T^{-1}$]; $R_{sink,ls}^{bio}$ is the substrate biodegradation sink term [$M_{ls}\,L^{-3}T^{-1}$]; $R_{source,ls}^{NAPL}$ is a substrate source term due to non-aqueous phase liquid (NAPL) dissolution [$M_{ls}\,L^{-3}T^{-1}$]; R_{ls} is the retardation factor for substrate ls [L^0]; t is the time [T]; and q_s is the volumetric flux of water per unit volume of aquifer [T^{-1}] with $q_s>0$ for sources and $q_s < 0$ for sinks.

For each of electron acceptor (EA) transport, (for this study, dissolved oxygen and sulfate), the equation is written as

$$-\frac{\partial}{\partial x_i}(\overline{V_i}E_{le}) + \frac{\partial}{\partial x_i}\left(D_{ij}\frac{\partial E_{le}}{\partial x_j}\right) + \frac{q_s}{\theta}E_{le}^{*} - R_{sink,le}^{bio} = \frac{\partial E_{le}}{\partial t} \quad (3.2)$$

where E_{le} is the EA concentration [$M_{le}\,L^{-3}$] for le=1, 2… NS (number of electron acceptors); E_{le}* is the EA point source concentration [$M_{le}\,L^{-3}$]; $R_{sink,le}^{bio}$ is the EA biodegradation sink term [$M_{le}\,L^{-3}T^{-1}$].

For each biodegradation product, (for this study, sulfide and methane), the transport equation is written as:

$$-\frac{\partial}{\partial x_i}\left(\overline{V_i}P_{lp}\right) + \frac{\partial}{\partial x_i}\left(D_{ij}\frac{\partial P_{lp}}{\partial x_j}\right) + \frac{q_s}{\theta}P_{lp}^{*} - \lambda_{lp}P_{lp} + R_{source}^{bio} = R_{lp}\frac{\partial P_{lp}}{\partial t} \quad (3.3)$$

where P_{lp} is the aqueous phase product concentration [M_{lp} L^{-3}] for lp=1, 2… NP (number of products); P_{lp}* is the point source concentration for product *lp* [M_{lp} L^{-3}]; λ_{lp} is the first order decay coefficient for product *lp* [T^{-1}]; R_{source}^{bio} is a biodegradation source term [M_{lp} L^{-3} T^{-1}]; and R_{lp} is the retardation factor for product *lp* [L^0].

3.2.2 NAPL Dissolution

Soluble components present in a non-aqueous phase liquid (NAPL) dissolve into the aqueous phase at the interface with groundwater. Dissolution is ongoing until equilibrium is reached or the NAPL mass is depleted. NAPL dissolution is a complex process that is influenced by several factors including NAPL composition, NAPL configuration, and groundwater flow condition (Nambi and Powers, 2000; Clement et al., 2004; Chu et al., 2004). In SEAM3D, for each of the substrates, concentration difference between the aqueous phase (S_{ls}) and equilibrium state (S_{ls}^{eq}) is the driving force for dissolution. Because NAPL dissolution is related to a high rate of transport processes, S_{ls} may remain lower than S_{ls}^{eq}. A mathematical equation (equation 3.4) was applied to simulate this effect by using a mass transfer rate coefficient (k^{NAPL}):

$$R_{source,ls}^{NAPL} = \max[0, k^{NAPL}(S_{ls}^{eq} - S_{ls})] \tag{3.4}$$

where the rate of mass transfer is a function of the concentration difference (Imhoff et al., 1994). Using Raoult's Law, S_{ls}^{eq} can be calculated (Parker et al., 1991) as

$$S_{ls}^{eq} = f_{ls} S_{ls}^{sol} \tag{3.5}$$

where f_{ls} is the mole fraction of substrate *ls* in the NAPL [mol_{ls} mol $_{NAPL}^{-1}$]; and S_{ls}^{sol} is the solubility of pure substrate *ls* in water. For each time step, f_{ls} is then calculated as

$$f_{ls} = \frac{S_{ls}^{NAPL} / \omega_{ls}}{I^{NAPL} / \omega_I + \sum_{ls=1}^{NS} S_{ls}^{NAPL} / \omega_{ls} + \sum_{lt=1}^{NT} T_{lt}^{NAPL} / \omega_{lt}} \tag{3.6}$$

where S_{ls}^{NAPL} is the constituent concentration in the NAPL phase expressed as NAPL mass of substrate *ls* per unit mass dry soil [M_{ls} M_{solid}^{-1}]; I^{NAPL} is the NAPL concentration of inert [M_i M_{solid}^{-1}]; T_{lt}^{NAPL} is the NAPL concentration of soluble, nonbiodegradable constituents *lt* [M_{ls} M_{solid}^{-1}]; and ω_j is the molecular weight of NAPL constituent j. With equations (3.4), (3.5), and (3.6), S_{ls}^{NAPL} for each time step is calculated as:

$$\frac{dS_{ls}^{NAPL}}{dt} = -\frac{\theta}{\rho_b} R_{source,ls}^{NAPL} \tag{3.7}$$

where ρ_b is the bulk density of the porous medium [M_{solid} L_{pm}^{-3}]. Thus, the NAPL concentration of substrate *ls* is decreased due to NAPL dissolution as the aqueous phase concentration increases.

3.2.3 Biodegradation

With multiple biodegradable hydrocarbon substrates and electron acceptors considered in this study, biodegradation of PHCs can be mathematically described through utilization of substrate linked to EA availability and bacterial growth. In general, a modified Monod equation is used in SEAM3D to calculate substrate uptake rate and microbial growth. A utilization equation of each substrate within microcolony *x* is written as

$$r_{x,ls} = \sum_{le} V_{x,ls,le} \tag{3.8}$$

where $V_{x,ls,le}$ [M_{ls} M_b^{-1} T^{-1}] is the specific rate of substrate utilization for microcolony *x* using substrate *ls* and EA *le* for growth, and the summation over *le* contains only the valid EAs for microcolony *x*. Similarly, a utilization equation of each electron acceptor could be written as

$$r_{x,le} = \sum_{ls} \gamma_{x,ls,le} V_{x,ls,le} \tag{3.9}$$

where $\gamma_{x,ls,le}$ is the EA use coefficient [M_{le} M_{ls}^{-1}], which is the mass of EA *le* used per unit mass of substrate *ls*.

The specific uptake rate of substrate $V_{x,ls,le}$ is described using Monod kinetics modified for EA availability as

$$V_{x,ls,le} = V_{x,ls,le}^{max}\left[\frac{\overline{S_{ls}}}{\overline{K}_{x,ls,le}^{s}+\overline{S_{ls}}}\right]\left[\frac{\bar{E}_{le}}{\overline{K}_{x,le}^{e}+\bar{E}_{le}}\right] I_{le,li} \tag{3.10}$$

where $V_{x,ls,le}^{max}$ is the maximum specific uptake rate of the substrate, $\overline{K}_{x,ls,le}^{s}$ is the effective half saturation constant for substrate *ls* utilizing EA le [M_{ls} L^{-3}]; $\overline{K}_{x,le}^{e}$ is the effective half saturation constant for EA le [M_{le} L^{-3}]; $\overline{S_{ls}}$ is the effective concentration of substrate ls [M_{ls} L^{-3}]; $\overline{E_{le}}$ is the effective concentration of EA le [M_{le} L^{-3}]; and $I_{le,li}$ is an inhibition function. The inhibition function (Widdowson et al., 1988) follows

$$I_{le,li} = 1 \tag{3.11a}$$

and

$$I_{le,li} = \prod_{li=1}^{le-1}\left[\frac{K_{le,li}}{K_{le,li}+\bar{E}_{li}}\right] \tag{3.11b}$$

where $K_{le,li}$ is the EA inhibition coefficient [M_{le} L^{-3}] describing inhibition of the use of EA *le* by EA *li*. However, a specific EA is included in this equation only when it is specified in a particular simulation. The inhibition function above shows that utilization of any EA may inhibit other EAs that provide less Gibbs free energy to the microbes. Equation (3.11a) is valid when electron acceptor is oxygen (O_2), while equation (3.11b) is valid when other electron acceptors present (NO_3, Mn (IV), Fe (III), SO_4, and CO_2).

In order to represent threshold concentrations below which microbes cannot grow, effective concentrations used in equation (3.10) and (3.11) follow

$$\bar{S}_{ls} = \max(S_{ls} - S_{ls}^{t}, 0) \tag{3.12}$$

$$\overline{K}_{x,ls,le}^{s} = \max(K_{x,ls,le}^{s} - S_{ls}^{t}, 0) \tag{3.13}$$

where S_{ls}^{t} is the threshold concentration of substrate ls; and $K_{x,ls,le}^{s}$ is the half saturation constant for substrate *ls* utilizing EA *le* [M_{ls} L^{-3}]. Likewise, $\overline{E_{le}}$, $\overline{K}_{x,le}^{e}$, $\overline{K}_{x,ln}^{n}$ are defined applying E_{le}^{t} as the threshold concentration.

The Monod equation is often used in terms of the maximum specific growth rate μ_{max} [$M_b M_b^{-1} T^{-1}$], however, SEAM3D uses the maximum specific rate of substrate utilization V_{max} [$M_s M_b^{-1} T^{-1}$] to estimate values of the use coefficients for electron acceptors and nutrients.

The metabolism of substrate will result in biomass growth if sufficient cellular nutrients are available. To derive the microbial growth equations, the SEAM3D Biodegradation Package calculates growth rates depending on background concentrations of EAs and hydrocarbon substrates. Background substrates are the carbon sources utilized by microbes prior to aquifer contamination by hydrocarbon substrates. Steady state concentrations are assumed for the background substrate, electron acceptor, nutrient, and biomass before the aquifer is contaminated. According to mass conservation, when it comes to steady state, the death rate ($K_{d_x}^{bk}$) of a specific microbe equals its growth rate, the background death equation follows

$$G_x^{bk,0} = Y_x^{bk} V_x^{max,bk} \left[\frac{\bar{E}_{le}}{\overline{K}_{x,le}^{e} + \bar{E}_{le}} \right] \qquad (3.14)$$

where $Y_x^{bk} = \frac{1}{NS} \sum_{ls} Y_{x,ls,le}$ is sum of the yield coefficients for different electron acceptors utilized by the microbial population *x* [M_b, M_{ls}^{-1}]. Because a steady state condition was assumed as the starting point of each simulation, the initial value for $\overline{E_{le}}$ was specified to represent pristine conditions. It should be noted that the inhibition term does not appear in equation (3.14) because of the steady state population assumption for the microbial population *x*.

When petroleum hydrocarbon oil is spilled into the aquifer, the steady state assumption is no longer valid. Petroleum hydrocarbon as a substrate, electron acceptor, and cellular nutrient concentrations

are used by microbes for biomass growth. The biomass growth rate equation for each population *x* could be written as

$$\frac{1}{M_x}\frac{dM_x}{dt} = -K_{d_x} + G_{x,ls,le} \tag{3.15}$$

where K_d represents the effective death rate [T^{-1}], and $G_{x,ls,le}$ is the growth rate due to metabolism of substrate. The equation for $G_{x,ls,le}$ is given by

$$G_{x,ls,le} = \sum_{le}\sum_{ls} Y_{x,ls,le} V_{x,ls,le} \tag{3.16}$$

where $Y_{x,ls,le}$ is the biomass yield coefficient [$M_b\ M_{ls}^{-1}$], which is the mass of bacteria produced per unit mass of substrate ls utilizing electron acceptor *le*.

The equation for effective death rate (3.17) is defined by the difference between $K_{d_x}^{bk}$ and the current growth rate

$$K_{d_x} = \max\left[0, K_{d_x}^{bk} - (G_x^{bk} + G_{x,ls,le})\right] \tag{3.17}$$

where G_x^{bk} is computed by equation (3.16) above with $\overline{E_{le}}$ calculated from current concentrations at each block in the model domain. From equation (3.17), for each of the model blocks the effective death rate K_{d_x} equals zero where no hydrocarbon substrate presents (no contamination), and biomass concentrations remain at background levels. However, when hydrocarbon substrate contaminate the region, utilization of electron acceptor and nutrients will decrease G_x^{bk} and $G_{x,ls,le}$, and thus, K_{d_x}>0.

3.3 Grid Design

The numerical modeling software GMS (Groundwater Modeling System, version 9.1) was used to set up model domains, specify input parameters, and simulate depletion and biodegradation of residual petroleum deposits in the saturated porous medium. Groundwater flow is simulated using the code MODFLOW. Both a two-dimensional model domain and a three-dimensional model domain were

constructed for this study. Two-dimensional models have their advantage in accurately simulating the tidal recharge boundary condition, while three-dimensional models have the advantage of portraying complicated geometry.

3.3.1 Two-Dimensional Model Grid

The two-dimensional model domain for flow and transport (Figure 3.1) depicts a flow field from top to bottom measuring 0.5 m by 0.5 m at the largest extent. The computational grid consists of 100 columns and 100 rows with a cell size of 0.005 m in all three dimensions. Therefore, each model block in the two-dimensional model has a volume of 1.25×10^{-7} m^3. The bulk density of soil is assumed to be 1.8 $\times 10^6$ g/m^3, which is typical of beach sand. Vertical flow is typically depicted in MODFLOW using model layers; however, the vertical dimension was simulated using model rows and the horizontal dimension was simulated using model columns (Anderson and Woessner, 1992). This allows the use of a single model layer, which was specified as a confined aquifer.

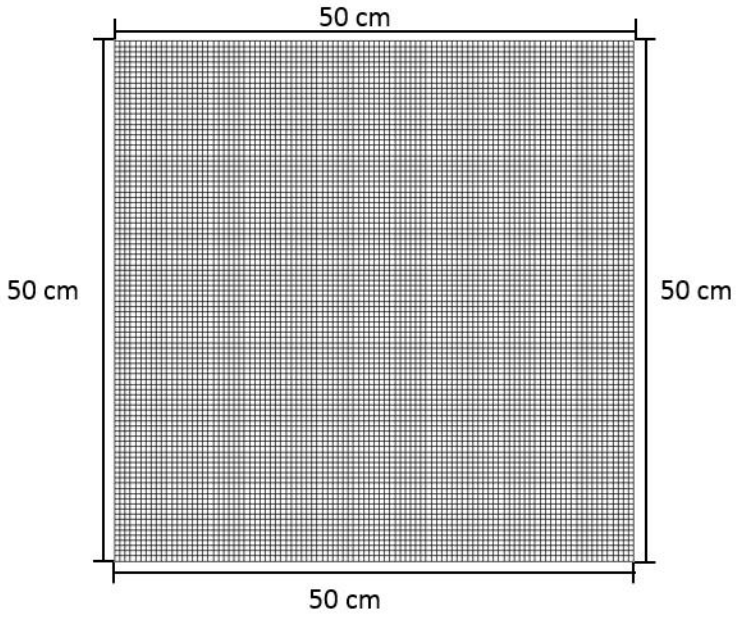

Figure 3.1. Schematic diagram of two dimensional model grid

3.3.2 Three-Dimensional Model Grid

The three-dimensional model domain for flow and transport (Figure 3.2), was 0.5 m in the longitudinal x-direction, 0.18 m in the transverse y-direction, and 0.5 m in the vertical z-direction. The computational grid composed of 100 columns, 36 rows and 100 layers using 0.005 by 0.005 by 0.005 m blocks. Each model block in the three-dimensional domain has a volume and bulk density identical to model cells in the two-dimensional problem. All the model layers were specified as confined.

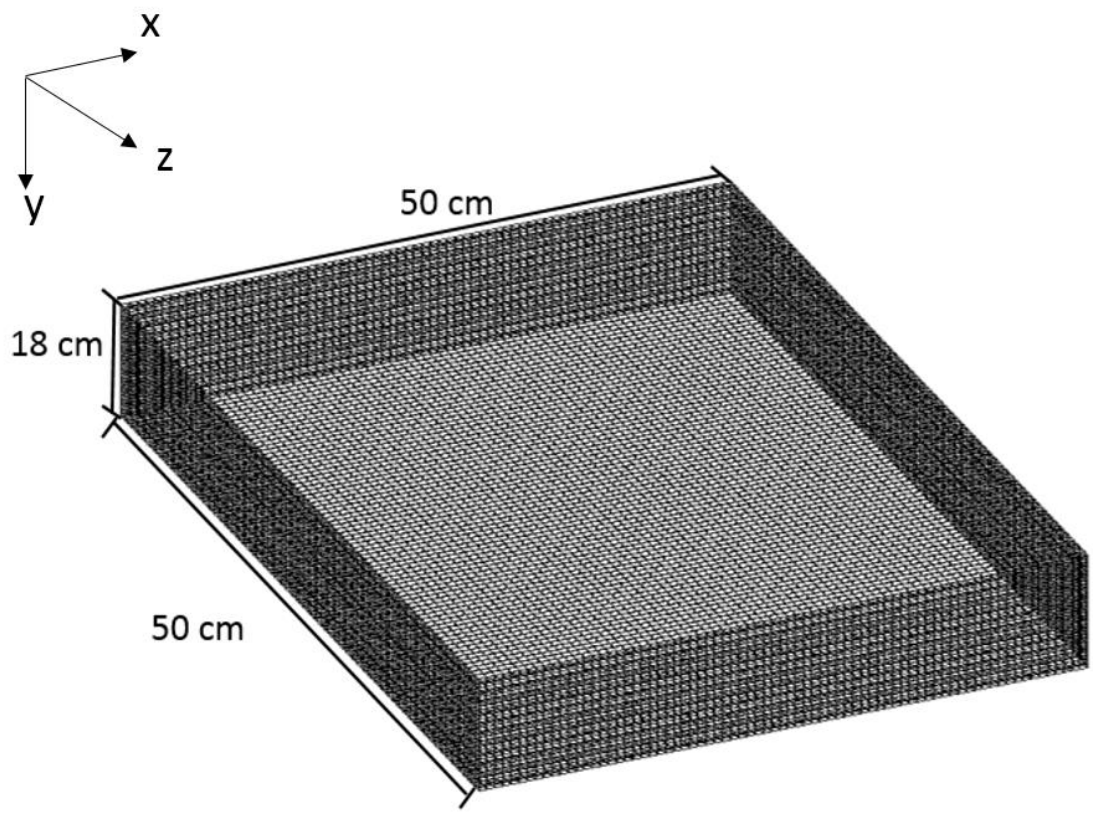

Figure 3.2. Schematic diagram of three-dimensional model grid

3.4 Boundary Conditions

Groundwater flows from the top boundary to the bottom boundary. The top boundary condition was specified as a time variant hydraulic head to simulate tidal wave recharge across the top of the aquifer. The bottom boundary condition was constant head. Therefore, the flow solution and transport solution were transient for the two-dimensional model. Both the transport time step and the biodegradation time step were set up 6 hours, which is in consistent with the time variant hydraulic head boundary condition.

Constant heads of 2.01 m and 2.00 m were specified at the top boundary and bottom boundary respectively, and thus, groundwater flows from top to bottom. The flow solution was steady state, while the transport simulations were transient. In order to be consistent with the two-dimensional grid design, both the transport time step and the biodegradation time step were also set up 6 hours.

Groundwater flows from the upper boundary to the lower boundary for both two-dimensional model and three-dimensional model. Assuming recharge to the system significantly reflects the seawater composition, it was anticipated that the input of electron acceptors (i.e., oxygen and sulfate) along the upper boundary facilitates biodegradation of PHCs dissolving out of the residual NAPL. Table 3.1 lists the initial and recharge concentrations used. The model was initialed as a clean aquifer with oxygenated water. The background dissolved oxygen concentration was 3.0 mg/L, while the sulfate concentration was 200 mg/L. Nitrate and iron concentration were zero for seawater (Gros et al., 2008).

Table 3.1. Initial and Recharge Water Concentrations

Solute	Initial Concentration (mg/L)	Recharge Concentration (mg/L)
DO	3	3
SO_4^{2-}	200	200
Methane	0	0

Chapter 4 Model Parameters

4.1 Oil Characterization

Previous field surveys on the beaches of West Point and Dauphin Islands, Alabama found a variety of petroleum deposits with distinct geometries, ranging from small tar balls to horizontal oil deposit sheets (Singh et al., 2012). In order to measure the amount of petroleum hydrocarbon that cannot be mobilized and recovered from the model block, residual saturation of NAPL was considered through the study. There are many different definitions in different organizations and many different methods of determining residual NAPL saturation (Adamski et al., 2004). To account for NAPL mobility, Morrow (1987) defines residual oil saturation as the "oil that remains in the swept zone of a waterflood when the produced ratio of water to oil has reached its economic limit." The residual saturation in this study is treated as the saturation at which the NAPL becomes discontinuous and is immobilized by capillary forces under ambient groundwater flow conditions (Mercer and Cohen, 1990). The equation of residual saturation (S_R) is given by

$$S_R = \frac{V^{NAPL}}{V^{voids}} \tag{4.1}$$

where V^{NAPL} is the volume of NAPL remains in the pore space, and V^{voids} is the total volume of the void space in a porous media. Oil saturations remaining in the swept zone of a waterflood typically can occupy 15 to 35% of the pore space (Chatzis et al., 1983). In this study, a residual saturation of 0.25 was assumed across all geometries, which indicated that 25% of the pore space is filled with NAPL. The mass loading rate for a specific block was then calculated through equation (4.1) to equation (4.3).

$$V^{NAPL} = \frac{V_t^c * \rho_b * C^{NAPL}}{\rho_{NAPL}} \tag{4.2}$$

$$V^{voids} = V_t^c * n \tag{4.3}$$

where V_t^c is the volume of a single block in the model domain [L^3], ρ_b is the bulk density of the soil [$M_{solid}\ L^{-3}$], C^{NAPL} is the NAPL concentration [$M_{NAPL}\ M_{solid}^{-1}$], ρ_{NAPL} is the density of the NAPL [$M_{NAPL}\ L^{-3}$], and n is the porosity of the porous media. Using a bulk density of 1.8 x 10^6 g/m^3, a NAPL density of

0.8×10^6 g/m^3, and a porosity of 0.3, a saturation of 0.25 corresponds to a soil concentration of 0.0333 g_{NAPL}/S_{olids}.

The mass fractions of the model constituents (Table 4.1) in the NAPL were based in part on the mass fraction of crude oil that leaked from the Deepwater Horizon blowout. However, GC-MS analyses of the field samples demonstrated that oil composition of the petroleum deposit was consistent across geometries and that the predominant hydrocarbon of the oil deposits were alkanes (Singh et al., 2012). Chemical composition study of the oil from the sea surface, salt marshes and sediments after the DWH oil spill revealed that the oil deposit was subjected to a light to moderate degree of weathering (Liu et al., 2012). Oil weathering is a relatively slow environmental process and creates uncertainty in terms of oil composition (Payne et al., 1983). Instead, this study focuses on an idealized unweathered crude oil (Ryerson et al., 2011; Zhou et al., 2013) Table 4.1 shows the eight PHC constituents that comprise the NAPL source: (1) Light alkanes (C9-C17); (2) Heavy alkanes (C21-C24); (3) Benzene; (4) Aromatics (toluene, ethylbenzene, xylenes); (5) Naphthalenes; (6) Light PAHs (phenanthrene and fluorene); (7) Heavy PAHs (chrysene, pyrene); and (8) one class of refractory compounds.

Table 4.1. NAPL composition for idealized model crude oil

Subscript	Description
1	Light alkanes (C9-C17)
2	Heavy alkanes (C21-C24)
3	Benzene
4	Aromatics (toluene, ethylbenzene, xylenes)
5	Naphthalenes
6	Phenanthrene & Fluorene
7	Heavy PAH (chrysene, pyrene)
8	Refractory compounds

Solubility and molecular weights of the model constituents were based on *CRC Handbook of Chemistry and Physics* (Haynes, 2013). Average values were assigned for Aromatics, Light PAHs and Heavy PAHs. Table 4.2 shows the detailed information of NAPL composition in this study.

Table 4.2. Properties and composition of NAPL constituents

	Initial Mass Fraction	Solubility(mg/L)	Molecular Weight
Light Alkanes	0.6757	0.135	128.3
Heavy Alkanes	0.1527	5.80E-10	338.6
Benzene	0.006	1780	78.1
Aromatics (TEX)	0.02	500	92.1
Naphthalenes	0.0546	34.8	128.2
Light PAHs	0.0294	2.23	166.2
Heavy PAHs	0.0077	0.0015	228.3

4.2 Model Parameter Estimates

The majority of the transport and biodegradation parameters needed to simulate the oil spill at the Gulf of Mexico were based on literature values, theoretical estimates, and field measurements. A description of the parameters, sources and estimation techniques are provided below.

4.2.1 Flow and Transport Parameters

Estimates of hydraulic conductivity (Li et al., 2007) and measurements of velocity have been made at oil polluted beaches (Garven, 1989). However, the values estimated from these studies range over several orders of magnitude. Beach sand located at the GOM was picked as a representative beach, and its physical properties were used in this study (Grubb, 1984). Uniform values of porosity (n = 0.3) and hydraulic conductivity ($K_{Aquifer}$ = 0.5 m/d) were assigned to the domain. However, within the NAPL source, the oil body reduces the flow of water through this zone. Assuming 25% of the pore space is filled with NAPL, the hydraulic conductivity for model block filled with oil is assumed to be K_{NAPL} = 0.011 m/d (Suthaker and Scott, 1996). The longitudinal dispersivity (α_L) was assumed to be α_L = 0.001 m, and a transverse dispersivity of 0.0001 m was also assumed (Grubb, 1984).

4.2.2 Biodegradation Parameters

Microbial parameters for biodegradation of petroleum hydrocarbons have been studied by researchers for different biodegradation pathways. Different measurements of the Monod kinetic

parameters were quantified in previous studies (Alvarez et al., 1991; Chen et al., 1992; Edwards and Grbić-Galić, 1994). Available parameters in the literature are taken to estimate Monod kinetic parameters. For simplicity, parameter values were assumed to be consistent among the aquifer layers for the three-dimensional model. This assumption is valid as the entire three-dimensional aquifer was considered relatively near the surface. For aerobic biodegradation of petroleum hydrocarbons, reported maximum specific uptake rate (V^{max}) values range from 0.01 to 9.9 d-1, half saturation factors (Ks) values range from 0.03 to 15.9 g/m3, and yield coefficient (Y) range from 0.01 to 1.56 g cells/g substrate. However, estimation of biodegradation kinetics for anaerobic biodecay are limited due to the slow reaction kinetics and uncertainty degradation pathways (Jones et al., 2008). Edwards and Grbić-Galić (1994) reported kinetic parameters for methanogenic degradation of toluene. Aharon and Fu (2000) reported kinetic parameters for crude oil under sulfate reduction and anaerobic methane oxidation. When available, literature values were used to help estimate the anaerobic biodegradation kinetics. In general, parameters were identical for each substrate and for each anaerobic process unless information existed to support different values. To account for the high rate and energy yield of aerobic biodegradation pathway, parameters controlling aerobic microbes' growth and death were higher than those of the anaerobic processes. Microbial kinetic parameters are summarized in Tables 4.3 through 4.5.

Table 4.3. Microbial parameters for aerobic biodegradation

Class	Aerobic			
	Biodegradation Rate μ (d^{-1})	Half Saturation Factor Ks (g m^{-3})	Yield Coefficient Y(g g^{-1})	Electron acceptor use coefficient (g g^{-1})
Light Alkanes	0.96	1	0.33	3
Heavy Alkanes	0.1	1	0.33	3
Benzene	0.64	3	0.27	3
Aromatics (TEX)	1.3	2	0.27	3
Naphthalenes	0.6144	1	0.33	3
Phenanthrene & Fluorene	0.3	2.2	0.33	3
Heavy PAH	0.1	0.69	0.33	3

Table 4.4. Microbial parameters for sulfate-reducing biodegradation

Class	Sulfate Reducing			
	Biodegradation Rate μ (d^{-1})	Half Saturation Factors Ks (g m^{-3})	Yield Coefficient Y(g g^{-1})	Electron acceptor use coefficient (g g-1)
Light Alkanes	0.096	2.5	0.06	4
Heavy Alkanes	0.076	2.5	0.06	4
Benzene	0.064	2.5	0.06	4
Aromatics (TEX)	0.26	2.5	0.06	4
Naphthalenes	0.061	2.5	0.06	4
Phenanthrene &Fluorene	0.0576	2.5	0.06	4
Heavy PAH	0.0576	2.5	0.06	4

Table 4.5. Microbial parameters for methanogenic biodegradation

Class	Methanogenesis			
	Biodegradation Rate μ (d^{-1})	Half Saturation Factors Ks (g m^{-3})	Yield Coefficient Y(g g^{-1})	Generation Coefficient (g g-1)
Light Alkanes	0.096	2.5	0.03	0.7
Heavy Alkanes	0.076	2.5	0.03	0.7
Benzene	0.064	2.5	0.03	0.77
Aromatics (TEX)	0.13	2.5	0.03	0.8
Naphthalenes	0.061	2.5	0.03	0.77
Phenanthrene & Fluorene	0.0576	2.5	0.03	0.77
Heavy PAH	0.02	2.5	0.03	0.77

The initial microbial biomass concentrations (Mx) of aerobes, sulfate reducers and methanogens were uniform throughout the domain (Table 4.6). The initial biomass of aerobes was higher that the sulfate reducers or methanogens. This difference was based on the assumption that aerobic biomass would predominate when the aquifer has a significant oxygen level under pristine conditions. The aerobic biomass of 2.5 g/m^3 roughly corresponded to $8x10^6$ cells/cm^3, assuming a cell volume of 1 μm and cell density of 1.0 g/cm^3. Thus, the high value of aerobic maximum specific uptake rate and the number of cells allowed significant aerobic utilization of substrates to occur immediately. However, under high oxygen pristine conditions, anaerobic microbes can only exist in anaerobic microenvironments within soil aggregates (Brock et al., 1994). Therefore, the sulfate reducers and methanogens concentrations were over an order of magnitude lower than the aerobic biomass.

Table 4.6.Initial biomass concentration of aerobes, sulfate reducers and methanogens

Biomass Concentration	Value (mg/L)
Aerobes	2.5
SO4 Reducers	0.05
Methanogens	0.05

4.2.3 Yield Coefficients

The yield coefficients ($Y_{x,ls,le}$) are used in the model to calculate theoretical microbe growth by the degradation of petroleum hydrocarbons (Tables 4.3 through 4.5). Christensen and McCarty (1975) developed the method of utilizing the stoichiometric half reaction to compute the yield coefficients. Walton and Smith (1992) adjust the calculation model to fit in nonstandard conditions. Essaid (1995) did a calculation using the stoichiometric and thermodynamic model to account for yield coefficients of BTEX under both aerobic and anaerobic conditions. According to the calculation, the yield coefficient for BTEX under aerobic conditions was set to 0.27 g/g. This relatively low value of yield coefficient assumes a low efficiency of energy transfer considering the field conditions. For anaerobic biodegradation, yield coefficient was calculated under methanogenic conditions with a value range of 0.008 g/g to 0.05 g/g. In

order to estimate yield coefficients for other model constituents, available literature values were used. Brauner (2002) conducted a laboratory microcosm study to estimate biomass growth for a mixture of five polycyclic aromatic hydrocarbon compounds (PAHs). The yield coefficients of PAH were estimated under both aerobic and sulfate-reducing conditions. The yield coefficients of PAH under aerobic conditions was 0.33 g/g while a value of 0.06 g/g was obtained under sulfate reducing condition. These values are corresponding to the value of theoretical calculation using a simple bioenergetics growth model (McFarland and Sims, 1991). In addition, McFarland and Sims (1991) also estimated the yield coefficient values under methanogenic conditions to be 0.03 g/g. With available information from the literature, summary tables (Table 4.3 to 4.5) show the yield coefficients used in the model.

Inhibition coefficients (Table 4.7) were relatively low to ensure each electron acceptor was essentially depleted before utilization of the next electron acceptor. Electron acceptor use coefficients ($\gamma_{x,ls,le}$) (Table 4.3, 4.4) were estimated based on the stoichiometric relationship between each electron acceptor and toluene (Borden et al., 1995). The generation coefficients ($\zeta_{x,ls}$) for methane (Table 4.5) were also based on the stoichiometric relationship between methane and toluene (Borden et al., 1995).

Table 4.7. Inhibition coefficients between SO_4, O_2, and methane

	inhibition coefficients
SO_4-O_2	0.1
methane-O_2	0.2
methane-SO_4	0.5

4.3 Modeling Approach to Investigate the Impact of Geometry

4.3.1 Two-Dimensional Modeling Approach

Prior to investigating the influence of geometry on long term persistence of residual oil deposits found at the coastal area in a three-dimensional setting, two-dimensional models were constructed as

described in Chapter 3. The upper boundary was specified as a time variant hydraulic head to simulate tidal-induced head changes with time (A detailed set up for the time variant head boundary is found in the Appendix Table A1). Specified hydraulic head of the upper boundary was always greater than the bottom despite its time variant nature. Therefore, groundwater flows vertically downward throughout the simulation.

For either geometry, the NAPL source representing a residual oil deposit extends from the left side of the model domain (Figure 4.1 and 4.2). Two different petroleum geometry patterns were considered in the two-dimensional model. For the first condition, horizontal tar sheet, a rectangular NAPL source extended from row 15 to row 29, column 1 to column 34. The second condition, an isolated tar ball, a semicircular NAPL source was centered at row 34 column 1 with a radius of 18 cells (Figure 4.1 and 4.2). Although MODFLOW and SEAM3D require construction of cell-centered blocks, this resulted in an approximate semicircular shape to the NAPL source because of the fine scale of the model grid. In order to compare NAPL mass depletion efficiency between the two geometry conditions, the total NAPL mass was independent of geometry. For both conditions, the NAPL deposit consisted of 510 cells initially to ensure the same amount of NAPL mass at the beginning.

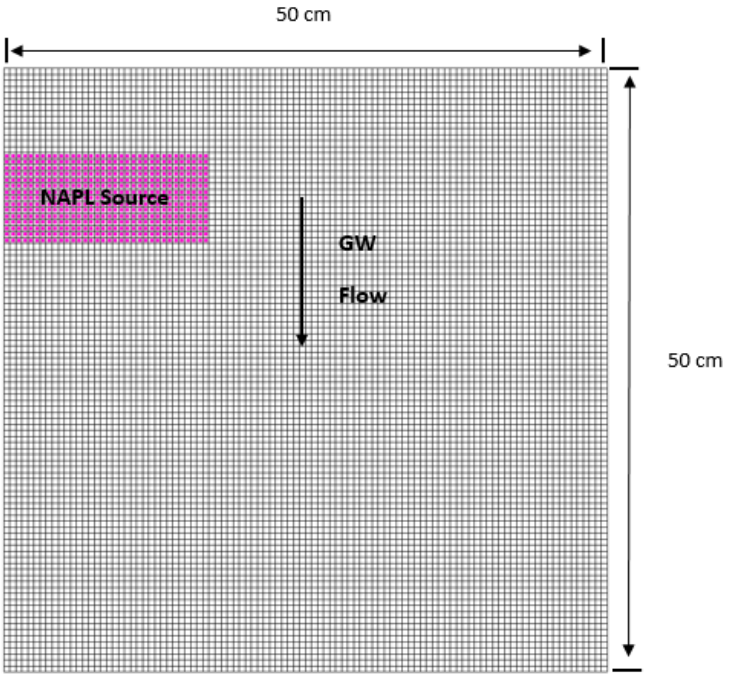

Figure 4.1. Horizontal tar sheet in the two-dimensional model domain

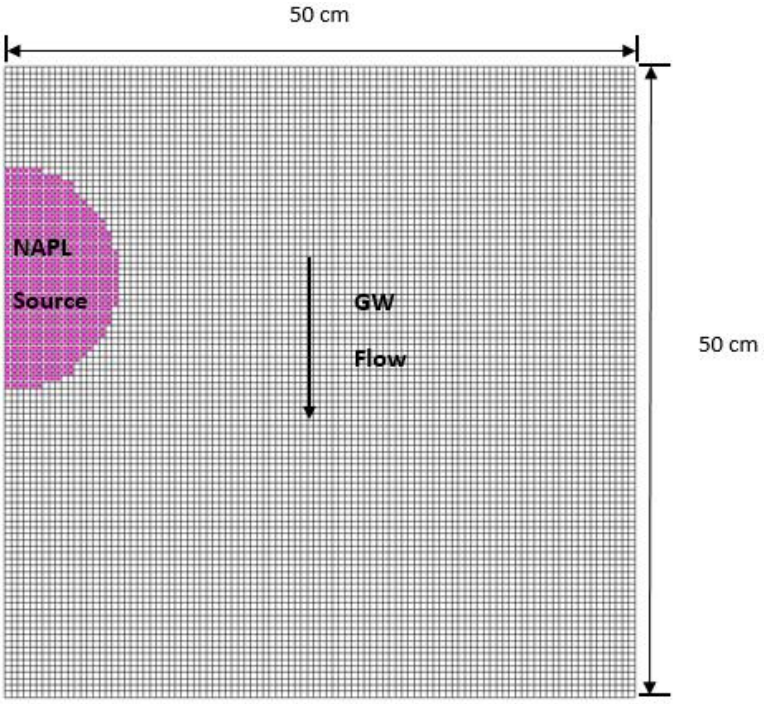

Figure 4.2. Sphere tar ball in the two-dimensional model domain

Three primary biodegradation pathways were considered throughout the study; aerobic respiration, sulfate reduction and methanogenesis. The predominant biodegradation in the shallow subsurface of coastal area has been attributed to aerobic bacterial hydrocarbon degradation (Harayama, 2004). However, more recent findings suggest that anaerobic degradation processes can be significant PHC biodegradation mechanisms in coastal environments (Röding et al., 2004). In order to compare results between the horizontal tar sheet model and the isolated tar ball model and the impact of different biodegradation pathways, four different cases were designed based on different biodegradation conditions. Table 4.8 shows the four cases designed to examine the geometry influence on long term persistence of residual oil deposits. Comparisons were based on the amount of NAPL mass depleted from the source area and the amount of NAPL mass biodegraded by microbes. The NAPL mass change in the source area was calculated from the output file of the SEAM3D package.

The first case considered both aerobic biodegradation and anaerobic biodegradation of petroleum hydrocarbons. Case 1 was set up to compare the horizontal tar sheet with the isolated tar ball model when three major microbes (aerobes, sulfate reducers and methanogens) all exist in the model domain. Case 2 was set up to compare two geometry models under aerobic biodegradation only conditions. The second case assumes biodegradation occurs in the model domain, however, because anaerobic microorganisms were absent from the model domain only aerobic biodegradation was possible. The third case assumes no biodegradation occurs in the model domain, and thus, the NAPL source mass depletion is only due to NAPL dissolved into the aqueous phase and transported out of the domain area. In order to set up the no biodegradation condition, three major microbes' concentrations were set to zero. Case 3 was set up to compare two geometry models in terms of NAPL dissolution and transportation. The fourth case assumes no water recharge from the top boundary. Therefore, methanogenesis becomes the predominant degradation process once oxygen and sulfate were consumed by aerobic microorganisms and sulfate reducers. Case 4 was set up to compare the two geometry models when methanogenesis degradation is the principle biodegradation pathway. A one year simulation time was applied for all the cases.

Table 4.8. Different cases of 2D model simulations

Case	Sheet Model	Sphere Model
1	Biodegradation (Aerobic + Anaerobic)	Biodegradation (Aerobic + Anaerobic)
2	Only Aerobic Biodegradation	Only Aerobic Biodegradation
3	No Biodegradation	No Biodegradation
4	No Recharge (Methanogenesis predominant)	No Recharge (Methanogenesis predominant)

4.3.2 Three-dimensional Modeling Approach

Three-dimensional models were constructed as described in Chapter 3. Similar to the two-dimensional model, the upper boundary of the three-dimensional model domain is specified head but was constant with time resulting in steady state flow. This approach dramatically reduced both the run time of MODFLOW/SEAM3D and the simulation output file size. A NAPL source is placed on the left part of the model domain to represent the residual oil deposit. Both the horizontal tar sheet model and the sphere tar ball model were simulated.

In order to assess influence of geometry on the horizontal tar sheet model and the sphere tar ball model, different key parameters affecting the geometry structure were taken into account. Because groundwater flows vertically from the upper to the lower boundary passing through and around the NAPL source, two key geometry parameters for the sheet model were (1) the upper horizontal area of the sheet deposit (width x length) and (2) the sheet thickness which represents the distance that groundwater travels through the deposit. For the sphere model, the radius was the key parameter affecting geometric structure. This is because both the sphere surface area and the groundwater travel distance are changed by altering sphere radius. Considering the symmetric nature of the sphere, only a quarter of the sphere was built to simplify the model. A detailed design regarding different geometry parameters is provided below.

4.3.2.1 Effect of upper horizontal area (horizontal tar sheet deposit)

A set of three-dimensional sheet models were constructed with different horizontal areas through which groundwater flow passes. Because two parameters may affect the sheet model at the same time,

sheet model thickness is set as a control variable. Table 4.9 shows five scenarios designed to examine how upper horizontal area affects the long term persistence of sheet deposit. Δx [cm] is the side length of a single cell; [cm] is the thickness of the sheet deposit; A [cm^2] is the upper horizontal area; V [cm3] is the volume of the sheet deposit; the last column on the right represents the total number of cells where residual NAPL is present. Figure 4.3 shows the model design of the first scenario (A1) in the three-dimensional grid, and figures of the rest four scenarios can be found in the appendix (Appendix Figure A1). Comparison between different model scenarios was based on percentage of NAPL mass depleted from the source area and percentage of NAPL mass biodegraded by microbes.

Table 4.9. Three-dimensional sheet model designs with different upper horizontal area

	Sheet Dimensions			**Upper Horizontal Area**	**Sheet Volume**	**Total Sheet Cells**
Model ID	Length (cm)	Width (cm)	Thickness (cm)	A (cm^2)	V (cm^3)	Cells
A1	17	6	7.5	102	765	6120
A2	13.5	5	7.5	67.5	506.25	4050
A3	10.5	4	7.5	42	315	2520
A4	8.5	3	7.5	25.5	191.25	1530
A5	4.5	2	7.5	9	67.5	540

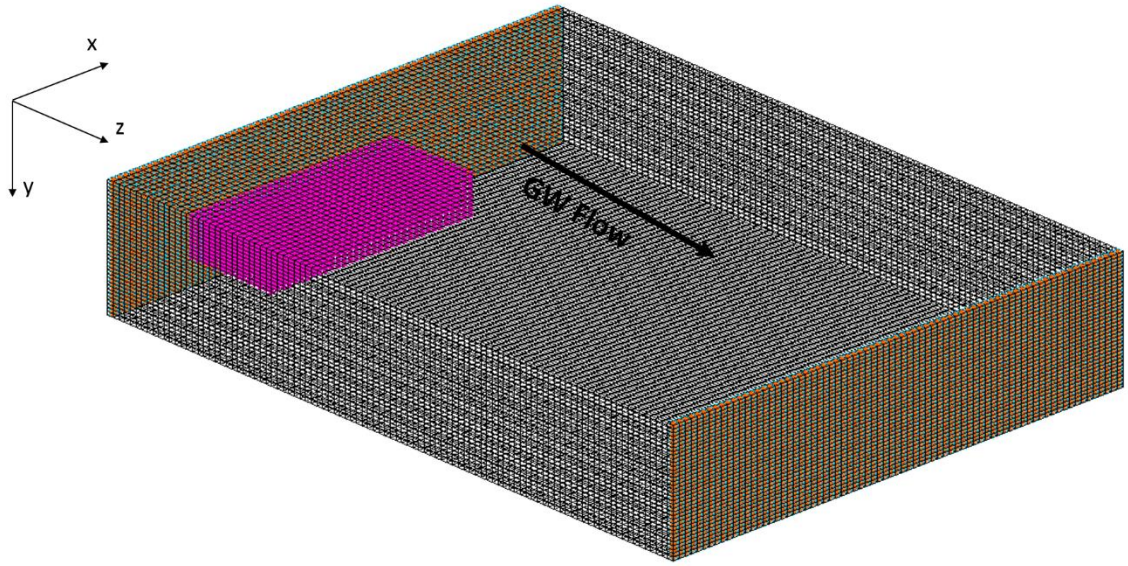

Figure 4.3. Horizontal tar sheet in the three-dimensional model domain (Scenario A1, T1)

4.3.2.2 Effect of thickness (horizontal tar sheet)

A set of three-dimensional sheet models were constructed with different thicknesses. The sheet model upper horizontal area is set as a control variable. Table 4.10 shows six scenarios designed to examine how thickness affects the long term persistence of sheet deposit. Figure 4.3 shows the model design of the first scenario (T1) in the three-dimensional grid, and figures of the other five scenarios can be found in the appendix (Appendix Figure A2). Comparison between different model scenarios was also based on the percentage of NAPL mass depleted from the source area and the percentage of NAPL mass biodegraded by microbes.

Table 4.10. Three-dimensional sheet model designs with different thickness

	Sheet Dimensions			Upper Horizontal Area	Sheet Volume	Total Sheet Cells
Model ID	Length (cm)	Width (cm)	Thickness (cm)	A (cm^2)	V (cm^3)	Cells
T1	17	6	7.5	102	765	6120
T2	17	6	6	102	612	4896
T3	17	6	4.5	102	459	3672
T4	17	6	3	102	306	2448
T5	17	6	2	102	204	1632
T6	17	6	1.5	102	153	1224

4.3.2.3 Effect of radius (sphere tar ball)

A set of three-dimensional sphere models were built with different radii. Table 4.11 shows six scenarios designed to examine how radius affects the long term persistence of the sphere deposit. Δx [cm] is the side length of a single cell; R [cm] is the radius of the sphere deposit; A [cm^2] is the surface area of the quarter sphere; V [cm^3] is the volume of the quarter sphere deposit; the last column on the right represents the total number of cells where residual NAPL is present. Figure 4.4 shows the model design of the first scenario (R1) in the three-dimensional grid, and figures of the other five scenarios can be found in the appendix (Appendix Figure A3). Comparison between different model scenarios was based on the percentage of NAPL mass depleted from the source area and the percentage of NAPL mass biodegraded by microbes.

Table 4.11. Three-dimensional sphere model designs with different radius

	Sphere Dimensions	Surface Area	Sphere Volume	Total Sphere Cells
Model ID	Radius (cm)	A (cm^2)	V (cm^3)	Cells
R1	9	254	763	6107
R2	7	154	359	2874
R3	5.5	95	174	1394
R4	4.5	64	95	763
R5	3	28	28	226
R6	2	13	8	67

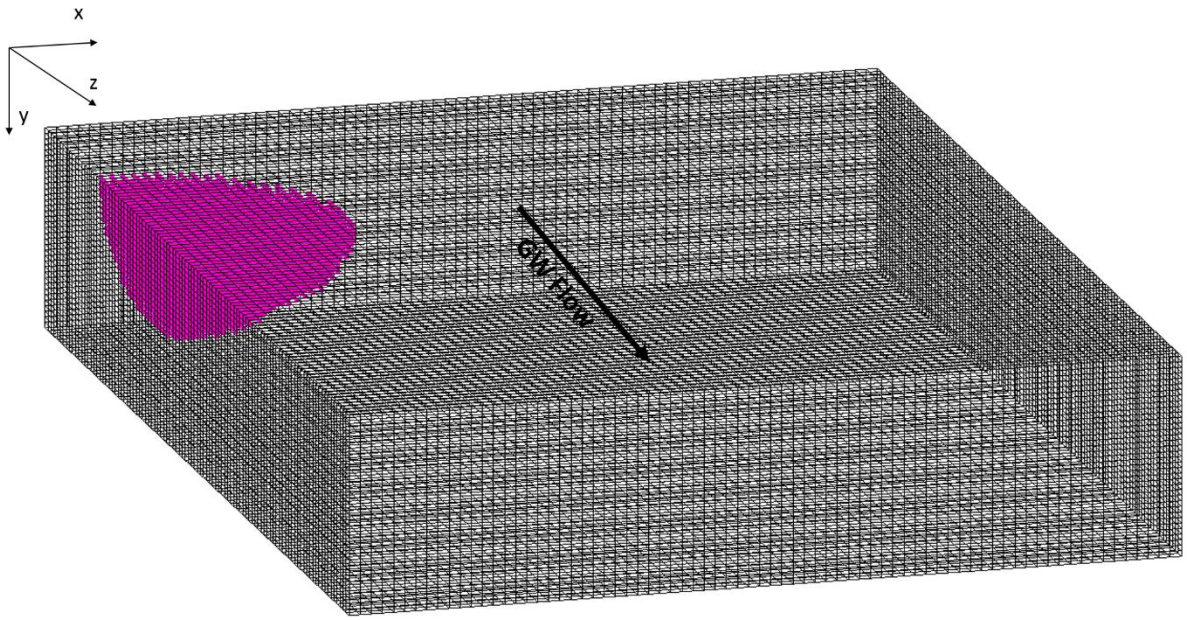

Figure 4.4. Sphere tar ball in the three-dimensional model domain (Scenario R1)

Chapter 5 Results and Discussion

The transport and fate of PHCs derived from a residual crude oil NAPL was analyzed using the MODFLOW/SEAM3D models. Both two-dimensional and three-dimensional modeling of residual oil depletion were computed using SEAM3D coupled with MODFLOW, which simulated flow in saturated porous media. This chapter presents the results and discussion of the data analyses for both two-dimensional and three-dimensional model approaches.

5.1 Two-dimensional Model Results

5.1.1 Effect of Oil Geometry on Groundwater Flow Distribution (Two-Dimensional Model)

In this study, groundwater flows vertically downward through the two-dimensional model grid. A constant head of 2.0 m was specified at the bottom boundary. However, the hydraulic head of the upper boundary changes with time in a range of 2.01 m to 2.05 m, thus, resulting in transient groundwater flow in terms of magnitude and direction of the flow. In order to investigate the influence of geometry on groundwater flow, groundwater hydraulic head contours were plotted in Figure 5.1 and 5.2 for the sheet and sphere models, respectively. In the case of transient flow, hydraulic head contours are shown every hour for a complete 6-hour tidal circulation.

The hydraulic head contour map shows that at the same elevation, the hydraulic head has a sharp decrease around the NAPL source compared with the porous medium. This is mainly because of the low hydraulic conductivity of residual oil. Convergence of hydraulic head equipotential lines around the residual oil indicates that the NAPL serves as an obstruction to groundwater flow. However, the obstructive influence to groundwater flow differs between the two geometries even though the two NAPL deposits both consists of 510 cells. The rectangular-shaped sheet model exhibits greater obstruction to the flow compared with the semicircular sphere model. After the convergence trend in and around the NAPL source, equipotential lines start to diverge downgradient of NAPL source, causing a relatively low flow

velocity zone in the aquifer. Figure 5.1 and 5.2 show that sheet deposit poses a bigger zone of low flow velocity downgradient of the NAPL source, and therefore, has greater obstructive influence to the groundwater flow.

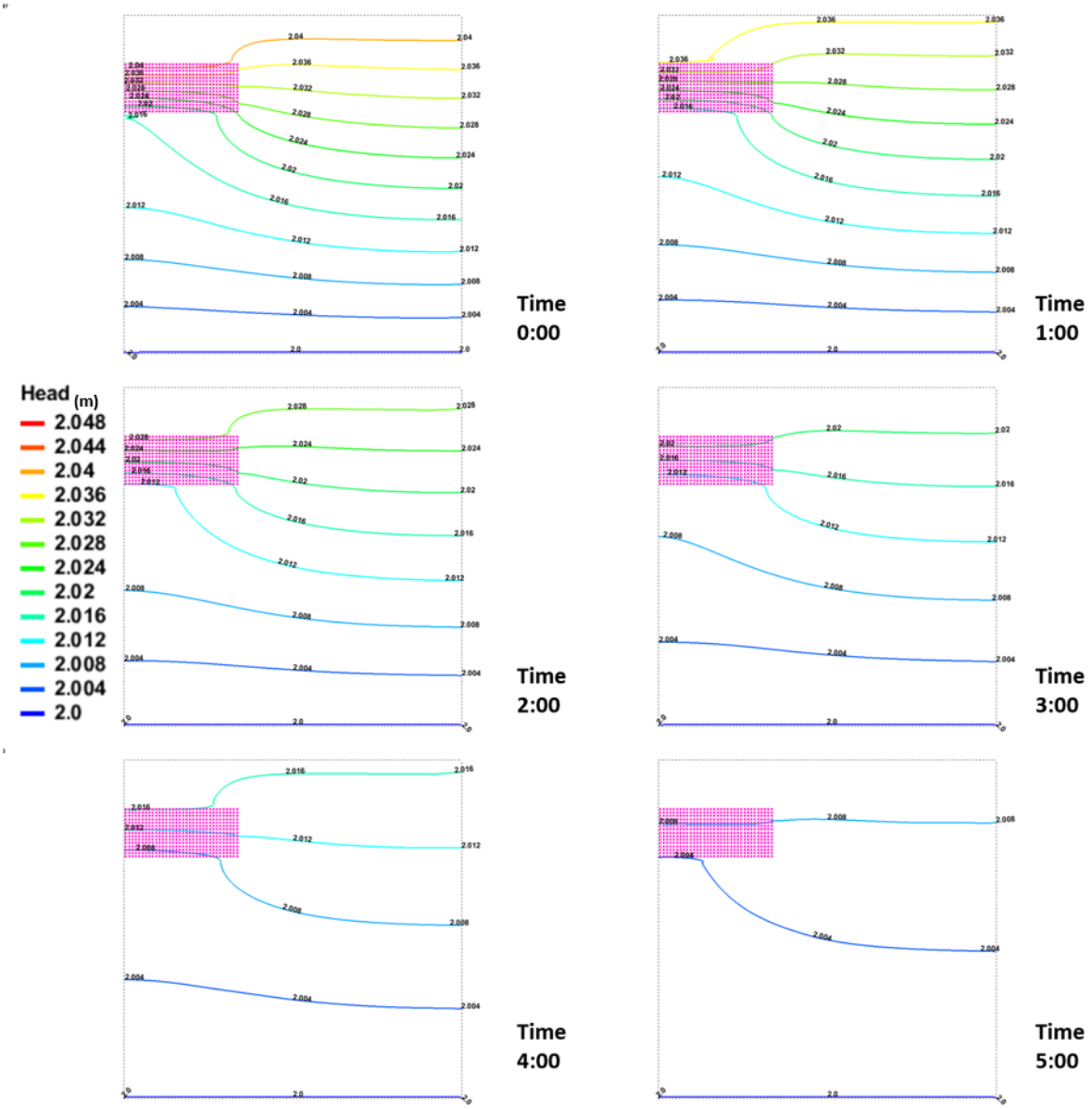

Figure 5.1. Groundwater hydraulic head contours of sheet model

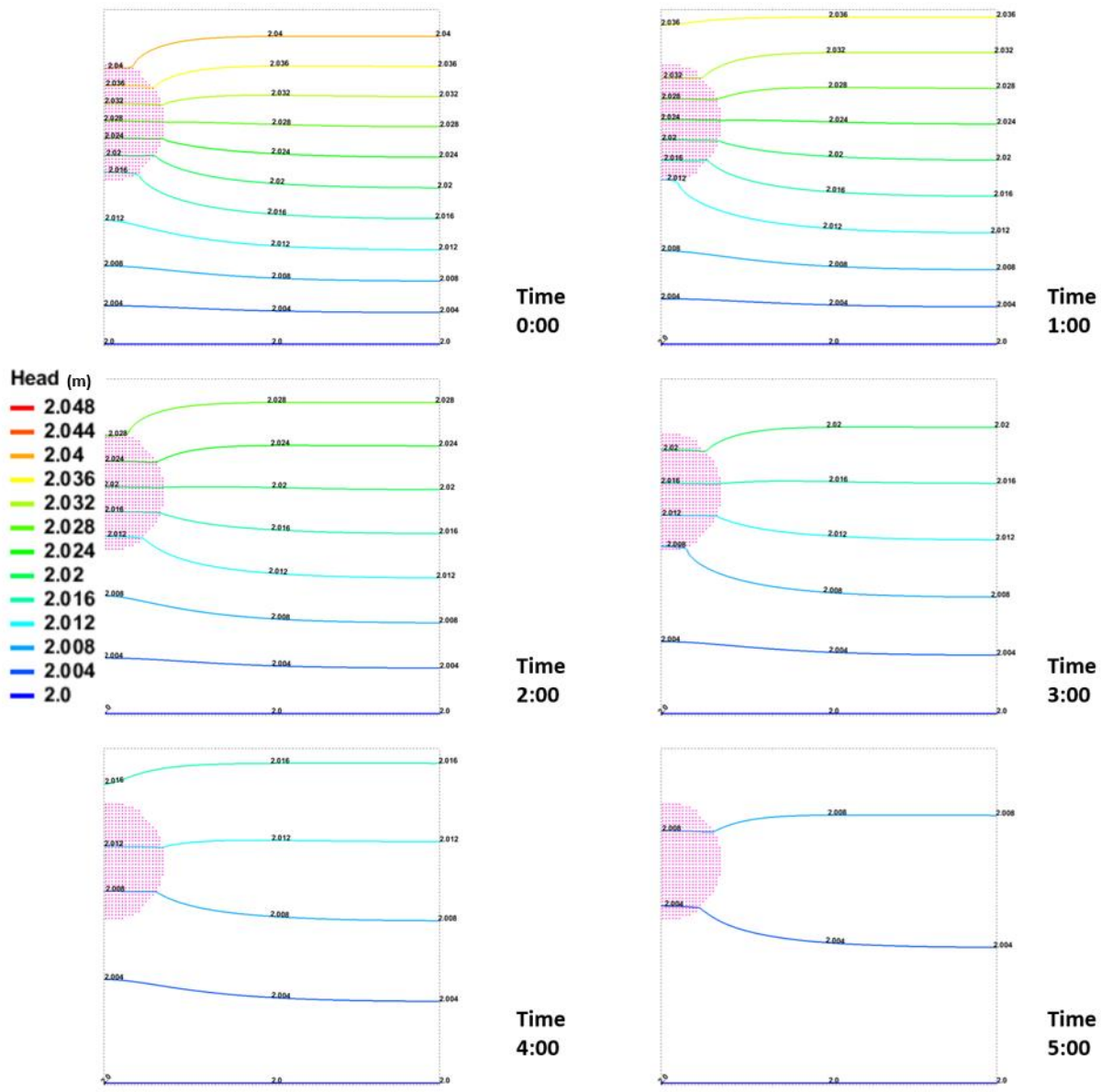

Figure 5.2. Groundwater hydraulic head contours of sphere model

5.1.2 Effect of Oil Geometry on Electron Acceptor Conditions

Figures 5.3 and 5.4 show the concentration distribution of dissolved oxygen (DO) and sulfate, respectively, for the two source geometries. Area distributions of the electron acceptors' concentration are plotted after 0, 5, 15, 30, 60 days for DO, and 0, 90, 120, 150, 180 days for sulfate. Because DO and sulfate are consumed during the biodegradation of PHCs, the concentration of electron acceptors decreases downgradient and within the oil deposit. Thus, an exhausted zone of both DO and sulfate forms

in proximity to the oil deposit, and a low electron acceptor concentration "shadow" is imposed downgradient of the oil deposit. After 60 days, the depleted zone of DO concentration becomes relatively stable, while for the sulfate concentration, a stable zone of depletion occurs after 120 days.

After the electron acceptor concentration shadow reaches stability, DO was completely consumed within and downgradient of the NAPL deposit of both geometries; however, distinct differences were noted between the two cases. Downgradient of the NAPL deposit, the area of DO deficiency associated with the sheet model is larger than that of the sphere model. As DO is consumed for aerobic biodegradation, this larger area of DO depletion may inhibit the aerobic biodegradation process of the sheet deposit model. In the case of anaerobic biodegradation, sulfate is depleted at the lower half of the sphere oil deposit, while for the sheet model, sulfate is still abundant after 180 days. With a higher sulfate concentration available in proximity to the sheet model, this finding suggests that sulfate reduction may have been established and occurred to a greater extent in the sheet oil deposit.

Figure 5.5 shows the concentration profiles of dissolved benzene in the aquifer for the two geometries at day 60 and day 365. The distribution figure reveals that, after 1 year simulation, benzene concentration within the sheet deposit is lower than within the sphere deposit. This finding suggests that the sheet oil deposit could potentially promote the biodegradation of benzene on a larger scale than the sphere deposit.

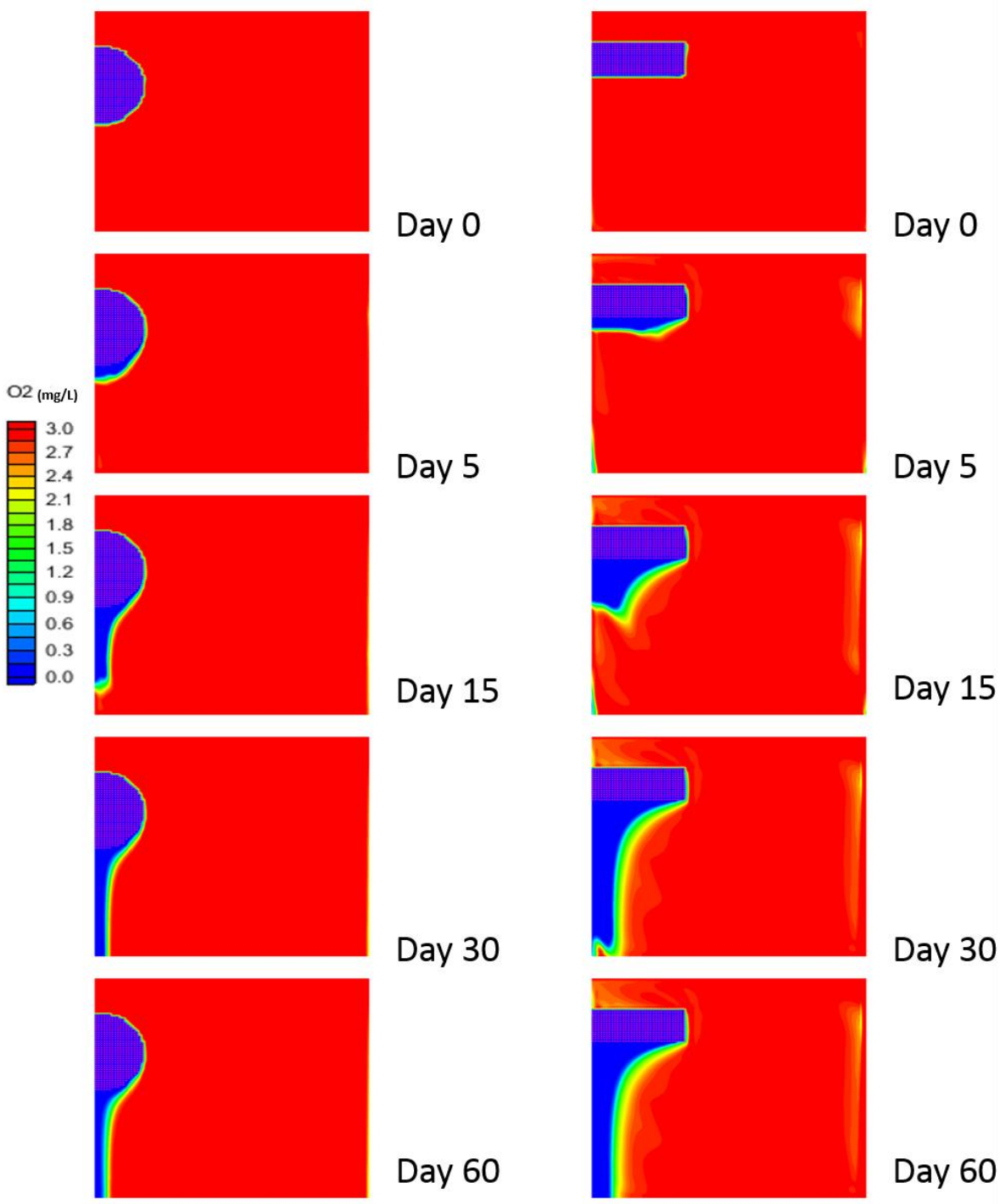

Figure 5.3. Concentration distribution of dissolved oxygen for sphere model (left) and sheet model (right)

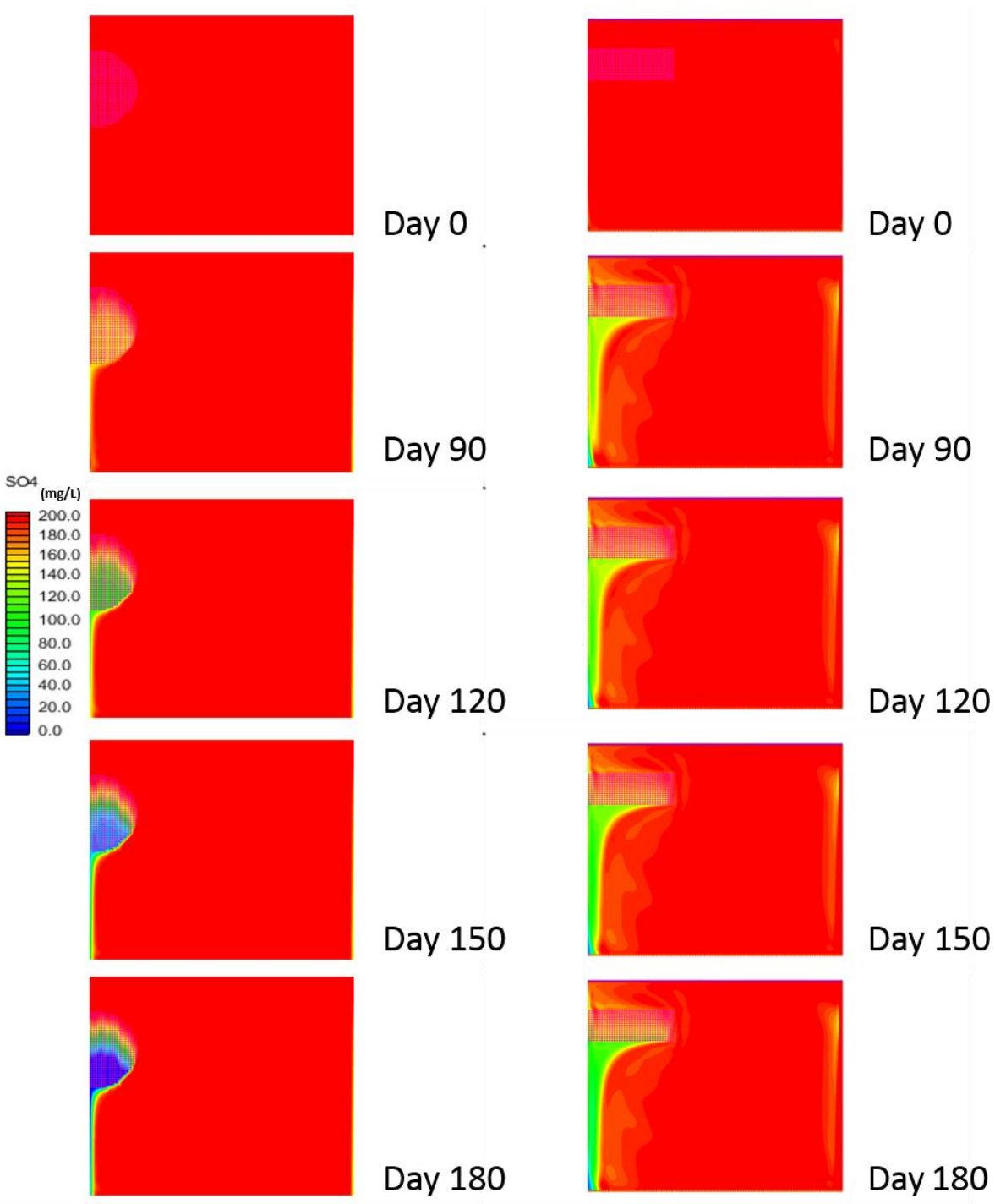

Figure 5.4. Concentration distribution of sulfate for sphere model (left) and sheet model (right)

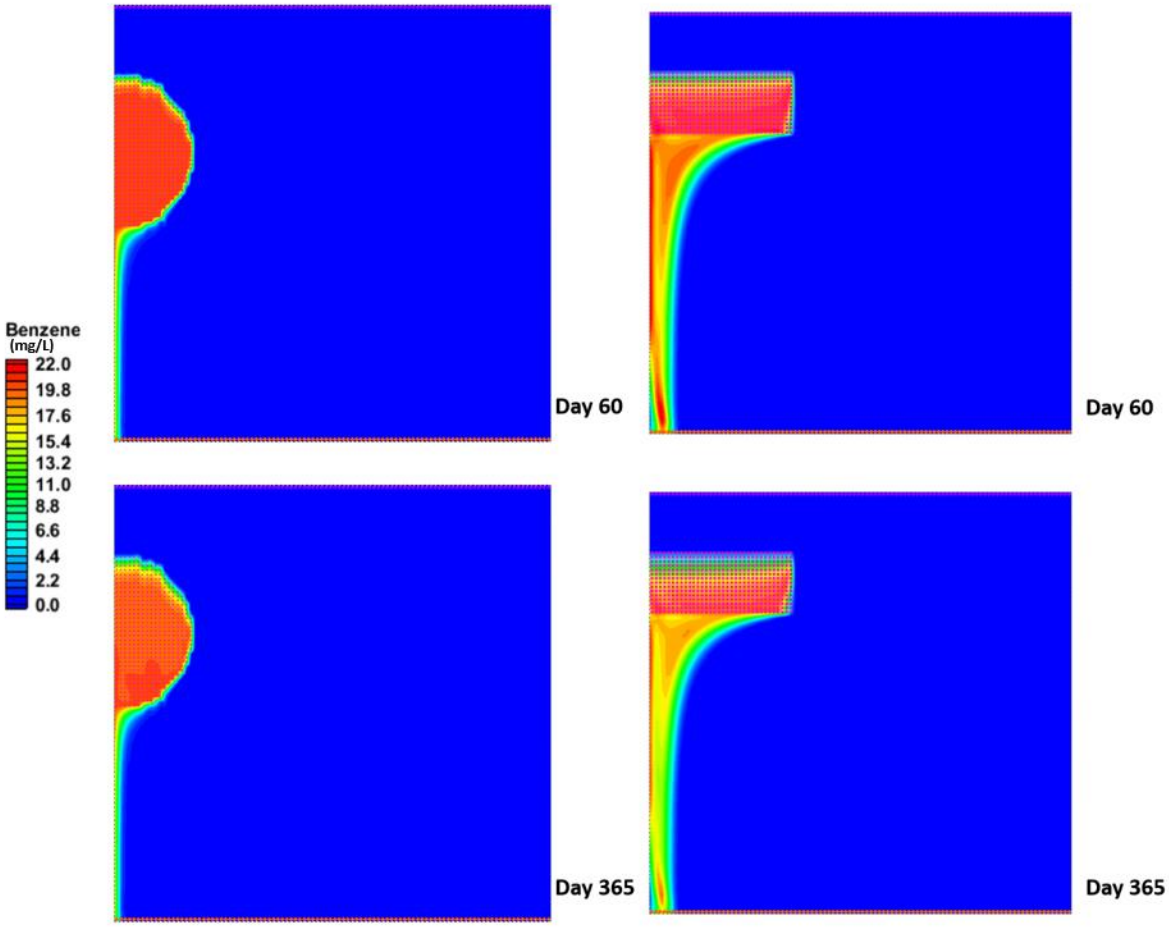

Figure 5.5. Concentration distribution of dissolved benzene for sphere model (left) and sheet model (right)

5.1.3 Effect of Oil Geometry Based on Different Biodegradation Pathway

In order to evaluate the influence of geometry under diverse biodegradation conditions, four cases were designed to compare the two geometry models under different biodegradation pathways (see Chapter 4). The percentage of mass biodegraded relative to the total NAPL mass for both benzene and naphthalene were calculated using the SEAM3D output file. Summary tables of mass change for the NAPL constituent benzene and naphthalene are presented in the appendix (Appendix Table A2 to A5) for both geometries. The results show that in contrast to benzene mass depletion, naphthalene is recalcitrant in the environment with a relatively small reduction in mass over the simulation time. Therefore, the following discussion will focus on benzene as a typical constituent of the NAPL oil deposit.

Figures 5.6 to 5.7 compare the percentage of biodegradation mass to the total NAPL mass between the four cases for the sheet model and sphere model, respectively. In Case 1, where both aerobic and anaerobic biodegradation are considered, sulfate-reducing biodegradation accounts for a much greater percentage of mass than aerobic biodegradation and methanogenesis for both geometries, which indicates that sulfate reduction dominated the biodegradation process at the end of the 1-year simulation . In Case 2, where only aerobic degradation is taken into account, the biodegraded benzene is consistent with the results of Case 1 with roughly 0.27 % of the total benzene degraded through an aerobic pathway for both the sheet model and the sphere model. In Case 4, without seawater recharge, anaerobic degradation dominates the overall biodegradation. The methanogenic pathway contributes relatively more after 1 year, but sulfate reducing still accounts for the greatest part of the biodegraded benzene mass.

Comparing between the sheet and sphere geometries (Figures 5.6 and 5.7, respectively), a significant difference is seen in Case 1 regarding sulfate-reducing biodegradation pathway. The biodegraded mass due to sulfate reduction in the sheet model (2.9%) is much greater than that of the sphere model (1.8%). This finding is consistent with the higher sulfate concentration in proximity to the sheet oil deposit, further supporting the notion that with recharging sea water present, sulfate reducing zones are induced by the sheet geometry to a greater extent than in the sphere geometry. Another interesting fact was noted in Case 4 when recharge seawater is unavailable. In this case, the biodegraded mass between the two geometries is almost the same, which indicates that the influence of geometry is negligible without the participation of groundwater movement.

Figures 5.8 to 5.9 illustrate the percentage of mass depletion from the NAPL source for benzene, naphthalene, and aromatics in the sheet and sphere models, respectively. Comparing the two geometric models in Case 1, total benzene mass depletion shows significant differences; 16.2% for the sheet model compared to only 5.5% of NAPL benzene in the sphere model. Therefore, a conclusion can be made that as recharge sea water flows vertically downward, NAPL benzene mass depletion of the sheet model is dramatically larger than the sphere model. To more clearly examine the NAPL benzene fate in the oil

deposit, biodegradation and mass flux are the two factors considered based on the conceptual model developed in this study. The contribution of the biodegradation and mass flux to the total NAPL benzene mass depletion for Case 1 is shown in Figure 5.10 for the sheet model and Figure 5.11 for the sphere model. The sheet model results show that 79.9% of benzene NAPL mass is depleted due to mass flux and 17.6% of mass is degraded by sulfate-reducing biodegradation (Figure 5.10). For the sphere model NAPL benzene depletion case, 59.5% of benzene NAPL mass is lost to mass flux and 33.5% of mass is lost due to sulfate-reducing biodegradation (Figure 5.11). The pie charts suggest that mass flux plays an important role in the long term persistence of benzene in the NAPL deposit independent of geometry. With regard to biodegradation of benzene, these results suggest that sulfate-reducing biodegradation is a major biodegradation pathway in the coastal area.

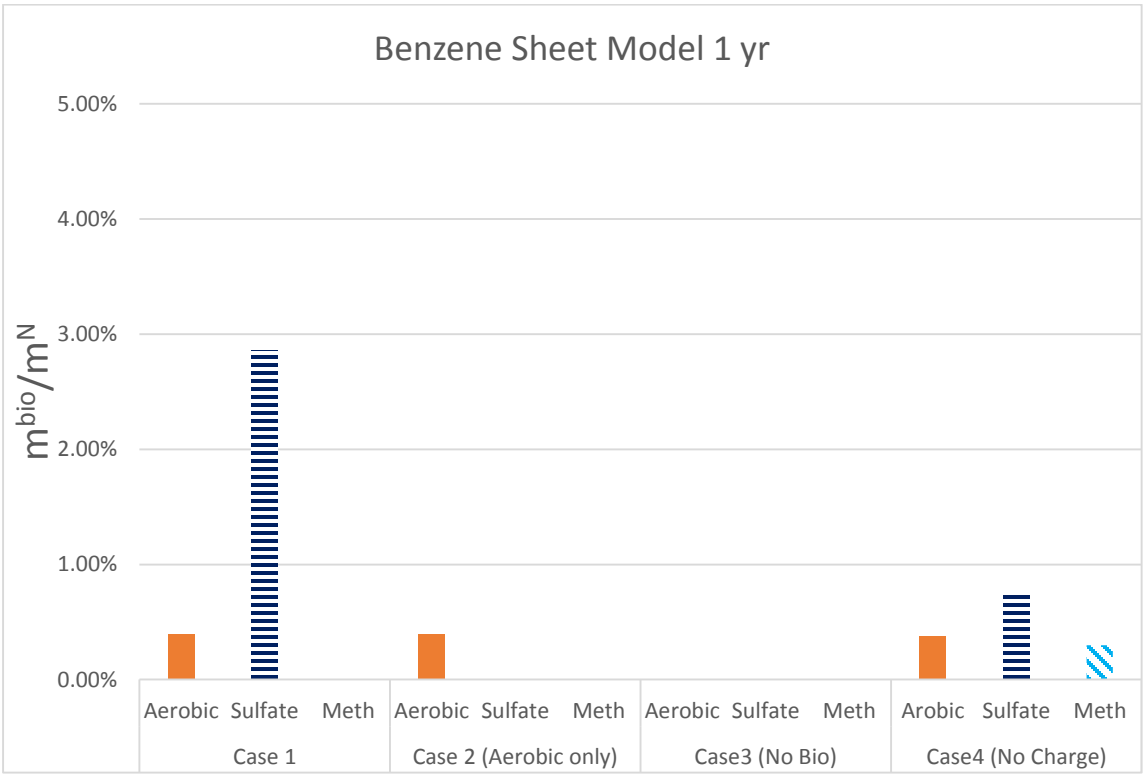

Figure 5.6. Percentage biodegradation mass of 4 cases for sheet model

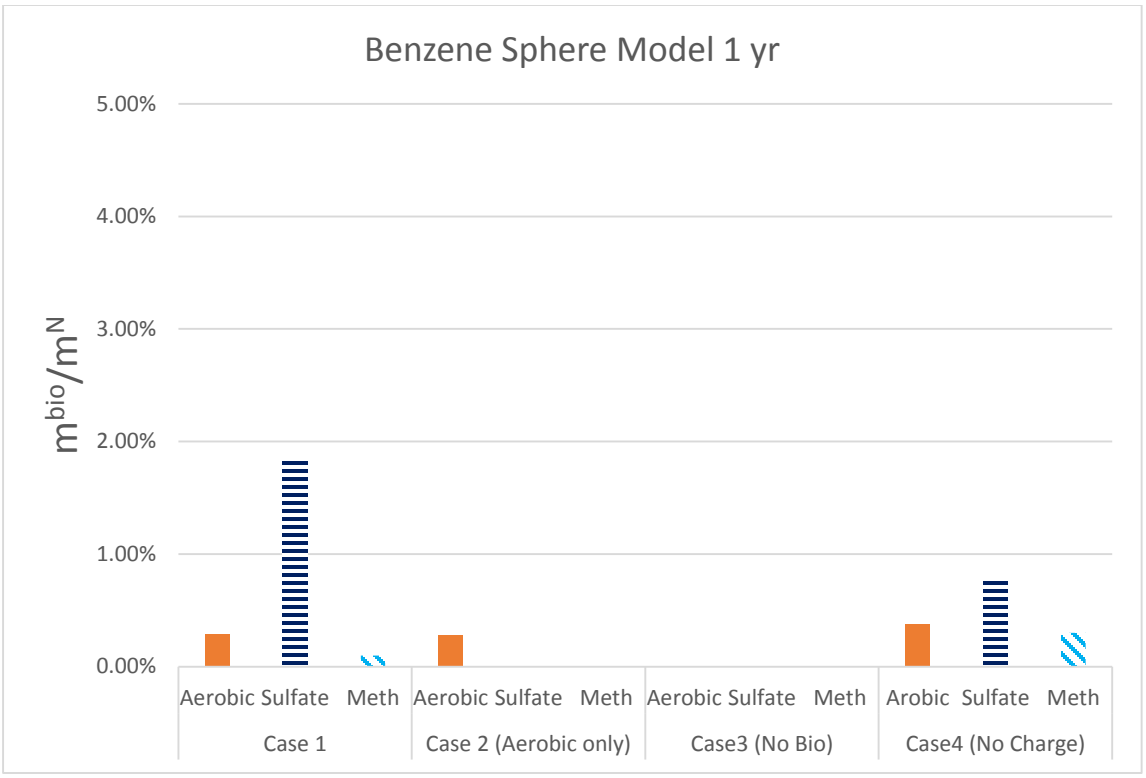

Figure 5.7. Percentage biodegradation mass of 4 cases for sphere model

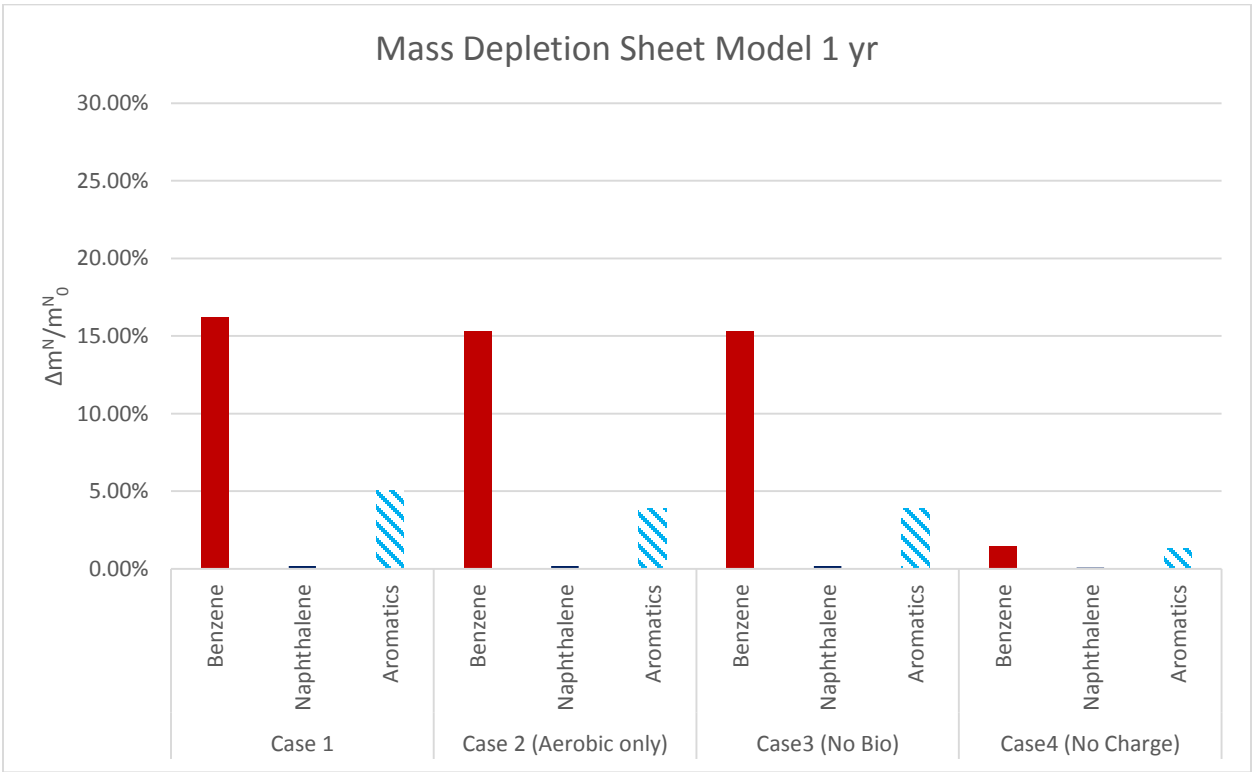

Figure 5.8. Percentage NAPL depletion of 4 cases for sheet model

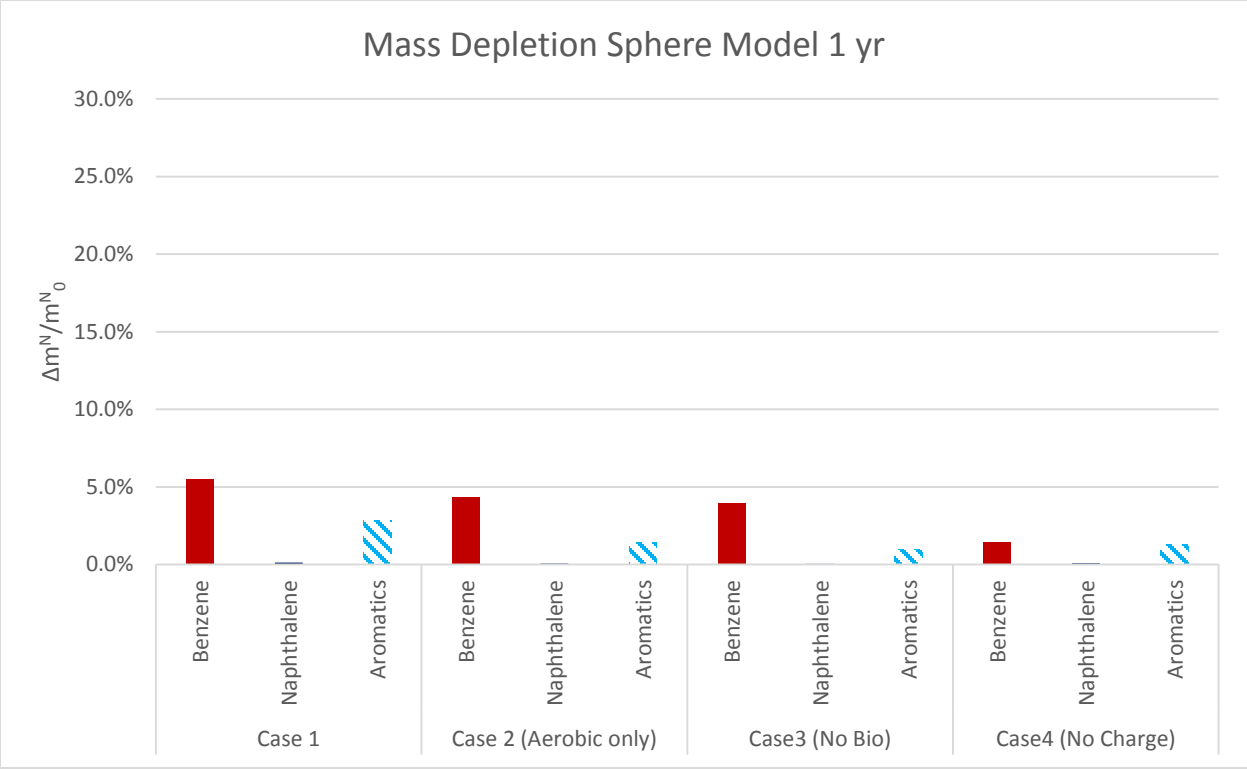

Figure 5.9. Percentage NAPL depletion of 4 cases for sphere model

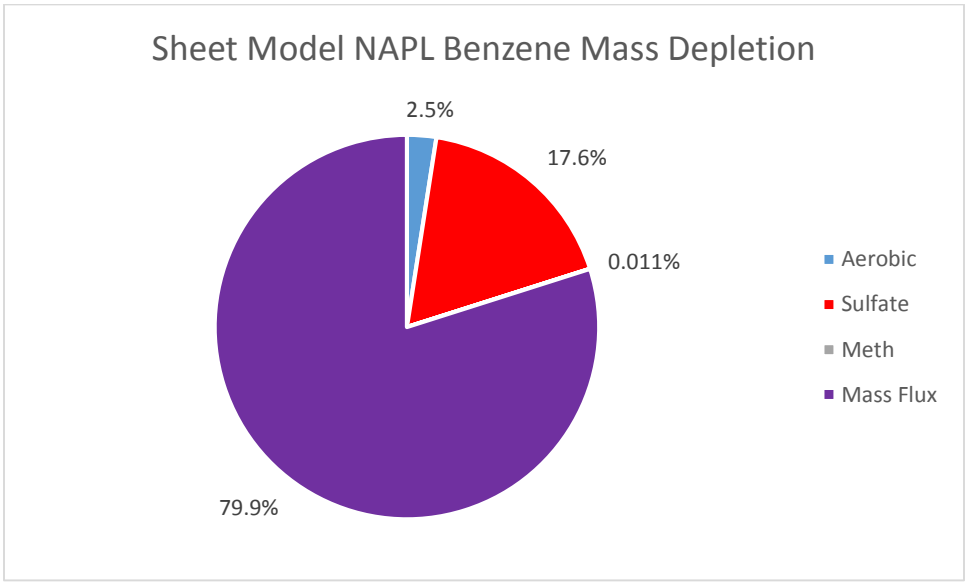

Figure 5.10. NAPL benzene depletion for sheet model in case 1

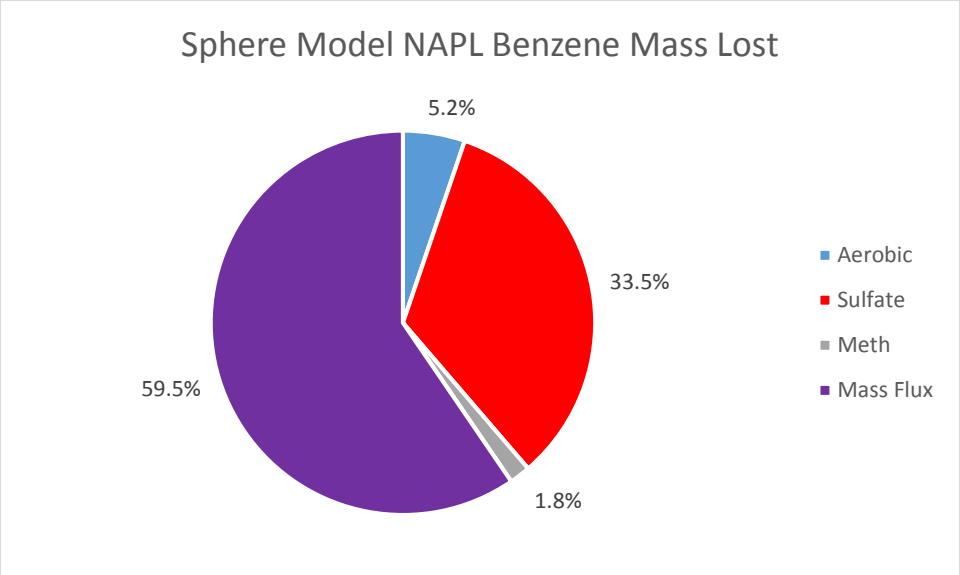

Figure 5.11. NAPL benzene depletion for sphere model in case 1

5.2 Three-dimensional Model Results

5.2.1 Effect of Oil Geometry on Groundwater Flow Distribution

In case of the three-dimensional model, groundwater flows vertically downward through the model domain. Unlike the two-dimensional model, the three-dimensional model flow is steady state as a constant head is specified at both the top and the bottom layer boundary (see Section 3.4). The influence of oil geometry on groundwater flow, groundwater hydraulic head contours is shown in Figures 5.12 and 5.13 for the sheet and sphere models, respectively. Both cross section and vertical section profiles were plotted for each of geometric structure.

According to the hydraulic contour profile, a clear decrease of hydraulic head is observed in the vicinity of the NAPL sources. This is attributed to the low hydraulic conductivity of the residual NAPL. This convergence trend of hydraulic head equipotential lines close to the NAPL source indicates NAPL's obstruction to groundwater flow. The obstructive effect is subject to the NAPL deposit geometry in the three-dimensional model. In case of the sheet oil deposit, since groundwater flows vertically through the NAPL source, the sheet model's upper horizontal area and thickness could greatly influence the

groundwater flow field. With regard to the sphere oil deposit, sphere models with different radii have different influences on the groundwater flow distribution.

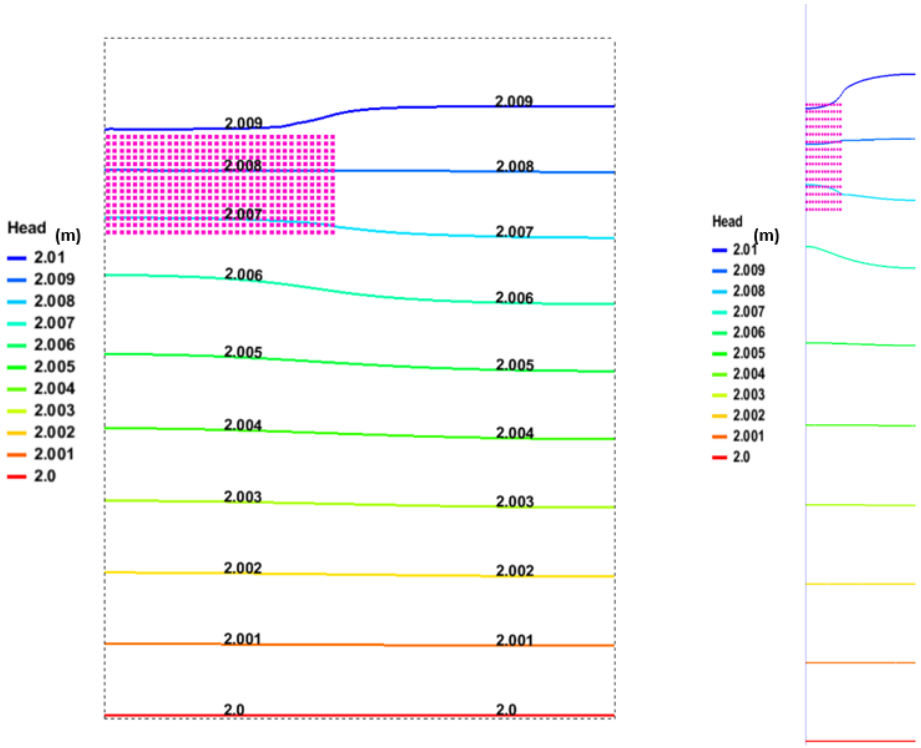

Figure 5.12. Groundwater hydraulic head contour for sheet model (left: front view right: side view)

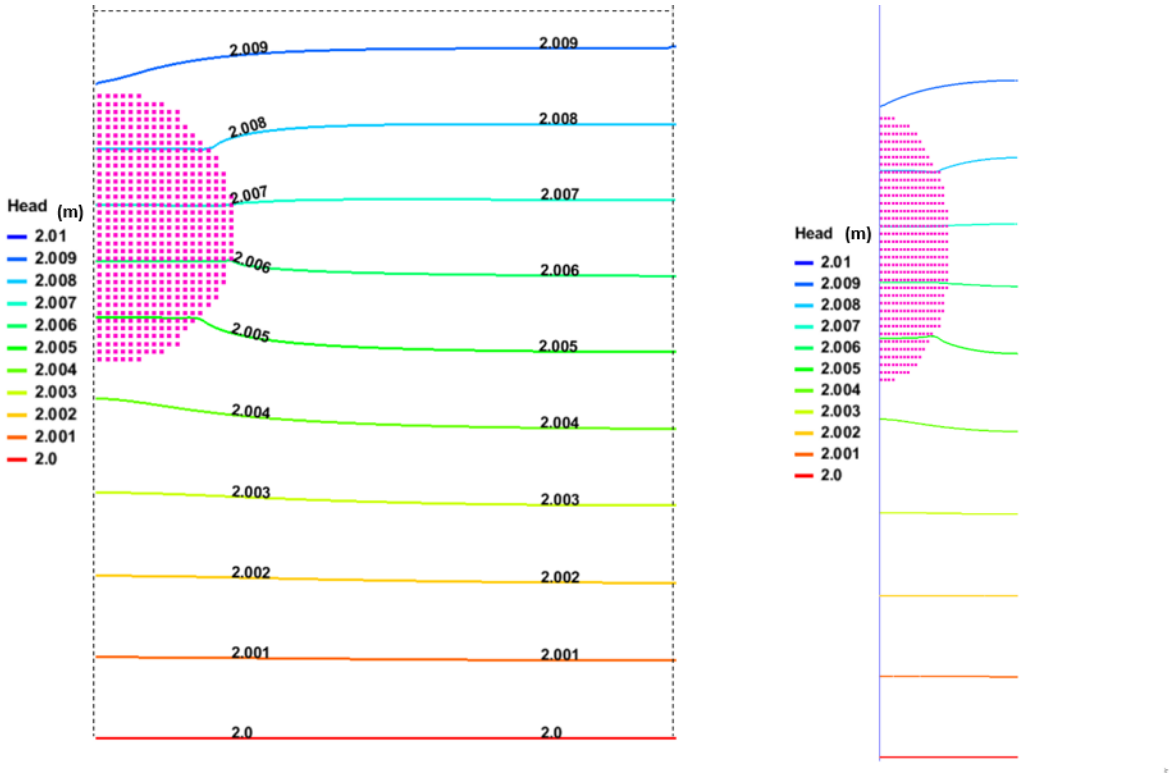

Figure 5.13. Groundwater hydraulic head contour for sphere model (left: front view right: side view)

5.2.2 Effect of Sheet Model's Upper Horizontal Area

Based on the results of the two-dimensional model, it is hypothesized that the upper horizontal area (width x length) and the thickness of the sheet model are the two parameters determining the influence of the sheet deposit geometric structure on the NAPL depletion. Starting with the upper horizontal area, five models with varying upper horizontal areas were constructed to investigate how this factor impacts NAPL depletion (see Chapter 4 for detailed design). After 1 year the ratio of biodegraded NAPL mass to initial total NAPL mass (biodegraded mass/ initial total mass) was calculated and compared between each model simulation. Figure 5.14 shows the calculated ratio for the NAPL component benzene, while Figure 5.15 shows naphthalene, another typical NAPL component. The figures reveal that there was a very slight increase in the calculated mass loss for the upper horizontal area range of 9 cm^2 to 102 cm^2; less than 0.2% increase for benzene, and less than 0.02% increase for naphthalene. This negligible increase indicates that the upper horizontal area of the sheet deposit has almost no influence on biodegradation of residual NAPL. Figures 5.16 to 5.17 illustrate the mass depletion ratio

(mass depleted/initial total mass) for benzene and naphthalene respectively. A similar trend can be seen in Figures 5.16 and 5.17, which further suggests that the upper horizontal area of sheet deposit has almost no effect on the long term persistence of residual NAPL.

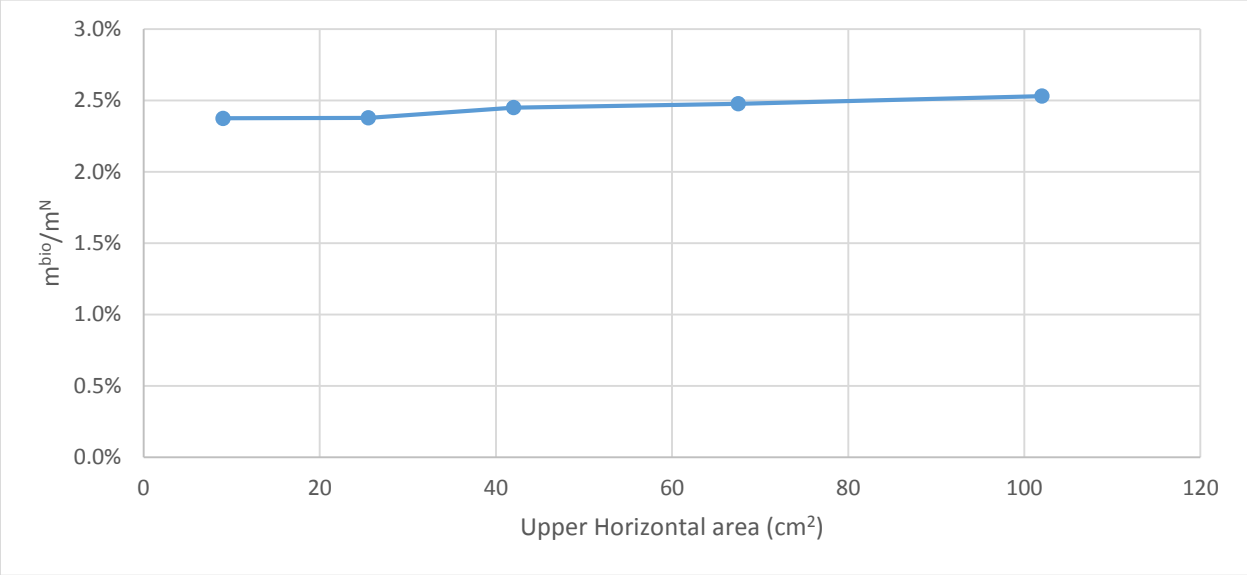

Figure 5.14. Ratio of biodegraded benzene to initial total NAPL benzene over upper horizontal area

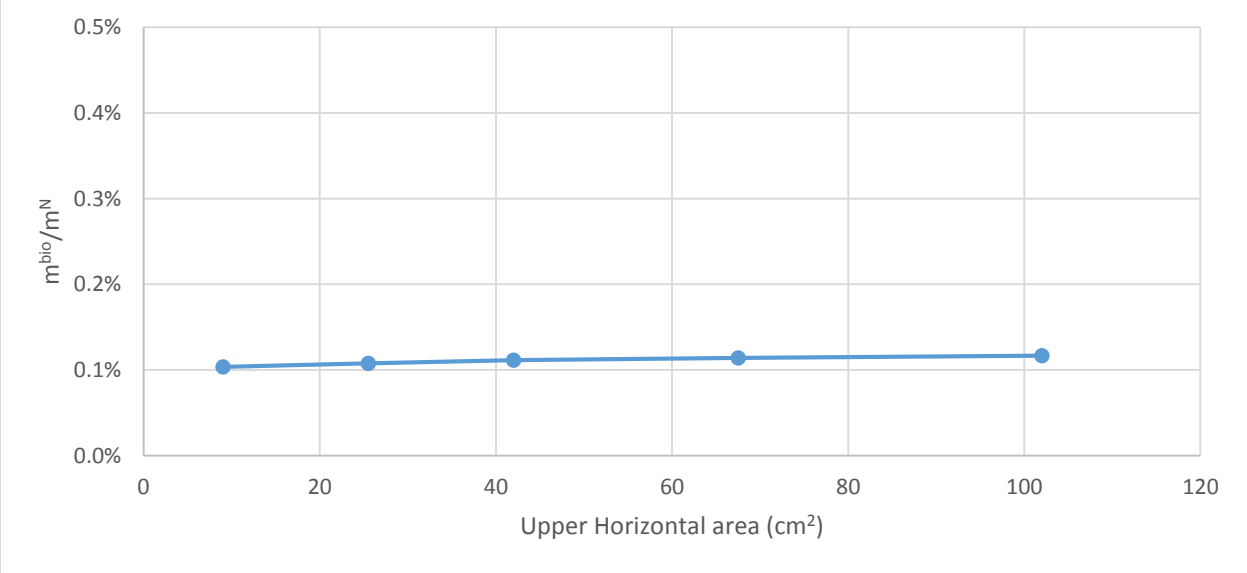

Figure 5.15. Ratio of biodegraded naphthalene to initial total NAPL naphthalene over horizontal area

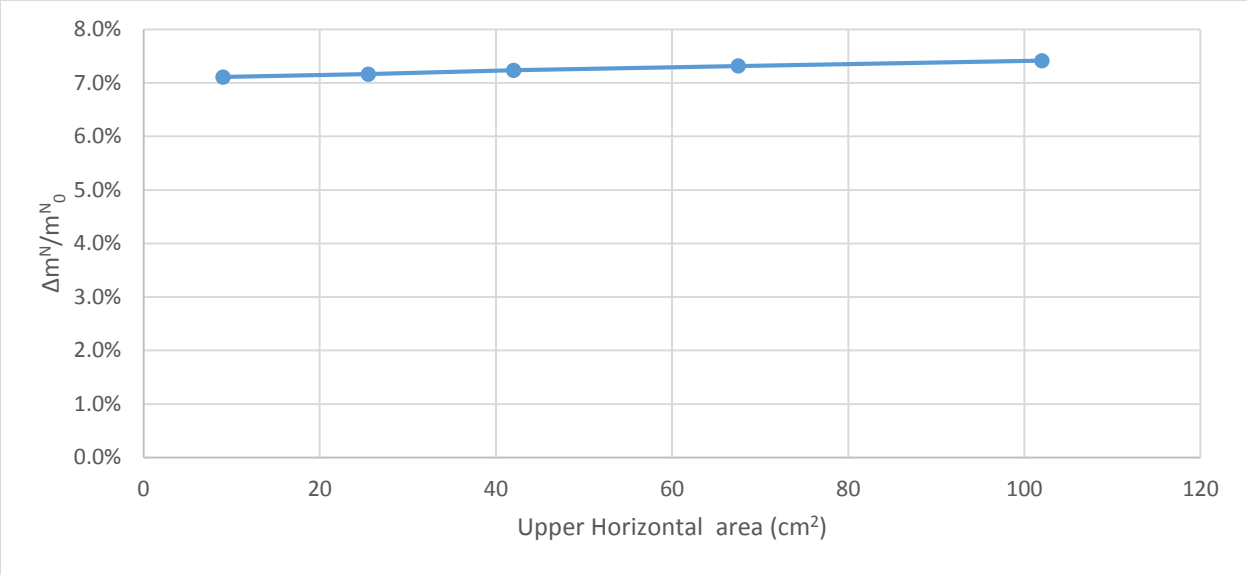

Figure 5.16. Ratio of benzene mass depleted to initial total NAPL benzene over horizontal area

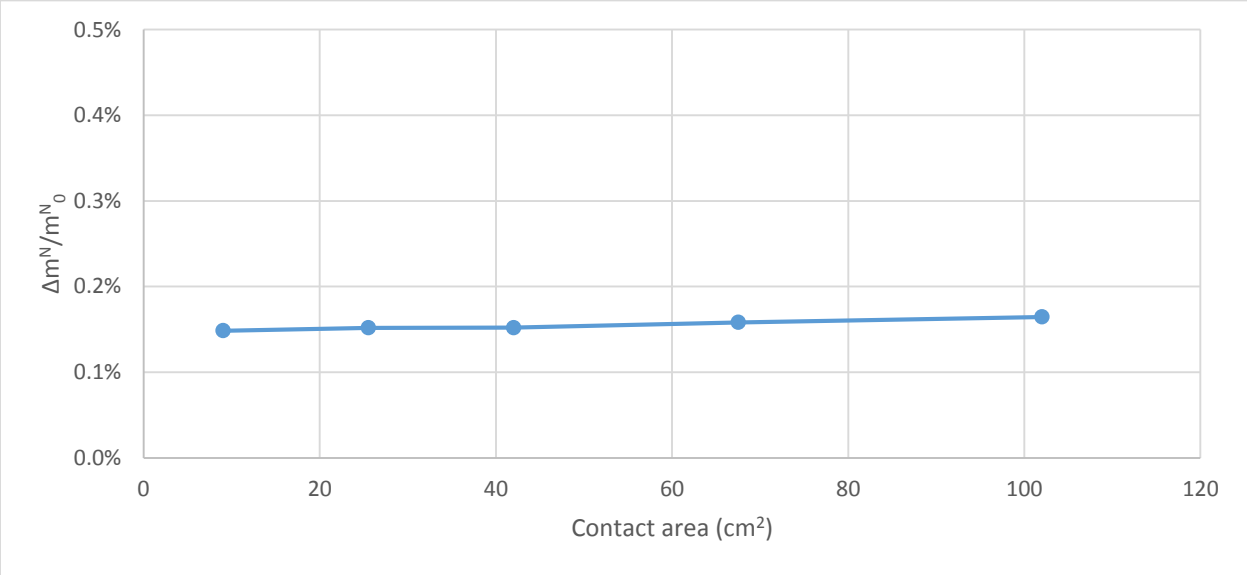

Figure 5.17. Ratio of naphthalene mass depleted to initial total NAPL naphthalene over horizontal area

5.2.3 Effect of Sheet Model Thickness

Sheet deposit thickness is another parameter dictating the geometric structure of the residual oil. The thickness of the sheet deposit represents the distance that groundwater travels through the deposit. Six models with varying sheet deposit thicknesses were constructed to evaluate its potential influence on fate of NAPL constituents (see Chapter 4 for detailed design). The percentage of biodegraded NAPL mass to initial total NAPL mass was calculated and compared for different deposit thicknesses. Figure 5.18 and

5.19 illustrate the ratio for benzene and naphthalene, respectively, for the range of thicknesses considered. Figure 5.18 shows a clear trend between the calculated ratio and thickness. A considerable decrease of m^{bio}/m^{N} occurred as sheet deposit thickness increased from 1.5 cm to 7.5 cm. In the smallest thickness scenario (1.5 cm), approximately 7% of NAPL benzene was biodegraded. However, only 2.5% of NAPL benzene was biodegraded when the sheet deposit thickness increased to 7.5 cm.

This negative correlation between the two variables indicates that the thickness of the sheet deposit plays an important role in terms of petroleum hydrocarbon biodegradation. The three-dimensional model in this study considered three major biodegradation pathways including aerobic biodegradation, sulfate reducing biodegradation, and methanogenesis biodegradation. Figure 5.20 shows the proportion of each individual biodegradation process contributed to the overall biodegradation with regard to each model thickness scenario. As can be seen from the figure, with the decrease of sheet deposit thickness, the proportion of aerobic biodegradation increased while the proportion of methanogenesis biodegradation dropped to almost zero. The proportion of sulfate reducing biodegradation, it increased slightly in the beginning, but started decreasing when methanogenesis dropped to nearly zero. This specific trend from Figure 5.20 suggests that smaller thickness of sheet deposit could encourage aerobic biodegradation processes, and potentially inhibit the anaerobic biodegradation process.

Figures 5.21 and 5.22 illustrate the mass depletion ratio (mass depleted/initial total mass) over thickness for benzene and naphthalene, respectively. Figure 5.21 shows the negative correlation between mass depletion ratio and thickness of sheet deposit. In the smallest thickness (1.5 cm) scenario, almost 30% of benzene was depleted from the NAPL source, while for the largest thickness (7.5 cm) scenario, only 8% of benzene was depleted. Therefore, thickness of the sheet oil deposit is a significant factor impacting the long term persistence of residual benzene in the oil deposit. However, in the case of naphthalene (see Figure 5.19 and Figure 5.22), thickness has almost no influence on the fate of residual naphthalene in the oil deposit.

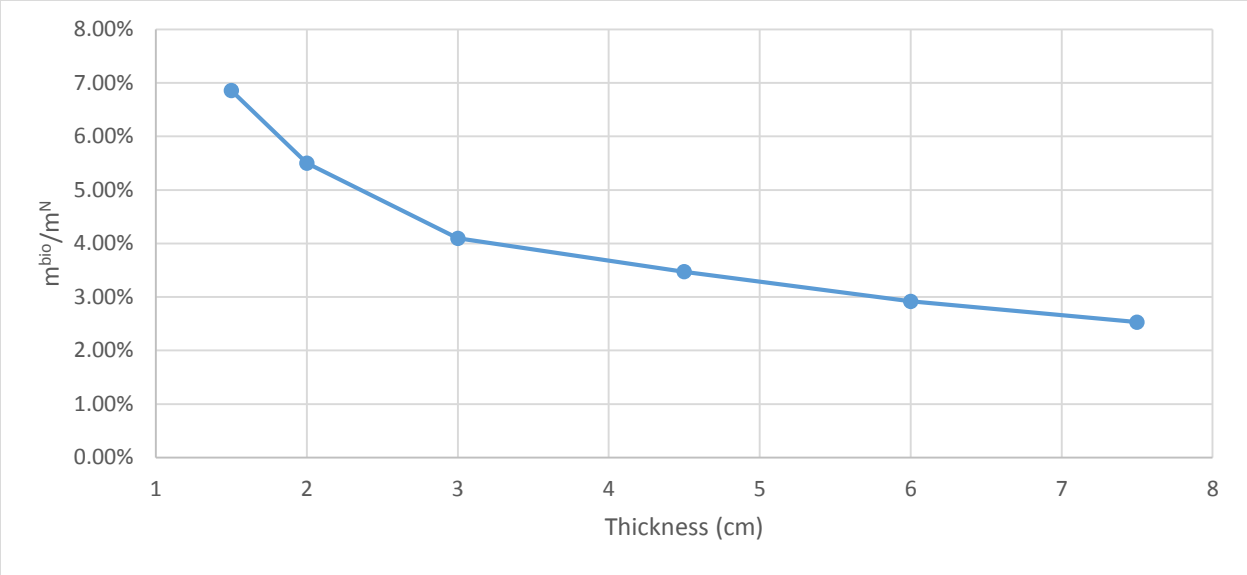

Figure 5.18. Ratio of biodegraded benzene to initial total NAPL benzene over thickness

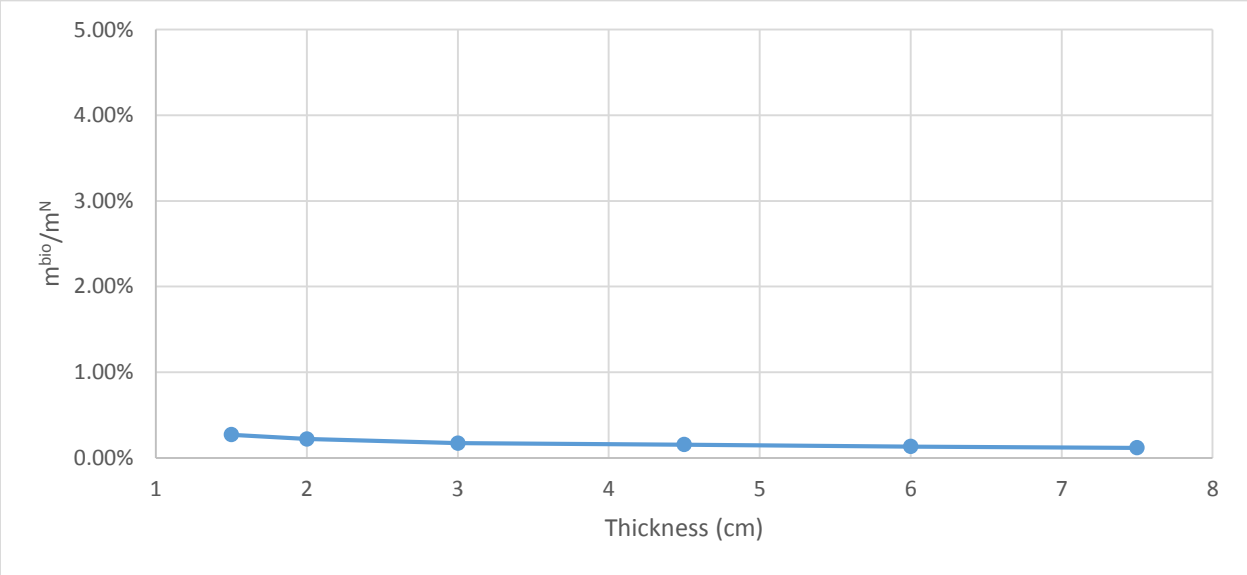

Figure 5.19. Ratio of biodegraded naphthalene to initial total NAPL naphthalene over thickness

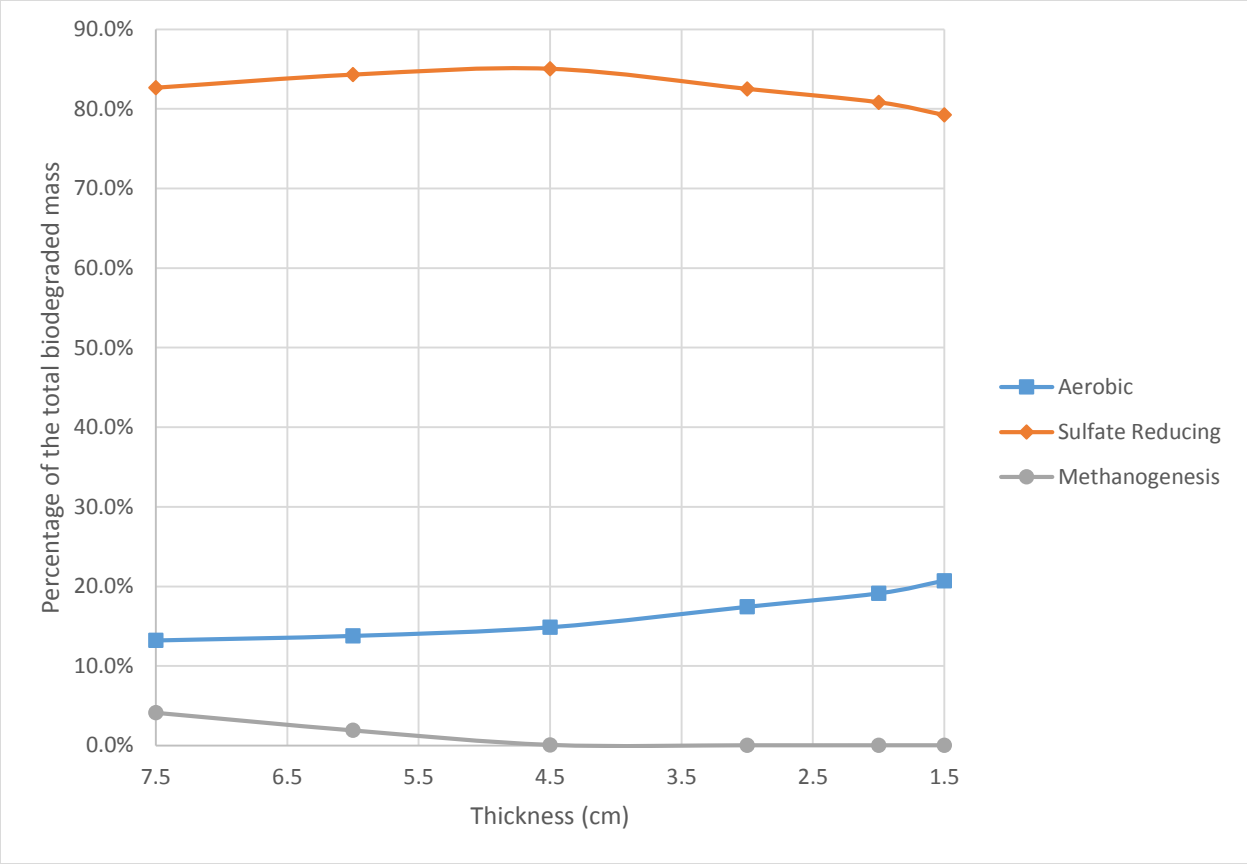

Figure 5.20. Relative contribution of different biodegradation processes as a function of thickness

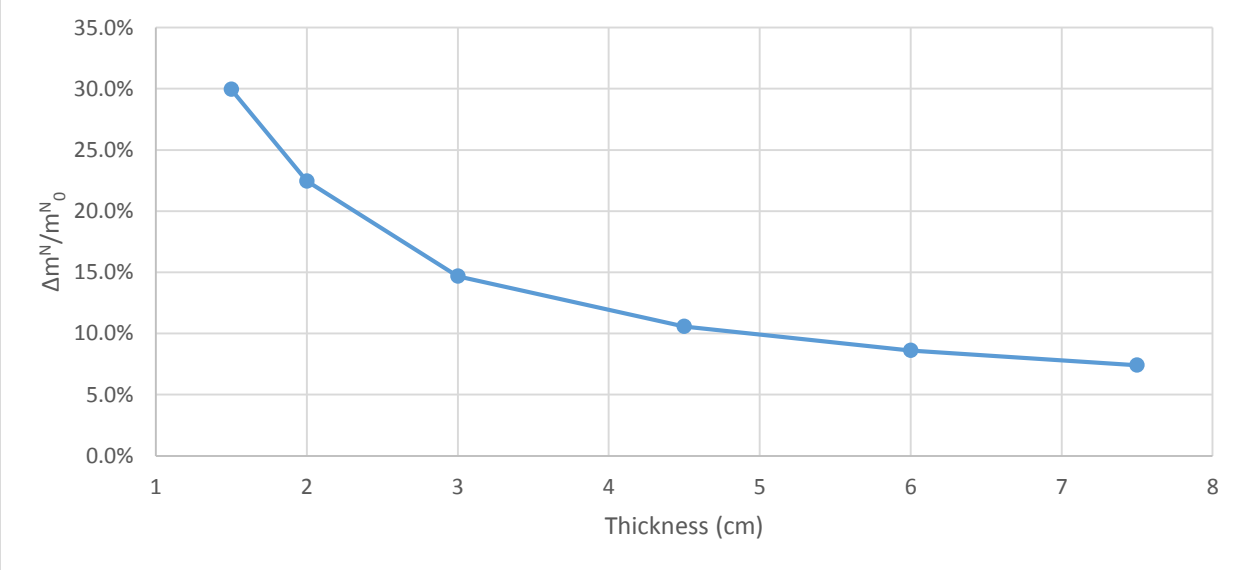

Figure 5.21. Ratio of benzene mass depleted to initial total NAPL benzene over thickness

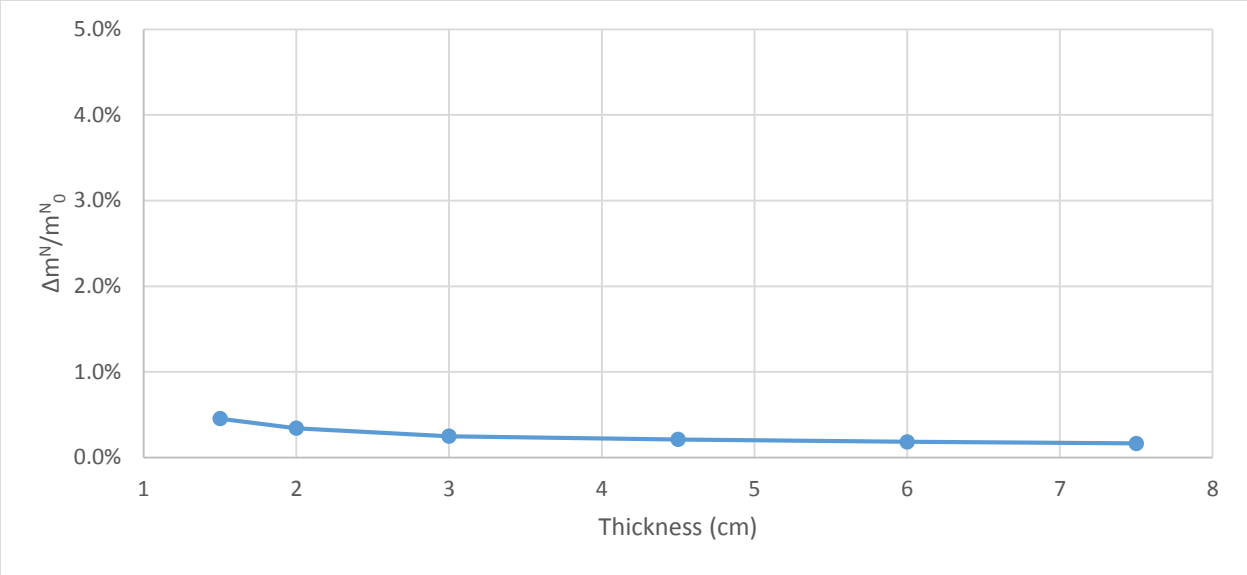

Figure 5.22. Ratio of naphthalene mass depleted to initial total NAPL naphthalene over thickness

5.2.4 Effect of Sphere Model Radius

To assess the geometric influence for the case of a spherical oil deposit, radius was evaluated as a parameter affecting geometry structure. Both sphere surface area and groundwater travel distance are altered by a changing sphere radius. Six sphere models with different radii were designed to examine the effect of volume and surface area on the long term persistence of spherical oil deposits (see Chapter 4 for detailed design). The percentage of biodegraded NAPL mass to initial total NAPL mass was calculated and compared between different radius scenarios. Similar to the sheet model results, benzene and naphthalene were selected as representative components. Figure 5.23 shows the calculated ratio of biodegradation for different radii for benzene. The figure exhibits a negative correlation between the two variables, which indicates that shrinking the radius of modeled sphere could stimulate the overall biodegradation. Similar to the discussion of sheet model's thickness, Figure 5.24 was constructed to show the contribution of different biodegradation pathways to the overall benzene biodegradation. The figure depicts that, with the decrease of sphere deposit radius, the proportion of aerobic biodegradation increased while the proportion of methanogenesis biodegradation dropped to almost zero. The proportion of sulfate reducing biodegradation also declines as sphere radius declines. This particular trend from Figure 5.24

indicates that aerobic biodegradation will have a greater impact on spherical oil deposits with relatively small radii, and may potentially inhibit the anaerobic biodegradation.

Figures 5.26 and 5.27 show the mass depletion ratio (mass depleted/initial total mass) over changing radius for benzene and naphthalene, respectively. A negative correlation between mass depletion ratio and radius of sphere deposit can be found in Figure 5.23. In the smallest radius (2 cm) scenario, approximately 11% of benzene was depleted from the NAPL source, while for the largest radius (7.5 cm) scenario, only 4.5% of benzene was depleted. Overall, sphere radius, as a key geometry parameter of sphere oil deposit, has a great influence on long term persistence of the residual benzene in the oil deposit. Nevertheless, for the fate of naphthalene in the environment (Figure 5.24 and Figure 5.27), the radius has almost no impact in this study.

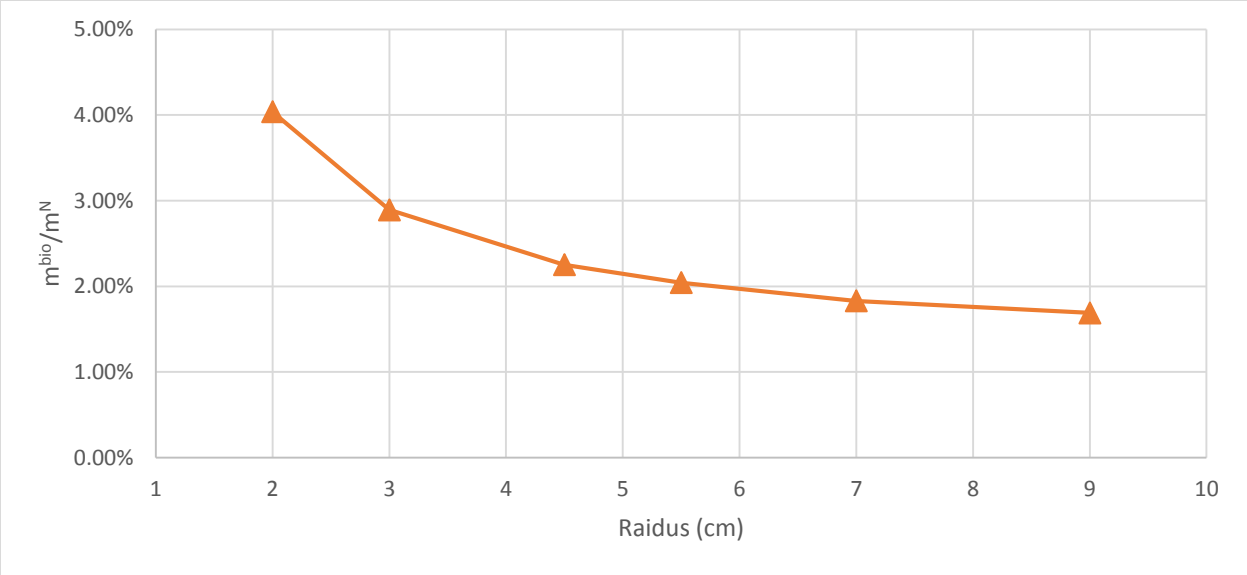

Figure 5.23. Ratio of biodegraded benzene to initial total NAPL benzene over sphere radius

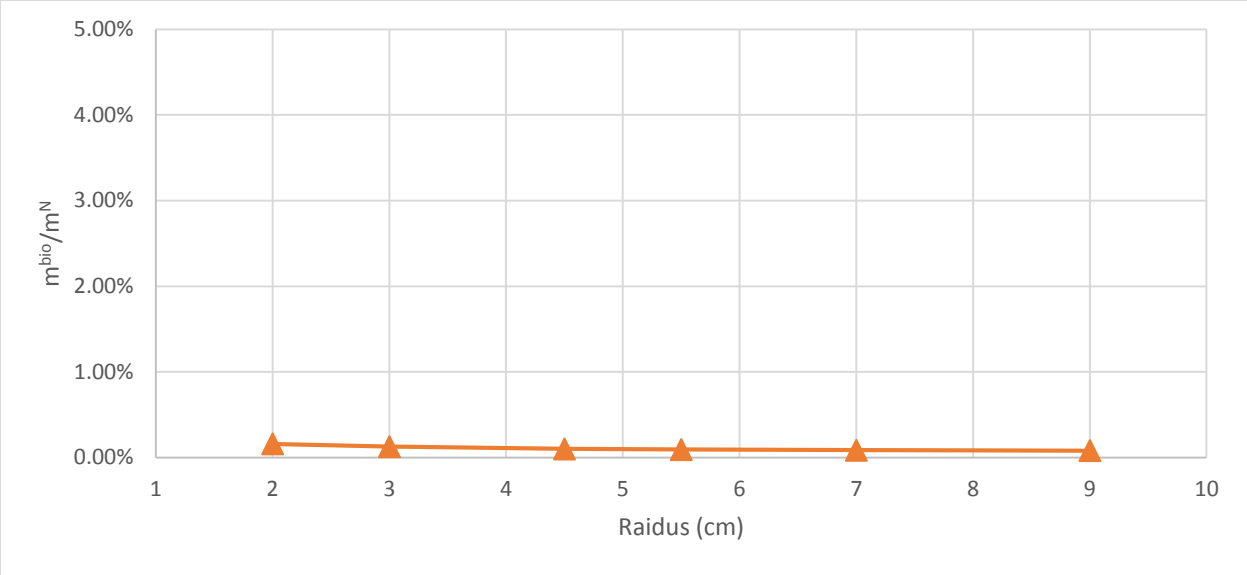

Figure 5.24. Ratio of biodegraded naphthalene to initial total NAPL naphthalene over different sphere radii

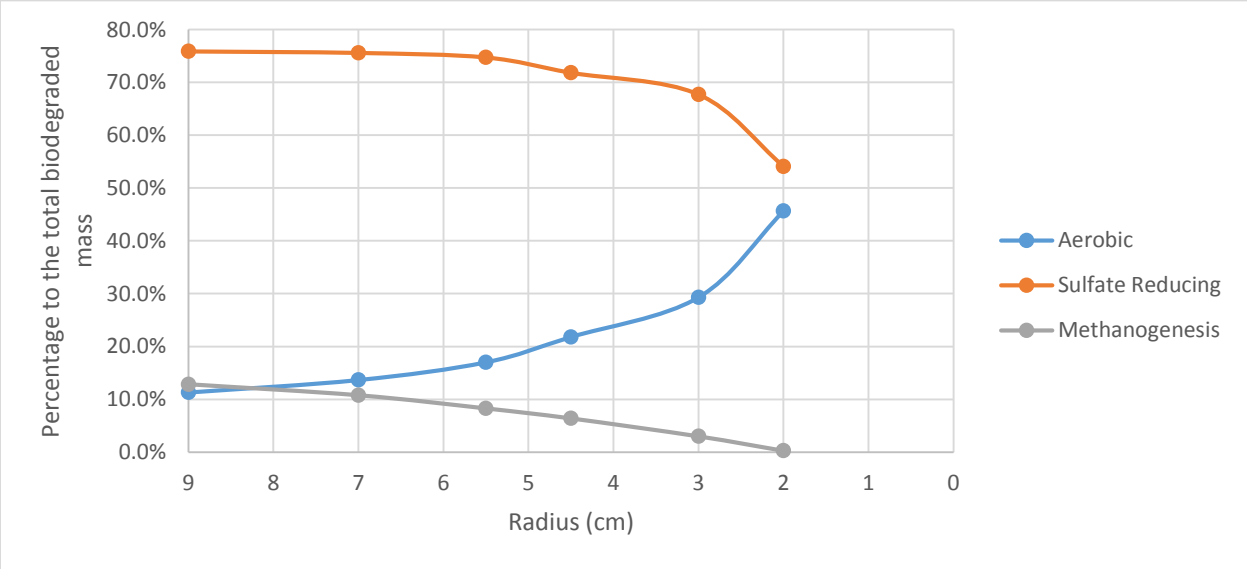

Figure 5.25. Proportion of different biodegradation processes contributed to the overall biodegradation over different sphere radii

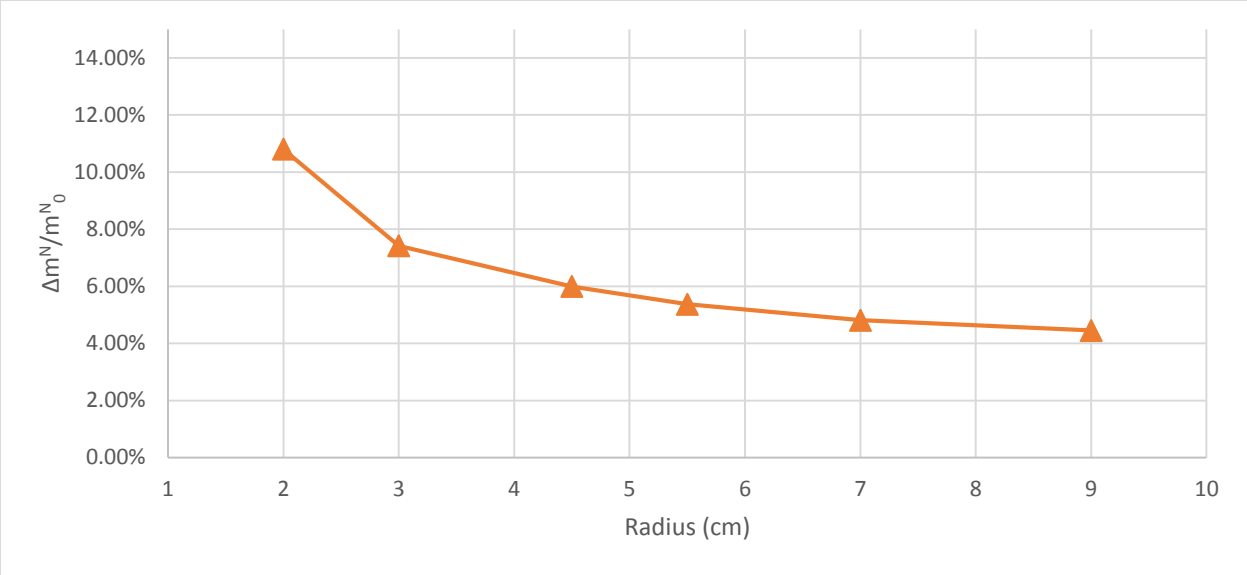

Figure 5.26. Ratio of benzene mass depleted to initial total NAPL benzene over different radii

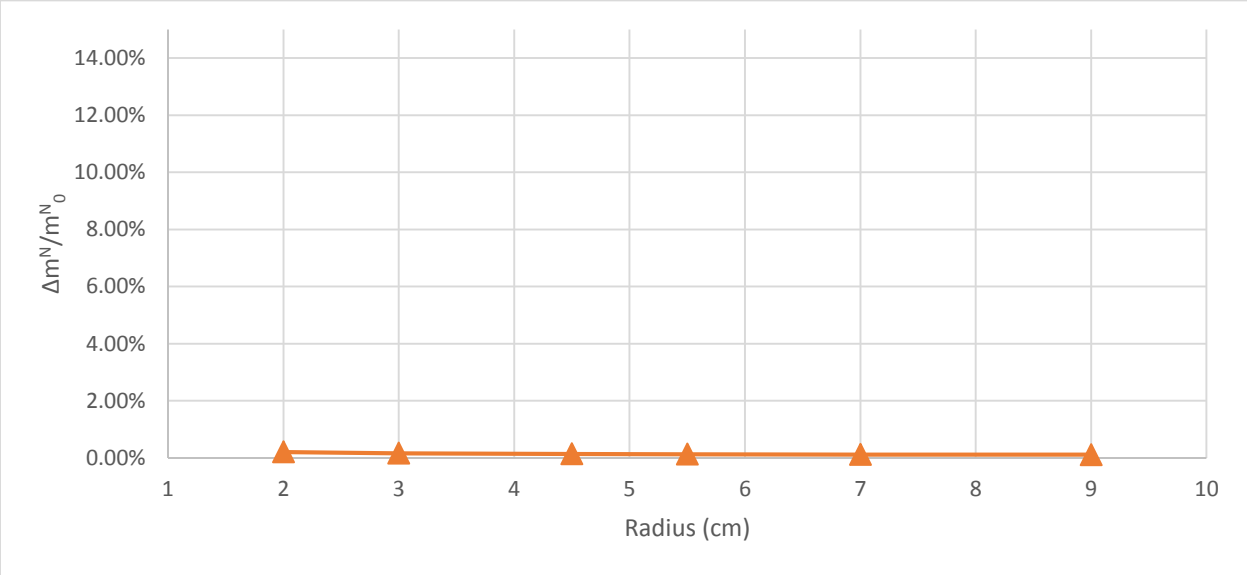

Figure 5.27. Ratio of naphthalene mass depleted to initial total NAPL naphthalene over different radii

Chapter 6 Conclusions

In order to understand the potential effect of crude oil deposit geometry on long term persistence of residual NAPL oil, numerical models were developed based on the Deep Water Horizon oil spill conditions. Two extreme deposit geometries were modeled in this study: the horizontal tar sheet and the spherical tar ball. In this study, groundwater flow was simulated using the code MODFLOW, and subsurface solute transport coupled with biodegradation and dissolution of PHCs from the NAPL source was simulated using the code SEAM3D (sequential electron acceptor model, 3 dimensional). Two-dimensional models were developed first for both geometries using the numerical modeling software GMS (Groundwater Modeling System, version 9.1). The two-dimensional model results showed that sheet geometry deposits exhibited a greater obstruction to groundwater flow relative to the spherical deposits and induced a larger sulfate reducing zone downgradient of the NAPL source, resulting in significantly greater sulfate-based biodegradation of benzene.

Three-dimensional models were constructed following the two-dimensional model development to assess the influence of key geometry parameters on oil deposit fate and persistence. Three parameters affecting deposit's geometric structure were taken into account: (1) the upper horizontal area of the sheet deposit, (2) the thickness of the sheet deposit, and (3) the radius of the sphere deposit. The three-dimensional model results suggested that thickness of the sheet deposit and radius of the sphere deposit were important geometry factors impacting the fate and long term persistence of residual NAPL oil in the coastal environment. However, the influence of deposit geometry differed depending on the solubility of the different NAPL components. When high solubility compound and low solubility compound both exist in the oil deposit, the influence on geometric factors on benzene degradation was significant, while the influence on naphthalene was almost negligible.

References

Abed, R. M., Musat, N., Musat, F., & Mußmann, M. (2011). Structure of microbial communities and hydrocarbon-dependent sulfate reduction in the anoxic layer of a polluted microbial mat. *Marine Pollution Bulletin*, *62*(3), 539-546.

Adamski, M., Kremesec, V., & Charbeneau, R. J. (2003). Residual Saturation: What is it? How is it measured? How should be use it?. In *Petroleum Hydrocarbons Conference, National Ground Water Association, Costa Mesa, CA, August* (pp. 19-20).

Aharon, P., & Fu, B. (2000). Microbial sulfate reduction rates and sulfur and oxygen isotope fractionations at oil and gas seeps in deepwater Gulf of Mexico. *Geochimica et Cosmochimica Acta*, *64*(2), 233-246.

Aigner, E., Burgess, J., Carter, S., Nurse, J., Park, H., Schoenfeld, A & Tse, A. (2010). Map of how much oil is on the Gulf of Mexico [Online image]. Retrieved April 30, 2015 from http://www.nytimes.com/interactive/2010/05/27/us/20100527-oil-landfall.html

Allan, S. E., Smith, B. W., & Anderson, K. A. (2012). Impact of the Deepwater Horizon oil spill on bioavailable polycyclic aromatic hydrocarbons in Gulf of Mexico coastal waters. *Environmental Science & Technology*, *46*(4), 2033-2039.

Alvarez, P. J., Anid, P. J., & Vogel, T. M. (1991). Kinetics of aerobic biodegradation of benzene and toluene in sandy aquifer material. *Biodegradation*, *2*(1), 43-51.

Amos, B. K., Suchomel, E. J., Pennell, K. D., & Löffler, F. E. (2008). Microbial activity and distribution during enhanced contaminant dissolution from a NAPL source zone. *Water Research*, *42*(12), 2963-2974.

Ancheyta, J., & Speight, J. G. (Eds.). (2007). *Hydroprocessing of heavy oils and residua*. CRC Press.

Anderson, M. P., & Woessner, W. W. (1992). *Applied groundwater modeling: simulation of flow and advective transport* (Vol. 4). Gulf Professional Publishing.

Atlas, R. M. (1975). Effects of temperature and crude oil composition on petroleum biodegradation. *Applied Microbiology*, *30*(3), 396-403.

Atlas, R. M. (1981). Microbial degradation of petroleum hydrocarbons: an environmental perspective. *Microbiological Reviews*, *45*(1), 180.

Atlas, R. M. (1985). Effects of hydrocarbons on microorganisms and petroleum biodegradation in arctic ecosystems. *Petroleum Effects in the Arctic Environment. Elsevier Applied Science Publishers*, 63-99.

Atlas, R. M. (1995). Petroleum biodegradation and oil spill bioremediation. *Marine Pollution Bulletin*, *31*(4), 178-182.

Atlas, R. M., & Hazen, T. C. (2011). Oil biodegradation and bioremediation: a tale of the two worst spills in US history. *Environmental Science & Technology*, *45*(16), 6709-6715.

Baehr, A. L., & Corapcioglu, M. Y. (1987). A compositional multiphase model for groundwater contamination by petroleum products: 2. Numerical solution. *Water Resources Research*, *23*(1), 201-213.

Banta, E. R., Hill, M. C., & McDonald, M. G. (2000). *MODFLOW-2000, the US Geological Survey modular ground-water model: User guide to modularization concepts and the ground-water flow process* (p. 121). Reston, VA: US Geological Survey.

Bailey, J. E., & Ollis, D. F. (1977). Kinetics of substrate utilization, product yield and biomass production in cell cultures. *Biochemical Engineering Fundamentals. McGraw-Hill, Tokyo*.

Blumer, M., Ehrhardt, M., & Jones, J. H. (1973). The environmental fate of stranded crude oil. In *Deep Sea Research and Oceanographic Abstracts* (Vol. 20, No. 3, pp. 239-259). Elsevier.

Board, M., & Board, O. S. (2002). *Spills of Emulsified Fuels: Risks and Responses*. National Academies Press.

Borden, R. C., Gomez, C. A., & Becker, M. T. (1995). Geochemical indicators of intrinsic bioremediation. *Groundwater*, *33*(2), 180-189.

Boll, M., & Heider, J. (2010). Anaerobic degradation of hydrocarbons: mechanisms of C–H-bond activation in the absence of oxygen. In *Handbook of Hydrocarbon and Lipid Microbiology* (pp. 1011-1024). Springer Berlin Heidelberg.

Boufadel, M. C., Suidan, M. T., & Venosa, A. D. (1999). A numerical model for density-and-viscosity-dependent flows in two-dimensional variably saturated porous media. *Journal of Contaminant Hydrology*, *37*(1), 1-20.

Brock, T. D., Madigan, M. T., Martinko, J. M., & Parker, J. (1994). Biology of Microorganisms. Prentice Hall, Englewood Cliffs, NJ.

Brun, A., & Engesgaard, P. (2002). Modelling of transport and biogeochemical processes in pollution plumes: literature review and model development. *Journal of Hydrology*, *256*(3), 211-227.

Brauner, J. S., Widdowson, M. A., Novak, J. T., & Love, N. G. (2002). Biodegradation of a PAH mixture by native subsurface microbiota. *Bioremediation Journal*, *6*(1), 9-24.

Butler, J. S. (2011). BP Macondo Well Incident U.S. Gulf of Mexico Pollution Containment and Remediation Efforts. Lillehammer Energy Claims Conference.

Button, D. K. (1985). Kinetics of nutrient-limited transport and microbial growth. *Microbiological Reviews*, *49*(3), 270.

Caldwell, M. E., Garrett, R. M., Prince, R. C., & Suflita, J. M. (1998). Anaerobic biodegradation of long-chain n-alkanes under sulfate-reducing conditions. *Environmental Science & Technology*, *32*(14), 2191-2195.

Chatzis, I., Morrow, N. R., & Lim, H. T. (1983). Magnitude and detailed structure of residual oil saturation. *Soc. Pet. Eng. J*, *23*(2), 311-326.

Chen, Y. M., Abriola, L. M., Alvarez, P. J., Anid, P. J., & Vogel, T. M. (1992). Modeling transport and biodegradation of benzene and toluene in sandy aquifer material: Comparisons with experimental measurements. *Water Resources Research*, *28*(7), 1833-1847.

Christensen, D. R., & McCarty, P. L. (1975). Multi-process biological treatment model. *Journal (Water Pollution Control Federation)*, 2652-2664.

Chu, M., Kitanidis, P. K., & McCarty, P. L. (2004). Possible factors controlling the effectiveness of bioenhanced dissolution of non-aqueous phase tetrachloroethene. *Advances in Water Resources*, *27*(6), 601-615.

Cirpka, O. A., Frind, E. O., & Helmig, R. (1999). Numerical simulation of biodegradation controlled by transverse mixing. *Journal of Contaminant Hydrology*, *40*(2), 159-182.

Clement, T. P., Kim, Y. C., Gautam, T. R., & Lee, K. K. (2004). Experimental and numerical investigation of DNAPL dissolution processes in a laboratory aquifer model. *Groundwater Monitoring & Remediation*, *24*(4), 88-96.

Corapcioglu, M. Y., & Baehr, A. L. (1987). A compositional multiphase model for groundwater contamination by petroleum products: 1. Theoretical considerations. *Water Resources Research*, *23*(1), 191-200.

Daling, P. S., Leirvik, F., Almås, I. K., Brandvik, P. J., Hansen, B. H., Lewis, A., & Reed, M. (2014). Surface weathering and dispersibility of MC252 crude oil. *Marine Pollution Bulletin*, *87*(1), 300-310

Das, N., & Chandran, P. (2010). Microbial degradation of petroleum hydrocarbon contaminants: an overview. *Biotechnology Research International*, *2011*.

Desai, A. M., Autenrieth, R. L., Dimitriou-Christidis, P., & McDonald, T. J. (2008). Biodegradation kinetics of select polycyclic aromatic hydrocarbon (PAH) mixtures by Sphingomonas paucimobilis EPA505. *Biodegradation*, *19*(2), 223-233.

Edwards, E. A., & Grbić-Galić, D. (1994). Anaerobic degradation of toluene and o-xylene by a methanogenic consortium. *Applied and Environmental Microbiology*, *60*(1), 313-322.

Elango, V., Urbano, M., Lemelle, K. R., & Pardue, J. H. (2014). Biodegradation of MC252 oil in oil: sand aggregates in a coastal headland beach environment. *Frontiers in Microbiology*, *5*.

Encyclopedia Britannica. (2011). Location of the Deepwater Horizon oil rig in the Gulf of Mexico [Online image]. Retrieved April 30, 2015 from http://kids.britannica.com/comptons/art-153348/This-map-depicts-the-location-of-the-Deepwater-Horizon-oil#cite

Essaid, H. I., Bekins, B. A., Godsy, E. M., Warren, E., Baedecker, M. J., & Cozzarelli, I. M. (1995). Simulation of aerobic and anaerobic biodegradation processes at a crude oil spill site. *Water Resources Research*, *31*(12), 3309-3327.

Essaid, H. I., Cozzarelli, I. M., Eganhouse, R. P., Herkelrath, W. N., Bekins, B. A., & Delin, G. N. (2003). Inverse modeling of BTEX dissolution and biodegradation at the Bemidji, MN crude-oil spill site. *Journal of Contaminant Hydrology*, *67*(1), 269-299.

Ewing, R. P., & Berkowitz, B. (1998). A generalized growth model for simulating initial migration of dense non-aqueous phase liquids. *Water Resources Research*, *34*(4), 611-622.

Fingas, M. F. (1999). The evaporation of oil spills: development and implementation of new prediction methodology. In *International Oil Spill Conference* (Vol. 1999, No. 1, pp. 281-287). American Petroleum Institute.

Fingas, M., & Brown, C. E. (2011). Oil spill remote sensing: a review. *Oil spill science and technology*, 111-169.

Garven, G. (1989). A hydrogeologic model for the formation of the giant oil sands deposits of the Western Canada sedimentary basin. *American Journal of Science*, *289*(2), 105-166.

Godsy, E. M., Warren, E., Cozzarelli, I. M., Bekins, B. A., & Eganhouse, R. P. (1999). Determining BTEX biodegradation rates using in situ microcosms at the Bemidji site, Minnesota: trials and tribulations. In *US Geological Survey Toxic Substances Hydrology Program—Proceedings of the Technical Meeting Charleston South Carolina March 8* (Vol. 12, p. 1999).

Gros, N., Camões, M. F., Oliveira, C., & Silva, M. C. R. (2008). Ionic composition of seawaters and derived saline solutions determined by ion chromatography and its relation to other water quality parameters. *Journal of Chromatography A*, *1210*(1), 92-98.

Grubb, H. F. (1984). *Planning report for the Gulf Coast Regional Aquifer-System Analysis in the Gulf of Mexico Coastal Plain, United States*. US Geological Survey.

Hamilton, J. D. (2011). *Historical oil shocks* (No. w16790). National Bureau of Economic Research.

Haritash, A. K., & Kaushik, C. P. (2009). Biodegradation aspects of polycyclic aromatic hydrocarbons (PAHs): a review. *Journal of Hazardous Materials*, *169*(1), 1-15.

Harayama, S., Kasai, Y., & Hara, A. (2004). Microbial communities in oil-contaminated seawater. *Current Opinion in Biotechnology*, *15*(3), 205-214.

Haynes, W. M. (Ed.). (2013). *CRC Handbook of Chemistry and Physics*. CRC press.

Hosseini, A. H., Deutsch, C. V., Mendoza, C. A., & Biggar, K. W. (2011). Inverse modeling for characterization of uncertainty in transport parameters under uncertainty of source geometry in heterogeneous aquifers. *Journal of Hydrology*, *405*(3), 402-416.

Hunt, A. (1996). Uncertainties remain in predicting paraffin deposition. *Oil and Gas Journal*, *94*(31), 96-103.

Imhoff, P. T., Jaffé, P. R., & Pinder, G. F. (1994). An experimental study of complete dissolution of a nonaqueous phase liquid in saturated porous media. *Water Resources Research*, *30*(2), 307-320.

Jacob, F., & Monod, J. (1961). Genetic regulatory mechanisms in the synthesis of proteins. *Journal of Molecular Biology*, *3*(3), 318-356.

Jakobsen, R. (2007). Redox microniches in groundwater: a model study on the geometric and kinetic conditions required for concomitant Fe oxide reduction, sulfate reduction, and methanogenesis. *Water Resources Research*, *43*(12).

Jakobsen, R., & Postma, D. (1999). Redox zoning, rates of sulfate reduction and interactions with Fe-reduction and methanogenesis in a shallow sandy aquifer, Rømø, Denmark. *Geochimica et Cosmochimica Acta*, *63*(1), 137-151.

Jefferson, J., & Bowling, N. (2011). The Economic and Biological Impacts of the BP Oil Spill. Hampden-Sydney College

Jobson, A., Cook, F. D., & Westlake, D. W. S. (1972). Microbial utilization of crude oil. *Applied Microbiology*, *23*(6), 1082-1089.

Jones, D. M., Head, I. M., Gray, N. D., Adams, J. J., Rowan, A. K., Aitken, C. M., ... & Larter, S. R. (2008). Crude-oil biodegradation via methanogenesis in subsurface petroleum reservoirs. *Nature*, *451*(7175), 176-180.

Jorgensen, S. E., & Gromiec, M. J. (1989). Mathematical submodels in water quality systems.

Kornacki, A. S., Kendrick, J. W., & Berry, J. L. (1994). Impact of oil and gas vents and slicks on petroleum exploration in the deepwater Gulf of Mexico. *Geo-Marine Letters*, *14*(2-3), 160-169.

Kerr, R. A. (2010). A lot of oil on the loose, not so much to be found. *Science*, *329*(5993), 734-735.

Kiruri, L. W., Dellinger, B., & Lomnicki, S. (2013). Tar balls from Deep Water Horizon oil spill: environmentally persistent free radicals (EPFR) formation during crude weathering. *Environmental Science & Technology*, *47*(9), 4220-4226.

Latham, M. A. (2011). Five Thousand Feet and Below: The Failure to Adequately Regulate Deepwater Oil Production Technology. *BC Envtl. Aff. L. Rev.*, *38*, 343.

Leahy, J. G., & Colwell, R. R. (1990). Microbial degradation of hydrocarbons in the environment. *Microbiological Reviews*, *54*(3), 305-315.

Lee, S. Y., & Choi, J. I. (1999). Production and degradation of polyhydroxyalkanoates in waste environment. *Waste Management*, *19*(2), 133-139.

Li, H., & Boufadel, M. C. (2010). Long-term persistence of oil from the Exxon Valdez spill in two-layer beaches. *Nature Geoscience*, *3*(2), 96-99.

Li, H., Li, G., Cheng, J., & Boufadel, M. C. (2007). Tide-induced head fluctuations in a confined aquifer with sediment covering its outlet at the sea floor. *Water Resources Research*, *43*(3).

Liu, Z., Liu, J., Zhu, Q., & Wu, W. (2012). The weathering of oil after the Deepwater Horizon oil spill: insights from the chemical composition of the oil from the sea surface, salt marshes and sediments. *Environmental Research Letters*, *7*(3), 035302.

McFarland, M. J., & Sims, R. C. (1991). Thermodynamic framework for evaluating PAH degradation in the subsurface. *Groundwater*, *29*(6), 885-896.

Mercer, J. W., & Cohen, R. M. (1990). A review of immiscible fluids in the subsurface: properties, models, characterization and remediation. *Journal of Contaminant Hydrology*, *6*(2), 107-163.

Molz, F. J., Widdowson, M. A., & Benefield, L. D. (1986). Simulation of microbial growth dynamics coupled to nutrient and oxygen transport in porous media. *Water Resources Research*, *22*(8), 1207-1216.

Morrow, N. R. (1987). A review of the effects of initial saturation, pore structure and wettability on oil recovery by waterflooding.

Nambi, I. M., & Powers, S. E. (2000). NAPL dissolution in heterogeneous systems: an experimental investigation in a simple heterogeneous system. *Journal of Contaminant Hydrology*, *44*(2), 161-184.

Nicol, J. P., Wise, W. R., Molz, F. J., & Benefield, L. D. (1994). Modeling biodegradation of residual petroleum in a saturated porous column. *Water Resources Research*, *30*(12), 3313-3325.

Nixon, L. D., Shepard, N. K., Bohannon, C. M., Montgomery, T. M., Kazanis, E. G., & Gravois, M. P. (2009). Deepwater Gulf of Mexico 2009: Interim report of 2008 highlights. *Minerals Management Service Gulf of Mexico OCS Region*.

Paganie, D. (2009, November). Gulf of Mexico. *Offshore Magazine*. Retrieved April 30, 2015 from http://www.offshore-mag.com/articles/print/volume-69/issue-11/departments/gulf-of_mexico/gulf-of-mexico.html

Parker, J. C., Katyal, A. K., Kaluarachchi, J. J., Lenhard, R. J., & Johnson, T. J. (1991). Modeling multiphase organic chemical transport in soils and ground water.

Payne, J. R., Kirstein, B. E., McNabb Jr, G. D., Lambach, J. L., de Oliveira, C., Jordan, R. E., & Hom, W. (1983, February). MULTIVARIATE ANALYSIS OF PETROLEUM HYDROCARBON WEATHERING IN THE SUBARCTIC MARINE ENVIRONMENT 1. In *International Oil Spill Conference* (Vol. 1983, No. 1, pp. 423-434). American Petroleum Institute.

Plata, D. L., Sharpless, C. M., & Reddy, C. M. (2008). Photochemical degradation of polycyclic aromatic hydrocarbons in oil films. *Environmental Science & Technology*, *42*(7), 2432-2438.

Reardon, K. F., Mosteller, D. C., & Rogers, J. D. B. (2000). Biodegradation kinetics of benzene, toluene, and phenol as single and mixed substrates for Pseudomonas putida F1. *Biotechnology and Bioengineering*, (69), 385-400.

Rojo, F. (2009). Degradation of alkanes by bacteria. *Environmental Microbiology*, *11*(10), 2477-2490.

Röling, W. F., Milner, M. G., Jones, D. M., Fratepietro, F., Swannell, R. P., Daniel, F., & Head, I. M. (2004). Bacterial community dynamics and hydrocarbon degradation during a field-scale evaluation of bioremediation on a mudflat beach contaminated with buried oil. *Applied and Environmental Microbiology*, *70*(5), 2603-2613.

Ryerson, T. B., Aikin, K. C., Angevine, W. M., Atlas, E. L., Blake, D. R., Brock, C. A., ... & Watts, L. A. (2011). Atmospheric emissions from the Deepwater Horizon spill constrain air-water partitioning, hydrocarbon fate, and leak rate. *Geophysical Research Letters*, *38*(7).

Schäfer, W., & Therrien, R. (1995). Simulating transport and removal of xylene during remediation of a sandy aquifer. *Journal of Contaminant Hydrology*, *19*(3), 205-236.

Singh, G., Pruden, A., & Widdowson, M. A. (2012). Influence of petroleum deposit geometry on local gradient of electron acceptors and microbial catabolic potential. *Environmental Science & Technology*, *46*(11), 5782-5788.

Suthaker, N. N., & Scott, J. D. (1996). Measurement of hydraulic conductivity in oil sand tailings slurries. *Canadian Geotechnical Journal*, *33*(4), 642-653.

Torlapati, J., & Boufadel, M. C. (2014). Evaluation of the biodegradation of Alaska North Slope oil in microcosms using the biodegradation model BIOB. *Frontiers in Microbiology*, *5*.

Uraizee, F. A., Venosa, A. D., & Suidan, M. T. (1997). A model for diffusion controlled bioavailability of crude oil components. *Biodegradation*, *8*(5), 287-296.

Urbano, M., Elango, V., & Pardue, J. H. (2013). Biogeochemical characterization of MC252 oil: sand aggregates on a coastal headland beach. *Marine Pollution Bulletin*, *77*(1), 183-191.

Vilc áez, J., Li, L., & Hubbard, S. S. (2013). A new model for the biodegradation kinetics of oil droplets: application to the Deepwater Horizon oil spill in the Gulf of Mexico. *Geochem. Trans*, *14*(4).

Waddill, D. W., & Widdowson, M. A. (1998). Three-dimensional model for subsurface transport and biodegradation. *Journal of Environmental Engineering*, *124*(4), 336-344.

Walton, J. C., & Smith, R. W. (1992). DISCUSSION OF "Thermodynamic Framework for Evaluating PAH Degradation in the Subsurface," by MJ McFarland and RC Sims, November-December 1991 issue, v. 29, no. 6, pp. 885-896. *Groundwater*, *30*(4), 624-624.

Wang, Z., & Fingas, M. (1995). Differentiation of the source of spilled oil and monitoring of the oil weathering process using gas chromatography-mass spectrometry. *Journal of Chromatography A*, *712*(2), 321-343.

Widdowson, M. A., Molz, F. J., & Benefield, L. D. (1988). A numerical transport model for oxygen-and nitrate-based respiration linked to substrate and nutrient availability in porous media. *Water Resources Research*, *24*(9), 1553-1565.

Widdowson, M. A. (2004). Modeling natural attenuation of chlorinated ethenes under spatially varying redox conditions. *Biodegradation*, *15*(6), 435-451.

Xu, Z., Chai, J., Wu, Y., & Qin, R. (2015). Transport and biodegradation modeling of gasoline spills in soil–aquifer system. *Environmental Earth Sciences*, 1-12.

Zhou, Z., Guo, L., Shiller, A. M., Lohrenz, S. E., Asper, V. L., & Osburn, C. L. (2013). Characterization of oil components from the Deepwater Horizon oil spill in the Gulf of Mexico using fluorescence EEM and PARAFAC techniques. *Marine Chemistry*, *148*, 10-21.

Appendix: Details of Numerical Model Design

Table A 1. time variant head package set up for 24 hours period in GMS (same set up between each day)

Stress Period	Start Time	End Time	Start head (m)	End head (m)
1	0:00	6:00	2.05	2.01
2	6:00	12:00	2.05	2.01
3	12:00	18:00	2.05	2.01
4	18:00	0:00	2.05	2.01

Table A 2. Summary tables of mass change for NAPL constituent benzene for sheet model (two-dimensional model)

Benzene	Case 1			Case 2 (Aerobic only)		
	Aerobic	Sulfate	Meth	Aerobic	Sulfate	Meth
m^{bio} (g)	7.31E-04	5.24E-03	3.38E-06	7.28E-04	0	0
m^{N} (g)	0.183416					
Δm^{N} (g)	2.97E-02			2.80E-02		
m^{bio}/m^{N}	0.40%	2.85%	0.00%	0.40%	0.00%	0.00%

Benzene	Case3 (No Bio)			Case4 (No Charge)		
	Aerobic	Sulfate	Meth	Aerobic	Sulfate	Meth
m^{bio} (g)	0	0	0	0.000697	0.001405	0.000547
m^{N} (g)	0.183416					
Δm^{N} (g)	2.80E-02			2.67E-03		
m^{bio}/m^{N}	0.00%	0.00%	0.00%	0.38%	0.77%	0.30%

Table A 3. Summary tables of mass change for NAPL constituent Naphthalene for sheet model (two-dimensional model)

Naphthalenes	Case 1			Case 2 (Aerobic only)		
	Aerobic	Sulfate	Meth	Aerobic	Sulfate	Meth
m^{bio} (g)	3.34E-04	2.19E-03	1.32E-06	3.35E-04	0	0
m^{N} (g)	0.61139					
Δm^{N} (g)	4.17E-03			3.25E-03		
m^{bio}/m^{N}	0.05%	0.36%	0.00%	0.05%	0.00%	0.00%

Naphthalenes	Case3 (No Bio)			Case4 (No Charge)		
	Aerobic	Sulfate	Meth	Aerobic	Sulfate	Meth
m^{bio} (g)	0	0	0	0.000413	0.000675	0.000271

m^N (g)	0.61139					
Δm^N (g)	3.24E-03			1.32E-03		
m^{bio}/m^N	0.00%	0.00%	0.00%	0.07%	0.11%	0.04%

Table A 4. Summary tables of mass change for NAPL constituent Benzene for sphere model (two-dimensional model)

Benzene	Case 1			Case 2 (Aerobic only)		
	Aerobic	Sulfate	Meth	Aerobic	Sulfate	Meth
m^{bio} (g)	5.28E-04	3.39E-03	1.78E-04	5.04E-04	0	0
m^N (g)	0.183416					
Δm^N (g)	0.010125			0.007995		
m^{bio}/m^N	0.29%	1.85%	0.10%	0.27%	0	0

Benzene	Case3 (No Bio)			Case4 (No Charge)		
	Aerobic	Sulfate	Meth	Arobic	Sulfate	Meth
m^{bio} (g)	0	0	0	0.000695	0.001401	0.000552
m^N (g)	0.183416					
Δm^N (g)	0.007239			0.002666		
m^{bio}/m^N	0.00%	0.00%	0.00%	0.38%	0.76%	0.30%

Table A 5. Summary tables of mass change for NAPL constituent Naphthalene for sphere model (two-dimensional model)

Naphthalenes	Case 1			Case 2 (Aerobic only)		
	Aerobic	Sulfate	Meth	Aerobic	Sulfate	Meth
m^{bio} (g)	2.01E-04	1.54E-03	8.78E-05	1.97E-04	0.00E+00	0.00E+00
m^N (g)	0.61139					
Δm^N (g)	0.00222			0.00114		
m^{bio}/m^N	0.03%	0.25%	0.01%	0.03%	0.00%	0.00%

Naphthalenes	Case3 (No Bio)			Case4 (No Charge)		
	Aerobic	Sulfate	Meth	Arobic	Sulfate	Meth
m^{bio} (g)	0	0	0	0.000413	0.000673	0.000274
m^N (g)						
Δm^N (g)	0.00078			0.00132		
m^{bio}/m^N	0.00%	0.00%	0.00%	0.07%	0.11%	0.04%

Table A 6. Documentation of GMS project files

	Project File Name	Description
Two-dimensional Modeling Approach	Sheetmodel_TracerBC.gpr	case 1 design for sheet model
	Sheetmodel_TracerBC_Aerobic.gpr	case 2 design for sheet model
	Sheetmodel_TracerBC_NOBIO.gpr	case 3 design for sheet model
	Sheetmodel_TracerBC_NoCharge.gpr	case 4 design for sheet model
	Spheremodel_TracerBC.gpr	case 1 design for sphere model
	Spheremodel_TracerBC_Aerobic.gpr	case 2 design for sphere model
	Spheremodel_TracerBC_NOBIO.gpr	case 3 design for sphere model
	Spheremodel_TracerBC_NoCharge.gpr	case 4 design for sphere model
Three-dimensional Modeling Approach	3D_Sheet365d_N1.gpr	Model ID A1,T1
	3D_Sheet365d_A2.gpr	Model ID A2
	3D_Sheet365d_A3.gpr	Model ID A3
	3D_Sheet365d_A4.gpr	Model ID A4
	3D_Sheet365d_A5.gpr	Model ID A5
	3D_Sheet365d_T2.gpr	Model ID T2
	3D_Sheet365d_T3.gpr	Model ID T3
	3D_Sheet365d_T4.gpr	Model ID T4
	3D_Sheet365d_T5.gpr	Model ID T5
	3D_Sheet365d_T6.gpr	Model ID T6
	3D_SphereNew365d_R1.gpr	Model ID R1
	3D_SphereNew365d_R2.gpr	Model ID R2
	3D_SphereNew365d_R3.gpr	Model ID R3
	3D_SphereNew365d_R4.gpr	Model ID R4
	3D_SphereNew365d_R5.gpr	Model ID R5
	3D_SphereNew365d_R6.gpr	Model ID R6

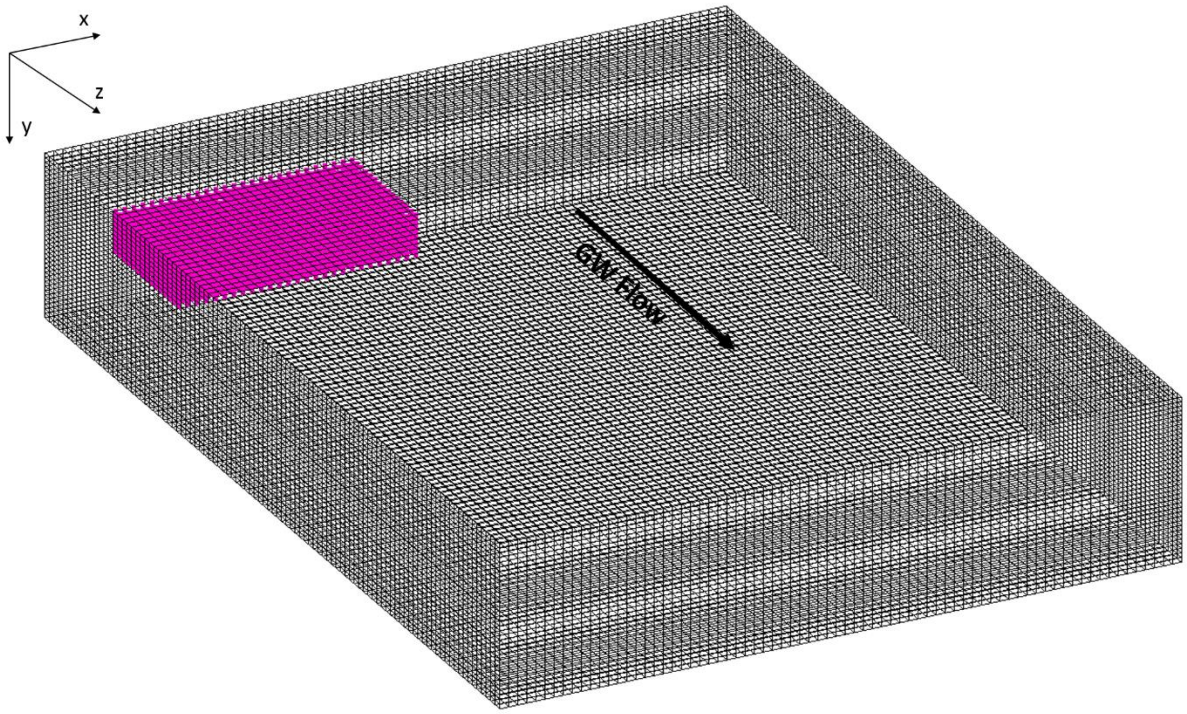
x
z
y
GW Flow

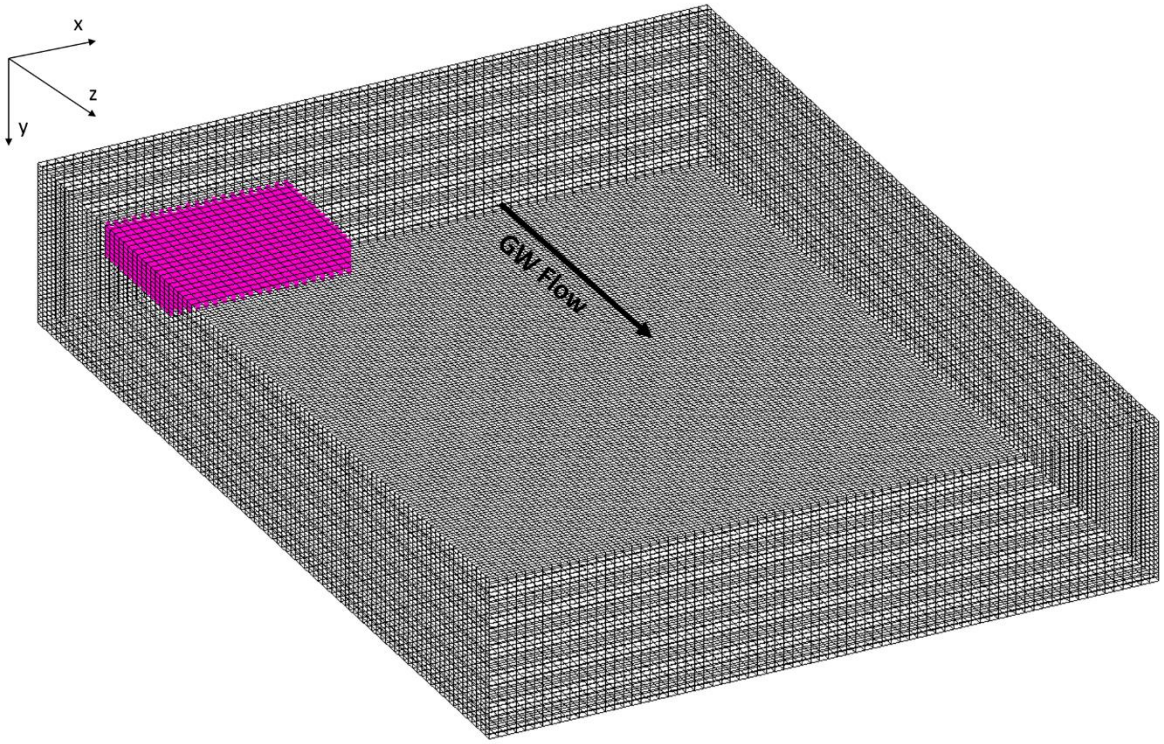
x
z
y
GW Flow

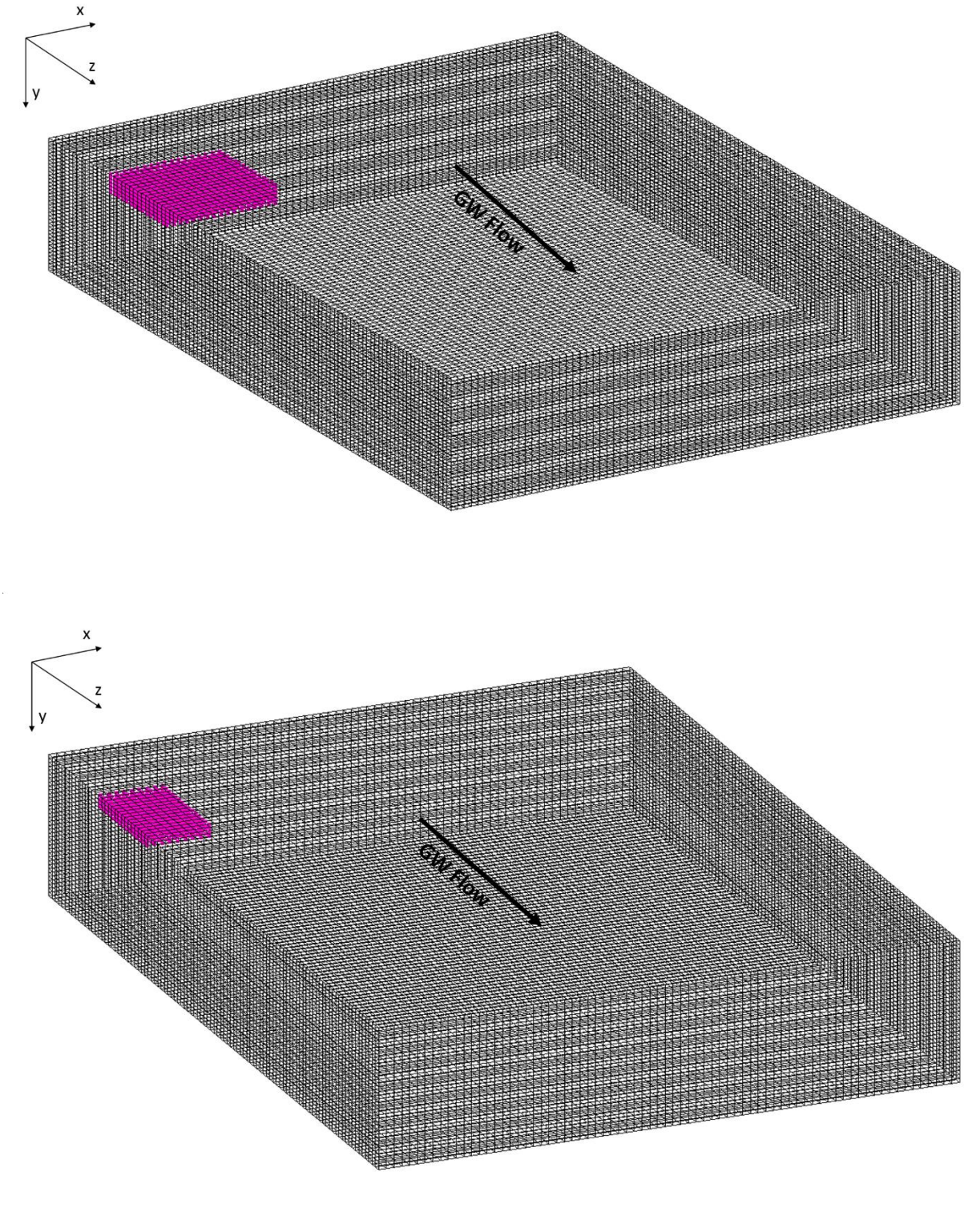

Figure A 1. Three-dimensional sheet model designs with different upper horizontal area (top to bottom: A2 to A5)

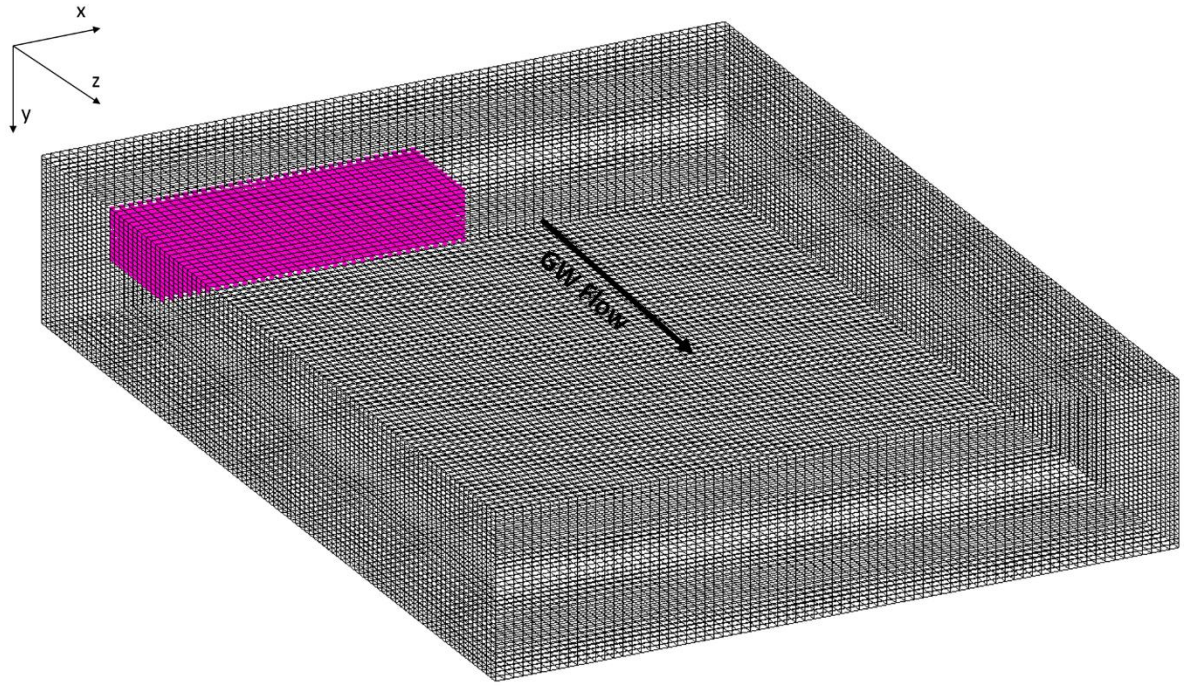
x
z
y
GW Flow

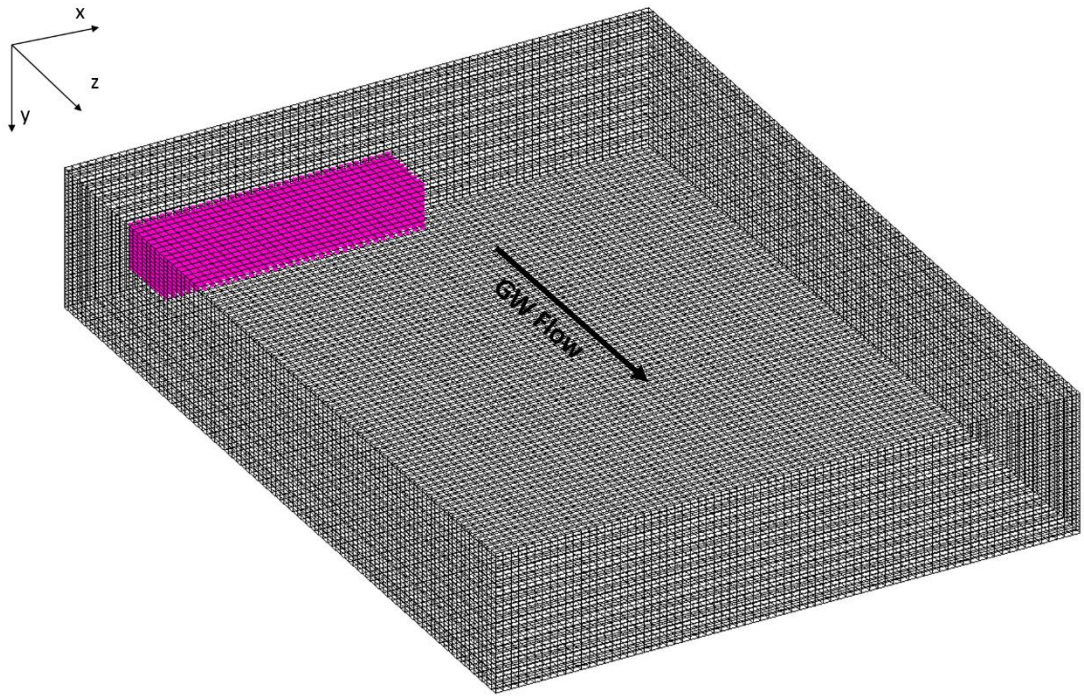
x
z
y
GW Flow

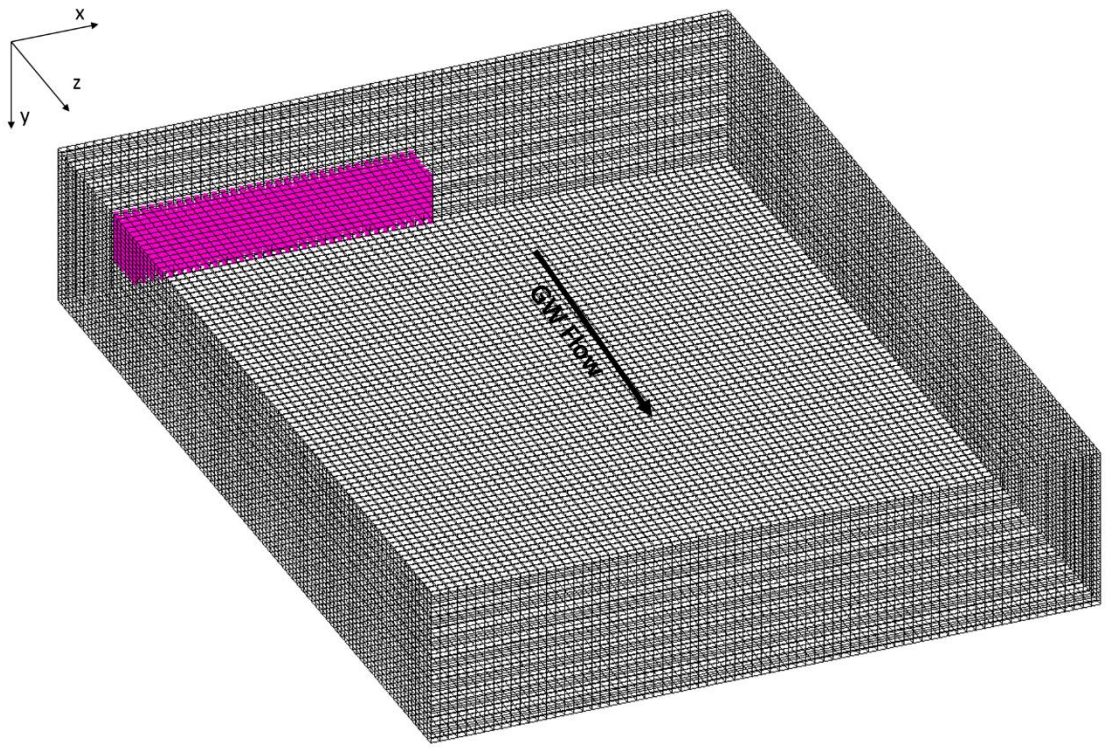
x
z
y
GW Flow

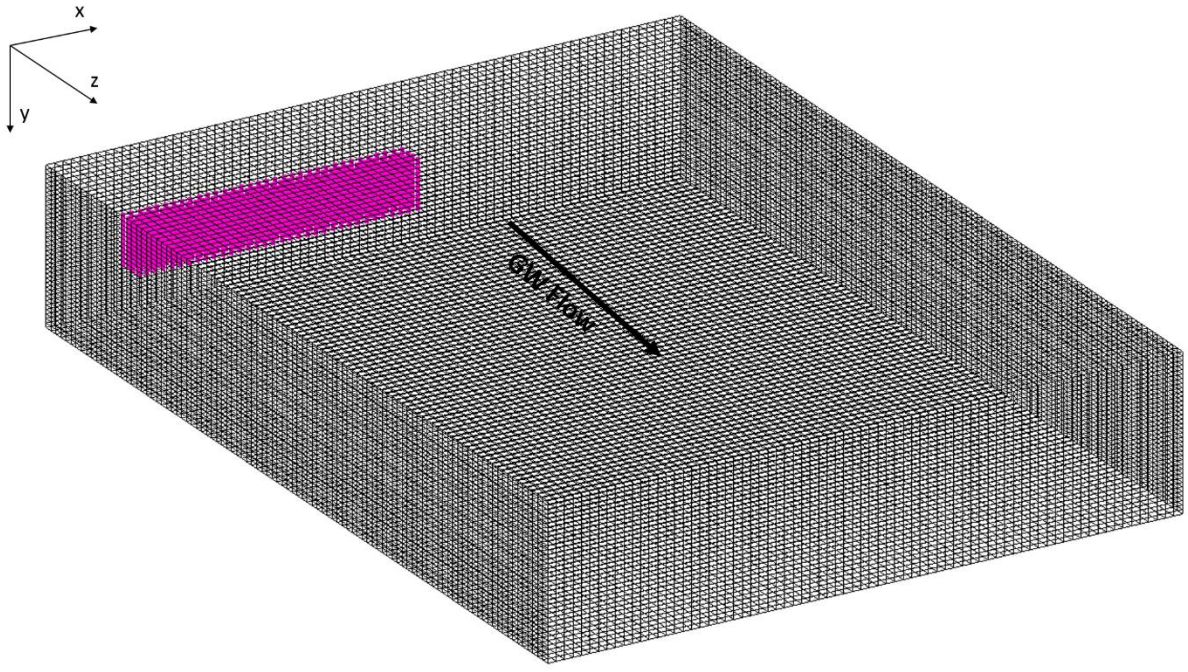
x
z
y
GW Flow

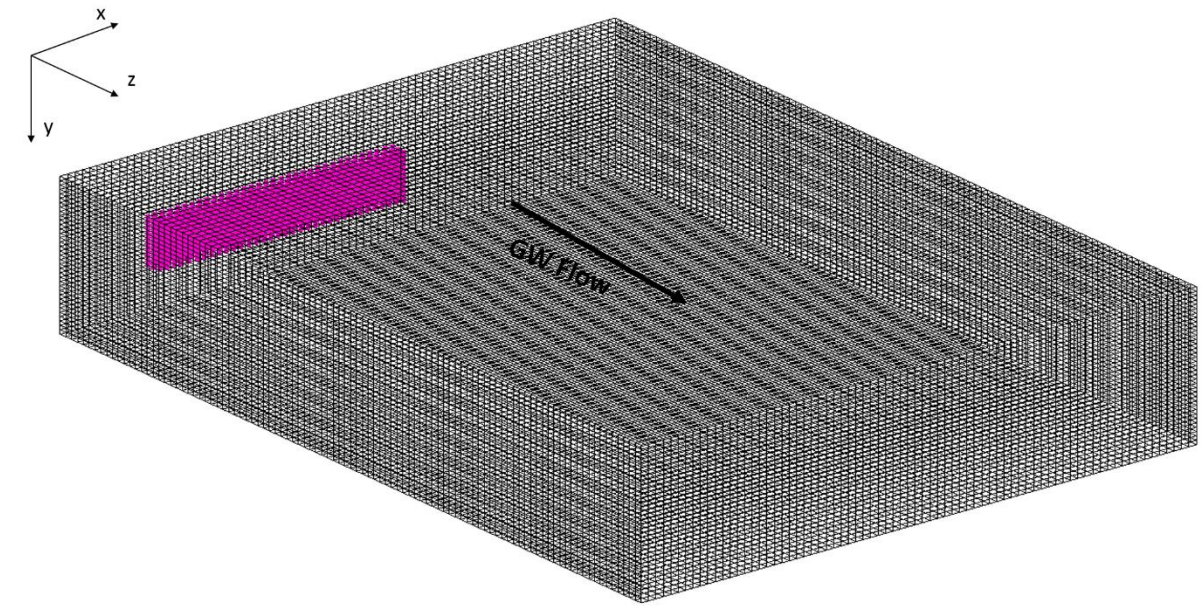

Figure A 2. Three-dimensional sheet model designs with different sheet thickness (top to bottom: T2 to T6)

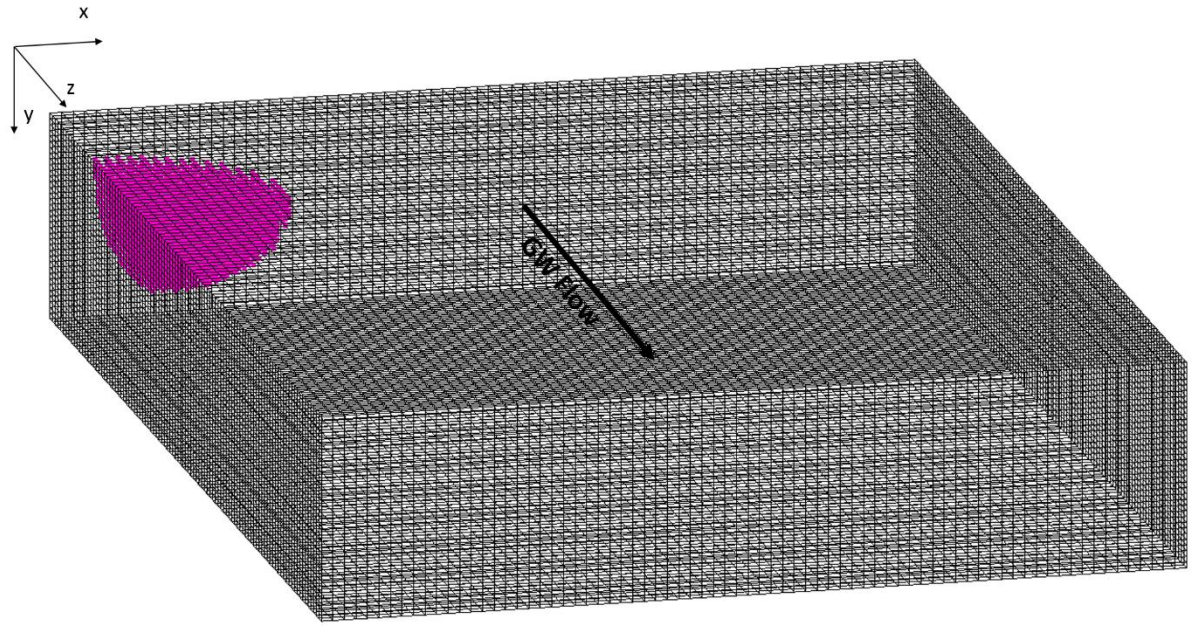
x
z
y
GW Flow

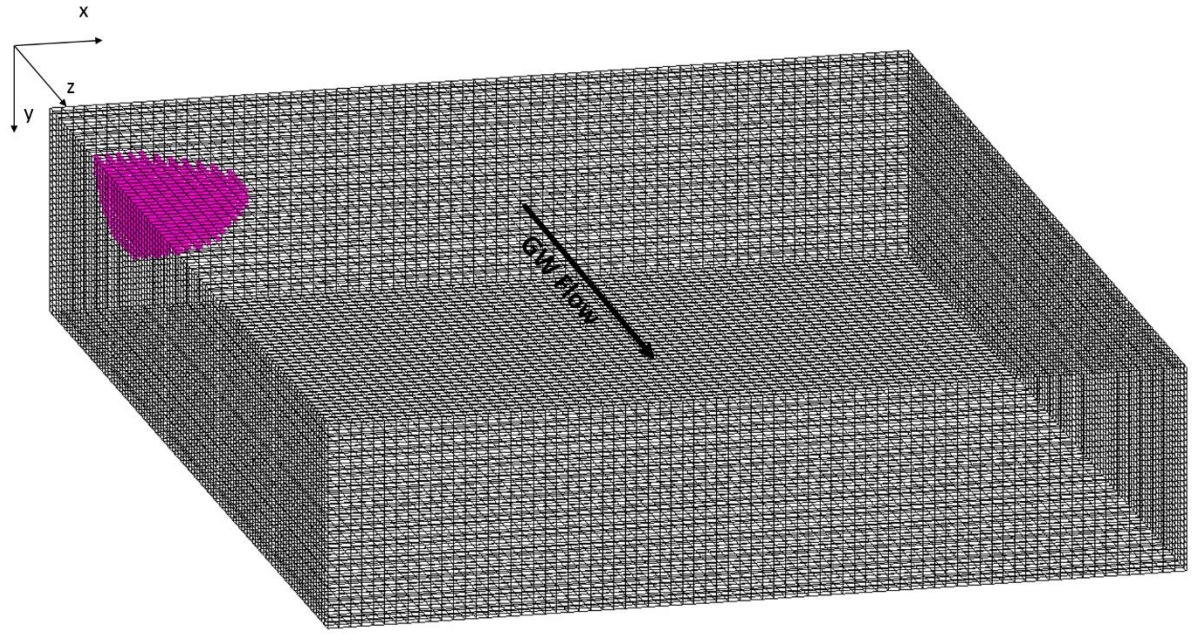
x
z
y
GW Flow

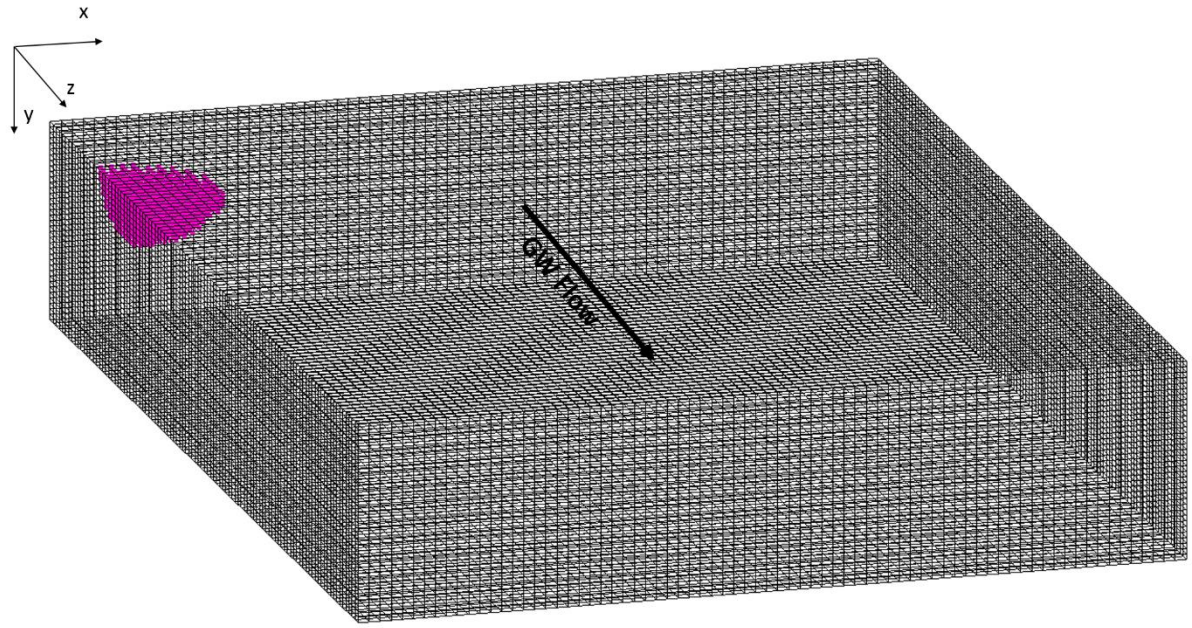
x
z
y
GW Flow

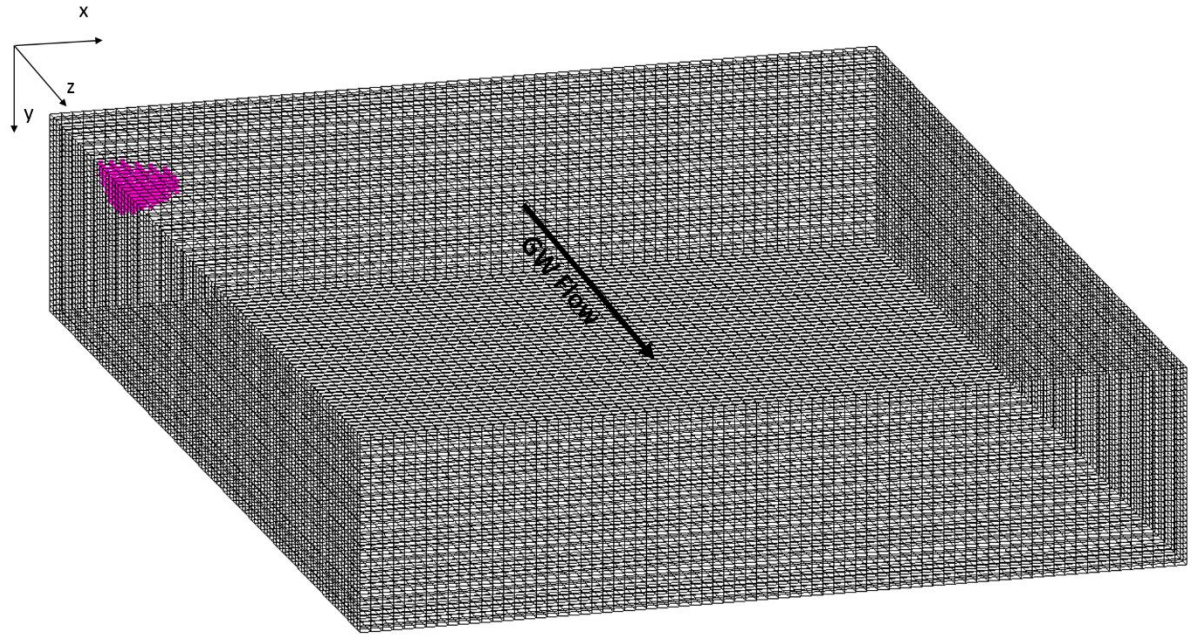
x
z
y
GW Flow

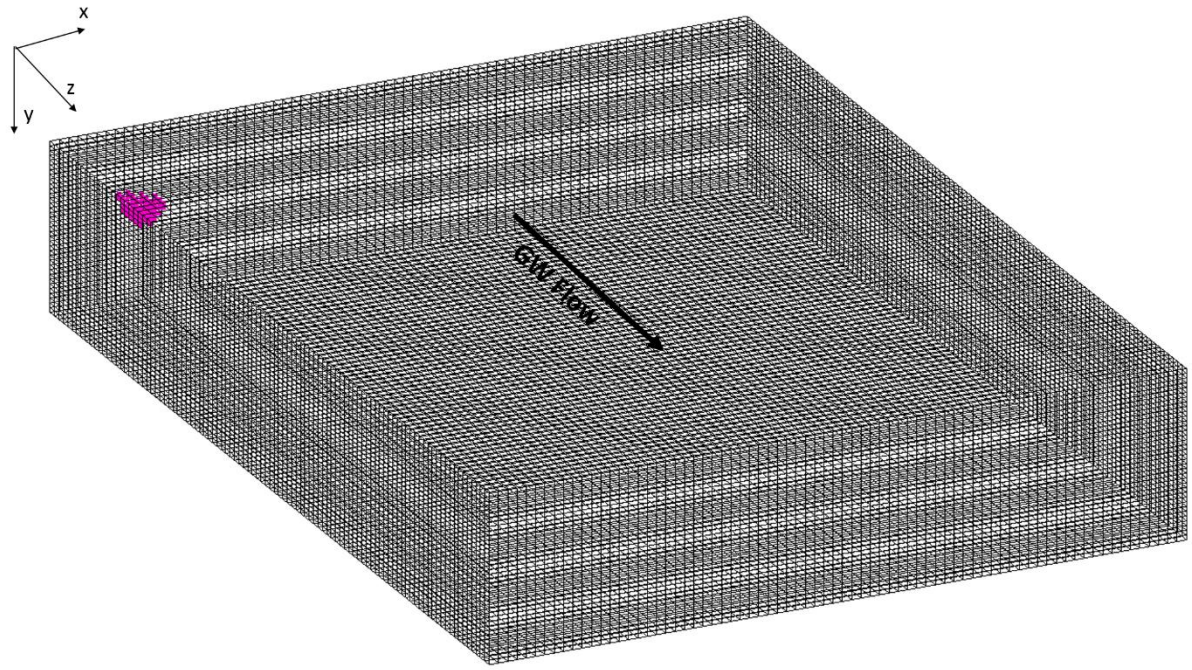

Figure A 3. Three-dimensional sphere model designs with different radius (top to bottom: R2 to R6)